

Review

Recent progress of carbon dots in targeted bioimaging and cancer therapy

Cheng-Long Shen^{1*}, Hang-Rui Liu^{2*}, Qing Lou¹, Feng Wang², Kai-Kai Liu¹, Lin Dong¹, Chong-Xin Shan¹

1. Laboratory of Materials Physics, Ministry of Education, and School of Physics and Microelectronics, Zhengzhou University, Zhengzhou 450052, China.
2. Department of Oncology, The First Affiliated Hospital of Zhengzhou University, Zhengzhou, 450052, China.

*These authors contributed equally.

 Corresponding authors: Qing Lou, Email: louqing1986@zzu.edu.cn; Prof. Feng Wang, Email: fengw010@163.com; Prof. Chong-Xin Shan, Email: cxshan@zzu.edu.cn

© The author(s). This is an open access article distributed under the terms of the Creative Commons Attribution License (<https://creativecommons.org/licenses/by/4.0/>). See <http://ivyspring.com/terms> for full terms and conditions.

Received: 2022.01.04; Accepted: 2022.02.28; Published: 2022.03.14

Abstract

Carbon dots (CDs), as one new class of carbon nanomaterials with various structure and extraordinary physicochemical properties, have attracted tremendous interest for their potential applications in tumor theranostics, especially in targeted bioimaging and therapy. In these areas, CDs and its derivatives have been employed as highly efficient imaging agent for photoluminescence bioimaging of tumors cells. With unique structure, optical and/or dose attention properties, CDs have been harnessed in various nanotheranostic strategies for diverse tumors through integrating with other functional nanoparticles or utilizing their inherent physical properties. Up to now, CDs have been approved as novel biomaterials by their excellent performances in precise targeted bioimaging and therapy for tumors. Herein, the latest progress in the development of CDs in targeted bioimaging and tumor therapy are reviewed. Meanwhile, the challenges and future prospects of the application of CDs in promising nanotheranostic strategies are discussed and proposed.

Key words: Carbon dots, targeted bioimaging, cancer therapy, nanotheranostic

1. Introduction

Cancer has been one of the widely spread diseases around the world, leading to millions of deaths every year [1-4]. Up to now, quite a few research has been carried out on the causes and biology of cancer, dramatically accelerating the development of diagnosis and treatment strategies of cancers [3, 5-12]. In the areas of cancer diagnosis, targeted imaging for tumor cells is considered as a promising technology to *in vivo* distinguishing the tumor sites efficiently and precisely, proving the promising diagnosis of cancer without trauma and expensive cost in common detailed physical examination [13-18]. Meanwhile, the *in vivo* imaging also provides the ability to monitor tumor morphologies in real-time, allowing doctors to understand the evolution of tumor tissues and enabling to adjust the dosing of drug to abate

overtreatment of harmful side-effects, or undertreatment of incomplete cancer remission [13-15, 17-28]. Yet, diverse models of targeted imaging have been established with the accumulation biodistribution of imaging agent in tumor sites [17-18, 26-28]. However, there are always various limitations for the common imaging agent, such as the inability to bypass biological barriers, poor biocompatibility, lack of stability, etc. In the areas of cancer therapy, there are various recommended guidelines of clinical oncology treatment for different kinds of tumors, such as operative treatment, chemotherapy, radiation therapy, etc. [10, 29-32]. Nevertheless, the common strategies for cancer therapy also still remind diverse restrictions such as serious damages to living body, potential drug resistance, ineffectiveness against metastatic disease, drug resistance of cancers, and

lack of effective modality for treatment monitoring. With the development of advanced technologies, the concept of precise targeted therapy for tumors are proposed, enabling the ability to overcome the limitations in common strategies of cancer therapy [17, 28, 33-36]

In recent years, the excellent performance of nanotheranostic strategies for diverse cancer has been approved with various experiments, enabling the engineered imaging agent or medicines to overcome the specific limitations of some cancers [37-41]. Up to now, several nanotheranostic strategies through targeted bioimaging and therapy have been designed to improve the targeting or therapies of cancers [42-46]. For examples, some nanomaterials, such as Au nanoparticles (Au NPs), semiconductor polymer nanoparticles (SPNPs), graphene and superparamagnetic iron oxide (SPIO), have been approved for targeted bioimaging with different models, such as photoluminescence (PL), afterglow, chemiluminescence (CL), photoacoustic (PA), and magnetism imaging and precise therapy through targeted drug delivery or advanced biological treatment [47-54]. Additionally, several nanomedicines have been approved and recommended as guidelines of clinical oncology treatment for several specific cancers [33, 35]. While these nanotheranostic strategies are complex and restricted in clinical treatment, their potential utility has substantiated the investment required at the front-end [27, 55-60]. Drawing back on these nanotheranostics strategies, the advanced nanotechnologies of targeted bioimaging and therapy for tumors have been utilized and developed with various approaches, enabling their advantages of efferent and precisely therapeutic effect.

Since the discovery in the process of electrophoretic purification of single walled carbon nanotubes in 2004, fluorescent carbon dots (CDs) have been proved one new class of carbon-related nanomaterials owing to their extraordinary physicochemical properties and diverse potential applications [61-83]. With different approaches to preparation, the obtained CDs can illustrate wide diversity in sizes, structures, surface function group and physicochemical properties [78-91]. Typically, CDs are always classified as one kind of 0 D carbon nanomaterials, which is consisted of sp^2/sp^3 carbon skeleton and abundant functional groups/polymer chains [87-101]. Compared with the other bio-nanomaterials, such as phosphorene, 2D Xenes, hydrogels, hydrophobic organic polymers, semi-conducting polymer nanoparticles, the CDs, as one zero-dimensional carbon-based nanomaterials, have illustrated obvious advantages in structure and properties for the application of nanotheranostics: (I)

CDs can achieve different luminescent models, such as PL, phosphorescence, thermally activated delayed fluorescence (TADF), chemiluminescence, etc., which can be used for diverse models of bioimaging; (II) CDs behave excellent biocompatibility and photostability compared with other imaging probes, which is favorable to be used as *in vivo* real-time imaging agents; (III) CDs exhibit tunable PL emission, especially the near-infrared (NIR) emission, which is suitable for tissue imaging with deep penetration; (IV) CDs are proved unique properties, such as penetration of blood brain barrier (BBB) and novel targeting for some cells, which is extraordinary advantages for imaging; (V) CDs exhibit clearable property in living body, which is excellent for long-term imaging. In addition to the applications as imaging agent, CDs have been approved to be as a nanoplatform to design biomaterials or directly used as nanomedicines for treatment of several special kinds of diseases [102-107]. On the one hand, the CDs possess a sp^2 hybridized structure with different surface functional groups, enabling their novel physical properties including excellent water solubility, biocompatibility, and photophysicochemical properties. Meanwhile, due to their special structure, some CDs present abundant superiority, such as modifiable surface, long-term permeation and metabolism in living body, approved unique properties of BBB penetration, special cells targeting, observed unique therapeutic effects for some diseases, etc. For examples, Rosenkrans *et al.* developed selenium-doped CDs as broad-spectrum antioxidants, and Kim *et al.* indicated the promising application of CDs in preventing α -synucleinopathy for Parkinson's disease [108, 109]. On the other hand, comprised with other larger nanomaterials, the smaller CDs (with the size of usually less than 10 nm) exhibit well-organized carbon atoms with a high aspect ratio, large surface area, and high thermal and chemical stabilities, enabling their promising capability for designing different biomaterials and nanomedicines. These CDs-based nanotheranostics have been approved in various works.

Recently, there have been some reviews about the nanotheranostics focus on bioimaging and cancer therapy, enabling the contrast and precise imaging of cell and organelle or improving the therapeutic effects of several tumor lines [110-115]. However, with the development of synthetic technique, the targeted bioimaging and cancer therapy have been expanded to a broader field, such as uptake accumulation, charge or pH, targeting agent, self-targeting, drug delivery, light-activate theranostic, metabolism and precise therapy via different CDs and their nanocomposites (Figure 1 and Table 1) [116-166].

Herein, the strategies of CDs-related nanotheranostics to achieve efficient targeted bioimaging and cancer therapy have been reviewed and discussed, and the challenge and prospect in the future development of this emerging field are also discussed and proposed.

2. Synthesis and classification of CDs

Since the CDs firstly prepared via electrophoretic purification of single walled carbon nanotubes, various synthetic methods to obtain CDs have been developed (Figure 2). Up to now, the strategies to prepare CDs are always based on the two main routes, naming top-down and bottom-up. Generally, the top-down strategy is considered to obtain nanosize nanoparticles from bulk carbon precursors by broking or exfoliating. Arc-discharge, laser ablation and electrochemical oxidation approaches are the common top-down strategies to achieve broking or exfoliating (Figure 2A-C) [61, 63, 80]. In the early stages, the CDs are usually synthesized via the top-down strategy and these CDs always illustrate excitation-dependent emission with low PL QY. Afterwards, with the practical requirement, these top-down strategies are reserved as a paradigm to solve the extensive concern and pioneering studies. By contrast, the bottom-up strategies to prepare CDs

are usually considered to obtain nanoparticles by the direct pyrolysis of small molecular. In the early years, researchers developed the template method to prepare CDs with different carriers as template. And the CDs can be obtained in the template through the pyrolysis of carbon-rich precursors, which can accurately control the size and structure of CDs (Figure 2D). With the development of synthetic technology, solvothermal strategy gradually become the most widespread routes to prepare CDs because of its low cost and easy manipulated parameters, such as temperature, time, and pressure of vessel. Among diverse precursors for preparing CDs in solvothermal method, citric acid and its related reactant are the most common ingredients. Since *Zhu et al.* firstly synthesized the fluorescent CDs with the high PL QY of ~80% with citric acid and ethylenediamine, various solvothermal strategies have been employed to achieve fluorescent CDs with high QY through tuning the pyrolysis of small-molecular (Figure 2E) [83]. Similarly, microwave-assisted pyrolysis is another fast, low cost and effective bottom-up strategy. In recent years, the microwave radiation has drawn researchers' more attention due to its short reaction times and potential introduced optical properties via special heating principle (Figure 2F). Up to now, fluorescent CDs with ultraviolet to infrared emission

have been achieved through bottom-up strategy, implying their great potential for practical applications.

Since the first discover of fluorescent carbon nanoparticles (CNPs) in 2004, diverse kinds of nanoparticles with carbon skeleton have been classified as CDs as shown in the Figure 3. Typically, with the development of synthesis strategies and raw materials, CDs have been defined as one kind of concept of 0 D nanomaterials whose main element is carbon. Recently, *Xia et al.* improved the classification and nomenclature to precisely distinguish different CDs, which are defined as carbon quantum dots (CQDs), graphene quantum dots (GQDs), carbon polymer dots (CPDs), and carbon nanodots (CNDs) via the summary and analysis of structure and properties features for different kinds of CDs (Figure 3A) [92]. In these classifications, CQDs are defined as spherical NPs with

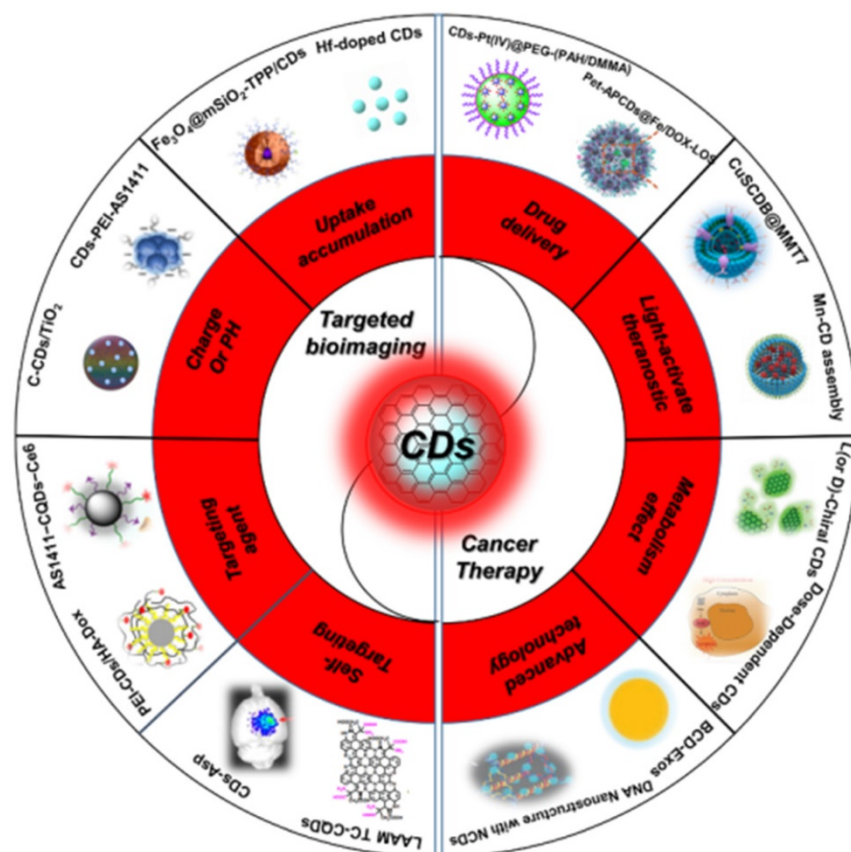


Figure 1. Schematic of the carbon dots in tumor for targeted bioimaging and cancer therapy.

obvious crystal lattices and chemical groups on the surface, possessing intrinsic state luminescence and quantum confinement effect. QDs are considered as small graphene fragments consisting of single or few graphene sheets with obvious graphene lattices and chemical groups on the edge or within the interlayer defect, which result in the quantum confinement

effect and edge effect. The CPDs are considered as a polymer/carbon hybrid structure comprising of abundant functional groups/polymer chains on the surface and a carbon core. For the CNDs, these NPs possess high carbonization degree with some chemical groups on the surface with no obvious crystal lattices structure and polymer features.

Table 1. Summary of the types of CDs and their nanocomposites with different sizes, morphology/composition, and photophysical properties.

Type	Shape	Chemical composition (elements)	Size [nm]	λ_{abs} / range [nm]	PL _{max} [nm]	PL lifetime [ns]	PL QY	PCE @ λ_{ex}	ROS, QY	Ref
CDs	Spherical	C, O, S	10 ± 4	400–750	640	2.3%	N/A	38.5%@671 nm	N/A	[116]
Supra-CDs	CD aggregates	C, O, N	12.4	600–800	N/A	N/A	N/A	53%	N/A	[117]
CyCD	Spherical	C, O	2.9 ± 0.5 (D) 2.8–5.0 (H)	770	820	N/A	5.7%	38.7%@808nm	N/A	[118]
CDs	Spherical	C, O, S	6–10 (D) 3–5 (H)	400–700	640	3.5		36.2%@808nm.	¹ O ₂ , 27%	[119]
R-CDs	Spherical	C, O, N	4	550	640	0.68	22.9%	44%	N/A	[120]
NIR-PCNDs	Disk-like	C, O, N	7.8 (D) 2.1 (H)	277, 450–631	710	3.7	26.28%	N/A	N/A	[121]
CDs	Platelet-like	C, O, N, S, Se	20 (D) 4 (H)	526	730, 820	N/A	0.2%	58%@635nm	N/A	[122]
R-NBE-T-CQDs	Triangular	C, O	3.9	582	598	6.6	54%	N/A	N/A	[87]
CDs	Spherical	C, O, N	7.6	268, 277, 634	750	2.1	43%	N/A	N/A	[123]
CDs	Disk-like	C, O, N, S	2–5 (D) 0.5–2 (H)	340, 455, 605, 650	720	N/A	0.2%	59%@655 nm	N/A	[39]
CDs	Spherical	C, O, N	2	270–400	450 nm	N/A	20%	N/A	¹ O ₂ , 0.82	[124]
N-O-CDs	Spherical	C, O, N	1.2–3.3 (D) 1.06 (H)	375/600–850 nm	475	16.1%	N/A	38.3%@808	N/A	[125]
CDs-650	Spherical	C, O, N	7 (D) 8.5 (H)	250, 365, 650	530	N/A	N/A	54.3%@655nm	N/A	[126]
DPP CDs	N/A	C, O, N, S	3.72 ± 0.67	530	N/A	N/A	N/A	N/A	¹ O ₂ , 27.6%	[127]
CuCD NSs	Sheet-like	C, O, N, S, Cu	23.4	340	N/A	N/A	N/A	41.3%@808 nm	N/A	[128]
CuSCDB@MMT7	Spherical	N/A	222.5 ± 20.1	N/A	N/A	N/A	N/A	39.7%@808nm	N/A	[129]
BCCGH	Sphere-like	C, O, N, S, Cu, Gd	7.9	605/ 640–700	655	N/A	N/A	68.4%@808nm	N/A	[130]
CDs	Spherical	C, O, N	5.6	226, 280, 615	648, 685	20	34%	N/A	N/A	[131]
CDs	Spherical	C, O, N	4–5	560	630, 670	N/A	25%	N/A	N/A	[132]
NIR-CDs	Disk-like	C, O, N	4 (D) 0.4–2 (H)	619, 720	770	0.561	11%	N/A	N/A	[133]
CNDs	Spherical	C, O, N	2.5	540	600–900	3.3	56%	N/A	N/A	[90]
Ce6-RCDs	Spherical	C, N, O	3.7	405, 640	653	N/A	N/A	46%@671 nm	N/A	[134]
Ni-pPCDs	Spherical	C, N, O, Ni	2.9 ± 0.5	204, 243, 286, 510	605	N/A	45.6%	N/A	N/A	[135]
NIR-CD/MoS ₂	Sheet	C, O, N, S, Mo	100	450	N/A	N/A	N/A	78.2%@808 nm	N/A	[136]
DA@N-CDs(Mn) NPs	Spherical	N/A	3.1	530	620 nm	4.5%	N/A	28.2%@808 nm	N/A	[137]
CQDs	Disk-like	C, O, N	2.42	628	665	2.49	47%	N/A	N/A	[138]
C-CD /TiO ₂	spherical	C, O, Ti	244.6	285, 400	N/A	N/A	N/A	9.54%@808nm	N/A	[139]
CDs	spherical	C, N, O, S	4.4	315, 355/ 320–750	930	4.59, 13.08	~8.0%	54.7%@808nm	N/A	[140]
SCDs	spherical	C, O, N	20	337, 600	N/A	N/A	N/A	41.7%@808 nm	N/A	[141]
CDs	Spherical	C, O, N, F	2.6	556, 624, 715, 847	658, 777	6.8	10	N/A	N/A	[142]
CDs	Spherical	C, O, N	4	295, 395, 580	642	5.9	N/A	N/A	N/A	[143]
CDs	Spherical	C, O, N	4–6	339	449	2.56	0.39%	N/A	O ₂ ^{•-} , 1.08%	[144]
Se/N-CDs	Spherical	C, O, N, Se	3.6 ± 0.6	317,550	607	N/A	3.70%	N/A	¹ O ₂ , 10.6%	[145]
CCOF @PEG	Spherical	N/A	235	200–900	650	N/A	N/A	N/A	N/A	[146]
NCDs	Spherical	C, O, N	4.1 ± 1.6 (D) 2.3 ± 0.8 (H)	610	623			77.6%@660	¹ O ₂ , 37%	[147]
S-CDs	Sphere-like	C, O, S	3.2 (H) 2.0 (H)	300, 360/ 400–900	440	N/A	N/A	55.4%@808 nm	N/A	[148]
Ni-CDs	Spherical	C, O, N, Ni	4.6 (D) 1.9 (H)	1002/ 750–1350	N/A	N/A	N/A	76.1%@1064 nm	N/A	[149]
S, N-CDs	Spherical	C, N, O, S	9	560/ 600–700	630	N/A	12.4%	34.4% @808nm	¹ O ₂ , 27%	[150]
TP-CDs	Quasi-spherical	C, O, N	4.0 ± 1.1	274/400–600	605	N/A	N/A	N/A	N/A	[151]
RGQDs	Spherical	C, O	3.54	230	532, 950	N/A	6%	N/A	N/A	[152]
CDs	spherical	C, O	3–4	310, 365	502	N/A	N/A	N/A	¹ O ₂ , 0.51	[153]
f-CDAs		C, O, N	12–22 (D) 7–13 (H)	550–700	675	2.3	15.6%	26.1%@655 nm	N/A	[154]
FA-CD/PPy-NPs	spherical	C, N, O	6.08 ± 2.07	260/ 700–1000 nm	520	N/A	20.39 ± 1.80 %	40.80 ± 1.54% @808nm	N/A	[155]
NIR-II-CD/BP Hybrids	Sheet-like	C, N, O, P	100–200 (D) 2.0 (H)	420	480	N/A	N/A	61.4%@1064 nm	N/A	[156]
anti-EpCAM@PDA-CDs@Pt(IV)	Spherical	C, N, O, Pt	1.7	275, 360	454	N/A	~22.5%	39.1%@808 nm	N/A	[157]

Abbreviations: D – diameter; H – height; λ_{abs} – Maximal absorption wavelength; λ_{ex} – excitation wavelength; λ_{em} – emission wavelength; PCE@ λ_{ex} – photothermal conversion efficiency @ corresponding excitation wavelength; and ROS, QY – reactive oxygen species, quantum yield.

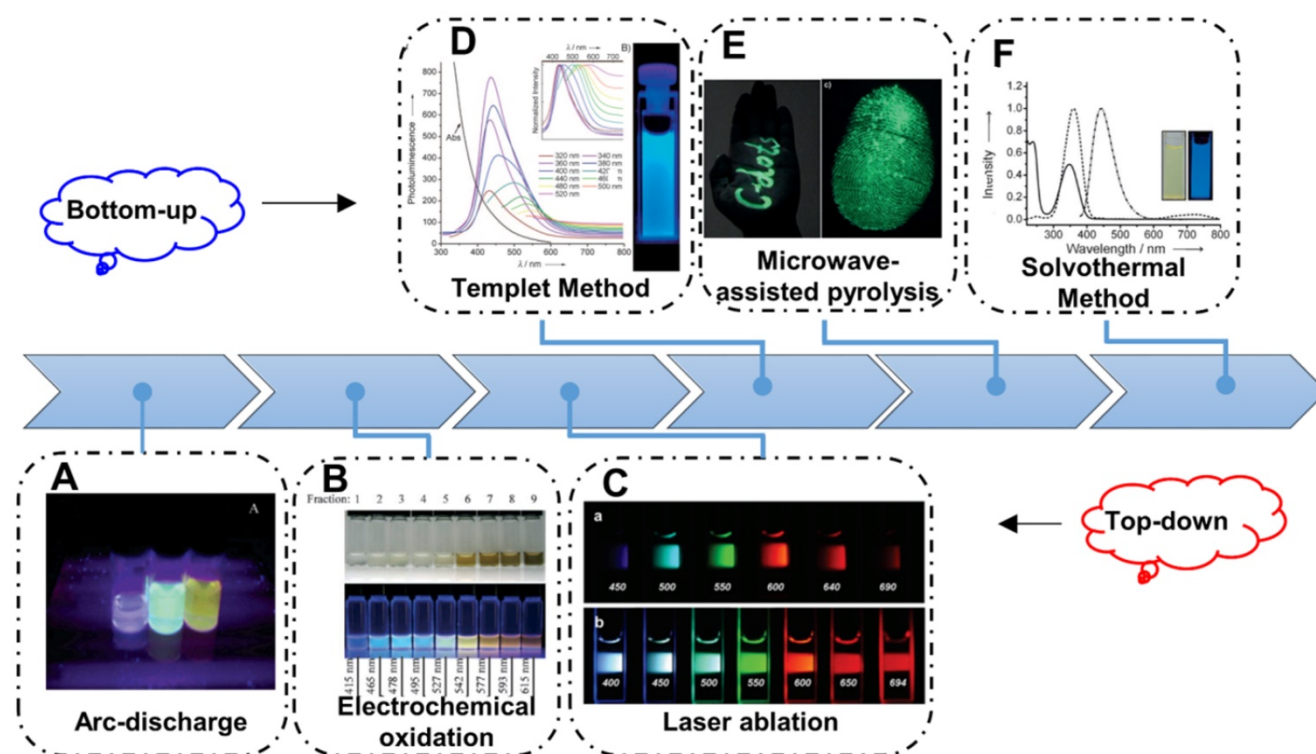


Figure 2. Schematic illustration of the synthetic strategies of CDs. (A) The CDs synthesized by arc-discharge. Adapted with permission from [61], copyright 2004, American Chemical Society. (B) The CDs synthesized by electrochemical oxidation. Adapted with permission from [79], copyright 2007, WILEY-VCH Verlag GmbH & Co. KGaA, Weinheim. (C) The CDs synthesized by laser ablation. Adapted with permission from [80], copyright 2006, American Chemical Society. (D) The CDs synthesized with templet method. Adapted with permission from [81], copyright 2009 WILEY-VCH Verlag GmbH & Co. KGaA, Weinheim. (E) The CDs synthesized by microwave-assisted pyrolysis. Adapted with permission from [82], copyright 2012 WILEY-VCH Verlag GmbH & Co. KGaA, Weinheim. (F) The CDs synthesized with solvothermal method. Adapted with permission from [83], copyright 2013 WILEY-VCH Verlag GmbH & Co. KGaA, Weinheim.

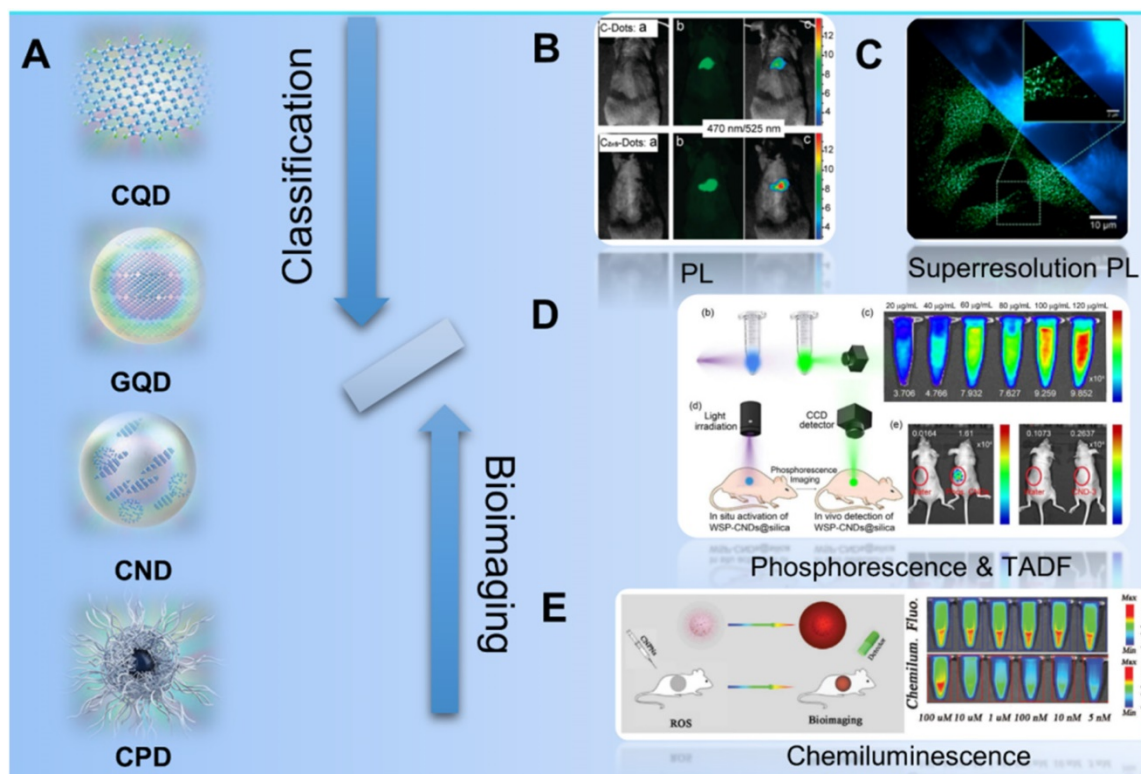


Figure 3. Schematic illustration of the classification of CDs and their different kinds of luminescence models for bioimaging. (A) The classification of CQDs, GQDs, CNDs and CPDs for different CDs. Adapted with permission from [69], copyright 2019 WILEY-VCH Verlag GmbH & Co. KGaA, Weinheim. (B) Schematic illustration of the PL bioimaging. Adapted with permission from [80], copyright 2009, American Chemical Society. (C) Schematic illustration of the bioimaging via superresolution PL. Adapted with permission from [91], copyright 2018, American Chemical Society. (D) Schematic illustration of the bioimaging by phosphorescence and TADF. Adapted with permission from [143], copyright 2020 Elsevier Ltd. (E) Schematic illustration of the bioimaging with CL. Adapted with permission from [167], copyright 2019 WILEY-VCH Verlag GmbH & Co. KGaA, Weinheim.

3. Targeted Bioimaging

Due to the novel photophysical properties, CDs has been employed as contrast agents for *in vivo* optical imaging (Figure 3B-E) [24, 80, 167-174]. In those approaches to optical imaging, the direct PL imaging with light irradiation is the most common strategy. With the down-conversion or multiphoton-excited upconversion fluorescence, the structure of cells or tissues can be reconstructed via the emitted photon of imaging agent (Figure 3B) [83, 90, 93-101]. However, the common PL imaging with conventional fluorescence microscopy is limited by the diffraction limit of light by the Abbe criterion. Thereby, two major approaches are employed to overcome the diffraction limit: the patterned illumination-based imaging, including stimulated emission depletion (STED) microscopy and structured illumination microscopy (SIM), and single molecule localization-based imaging, including stochastic optical reconstruction microscopy (STORM) and photoactivated localization microscopy (PALM). For the single molecule localization-based imaging, closely clustered fluorescent particles are resolved by stochastically turning each particle's signal on and off, and then the centroid of on-state particle is mathematically determined in each imaging frame. On the condition, the super-resolution PL image can be reconstructed via the combination of multiple iterations (Figure 3C) [167]. In addition to the direct PL imaging, afterglow imaging is considered as another excellent strategy for bioimaging. In general, the afterglow imaging through the phosphorescence and TADF can decrease the noise of photoexcited autofluorescence from the background because of the novel delay luminescence (Figure 3D) [13, 69]. Similarly, CL is also employed as a contrast optical imaging strategy. Owing to the CL emission as the result of a chemical reaction without photoexcitation, the CL imaging can be employed as special biomolecularr sensor with ultrahigh sensitivity and provide their distinguished bioimaging without photoexcited autofluorescence from the background (Figure 3E) [20, 22-27]. Thereupon, different strategies have been developed to further achieve targeting bioimaging of cancer cells. In the early stage, researchers found the accumulation effect of CDs in tumors sites and further developed the uptake accumulation targeted imaging. With the development of nanotechnologies, CDs was further developed to achieve tumor targeting imaging with rational design, such as the stimulus-responsive imaging triggered by the novel charge and pH in tumor microenvironment and *in vivo* biomarker imaging with the interaction between CDs and

various biomoleculars. More importantly, several researches have observed and approved the special targeting cancer cells marker of CDs in several special tumors, enabling a novel application in self-targeting bioimaging and promising approaches to dignosis of cancer. Up to now, the CDs-related targeted bioimaging for tumor have been approved for the promising clinical diagnosis for various cancers.

3.1. Uptake accumulation

As one new class of powerful nanoprobess, CDs have been proved one kind of contrast agents for diverse models of bioimaging since its discover [175, 176]. Ideally, the CDs for bioimaging exhibit high PL quantum yield (QY), long-wavelength PL emission, minimum toxicity and renal cleavability, enabling the rational use of inherent CDs in visualizing biological systems both *in vitro* and *in vivo* [177-183]. At early stage, CDs exhibit homogeneous permeation and distribution in all cells, endowing similar uptake accumulation for the normal and cancer cells [80, 167]. However, several researchers have observed the distinctive accumulation of CDs in tumor tissues due to the enhanced permeability and retention (EPR) effect. For example, Su *et al.* reported the preferential accumulation and efficient renal clearance of CDs at the tumor site [184]. In their work, a novel kind of Hafnium-doped CDs (Hf-CDs) exhibited preferential targeted tumor accumulation capability with significant advantages including robust stability, good biocompatibility, excellent water solubility, remarkable computed tomography (CT) contrast performance, enabling the CDs in particular CT/fluorescence imaging for orthotopic liver cancer (Figure 4A-B). In their experiments, researchers found that the Hf-CDs could accumulate at the tumor site for rapid bioimaging (Figure 4C-E), implying a facile and universal method to multimodal imaging. In addition, these researchers further strengthen the distinctive cancer cells uptake accumulation through various approaches. For example, Zhang *et al.* constructed a biocompatible nanoplatform for long time mitochondria-targeting cellular imaging with CDs and further develop the magnetic field-enhanced cellular uptake functionalities to increase the distinctive accumulation [185]. With the magnetic mesoporous silica nanoparticles ($\text{Fe}_3\text{O}_4@m\text{SiO}_2$) via surface modified triphenylphospine (TPP) and conjugated fluorescent CDs (Figure 4F), researchers have proved the novel time-dependent mitochondrial colocalization of the $\text{Fe}_3\text{O}_4@m\text{SiO}_2$ -TPP/CDs nanoplatform in various cell lines such as A549, CHO, HeLa, SH-SY5Y, HFF and HMEC-1. Furthermore, researchers indicated that the cellular uptake efficiency of A549 and HFF cell lines could be

enhanced in a short time under a static magnetic field (Figure 4G-J). These distinctive accumulations of CDs in tumors sites provided the basis of targeted uptake and paved the abundant approaches to targeted bioimaging.

3.2. Charge or pH

In addition to the direct uptake accumulation, these stimulus-responsive strategies to achieve targeted uptake of CDs based on the distinctive microenvironment in tumor sites, such as charge or the pH, also been explored [186]. For example, the zwitterionic CDs can easily bioconjugate with various biomolecules through the interaction between biomolecules and their carboxylic moieties, shed their anionic component and leave a positive charge on their surface when they achieve interaction with cancer cell microenvironment, enhancing their targeted uptake in cancer cells [187-189]. On the basis, Sri et al. developed one kind of zwitterionic CDs and indicated their targeted bioimaging for the oral cancer cell lines of FaDu (human pharyngeal carcinoma) and Cal-27 (human tongue carcinoma) (Figure 5A-B) [189]. Similarly, Kong et al. developed an efficient detected and targeted nanosystem based on the DNA aptamer AS1411 modified CDs with polyethyleneimine (PEI) as connecting bridge (Figure 5C) [190]. In their work, researchers confirmed the higher cellular uptake of

CDs-PEI-AS1411 nanosystem in MCF-7 cells compared with that of L929 cells, which revealed the highly selective detection ability of nucleolin-positive cells. In addition to the charge interaction, pH-responsive interaction was indicated another factor to increase the cellular uptake selectivity of free CDs. For example, Phuong et al. developed a selective and sensitive nanotheranostic nanoplatform based on the pH-responsive TiO₂-integrated cross-linked CDs (C-CD/TiO₂) for tumor diagnosis by the specific targeted capability of the tumor cell membrane and nuclei (Figure 5D) [139]. In their work, researchers designed the zwitterionic-formed CD (Z-CD) which could target the nucleus and the hydrophobic Dopa-decyl (D-CD) which could penetrate the hydrophobic sites of cell membrane. With the boronate ester linkages between the TiO₂-immobilized D-CD and Z-CD for nuclear targeting, the fluorescence “off” state at physiological pH and the fluorescence “on” state in acidic cancer cells were employed for tumor-selective biosensors through the cleavages of the boronate ester bonds by the disruption of the FRET. In the *in vivo* tumor model, the C-CD/TiO₂ could efficiently ablate tumors under NIR light irradiation with up-regulation of the pro-apoptotic markers in tumor, illustrating excellent targeted bioimaging and therapy capability.

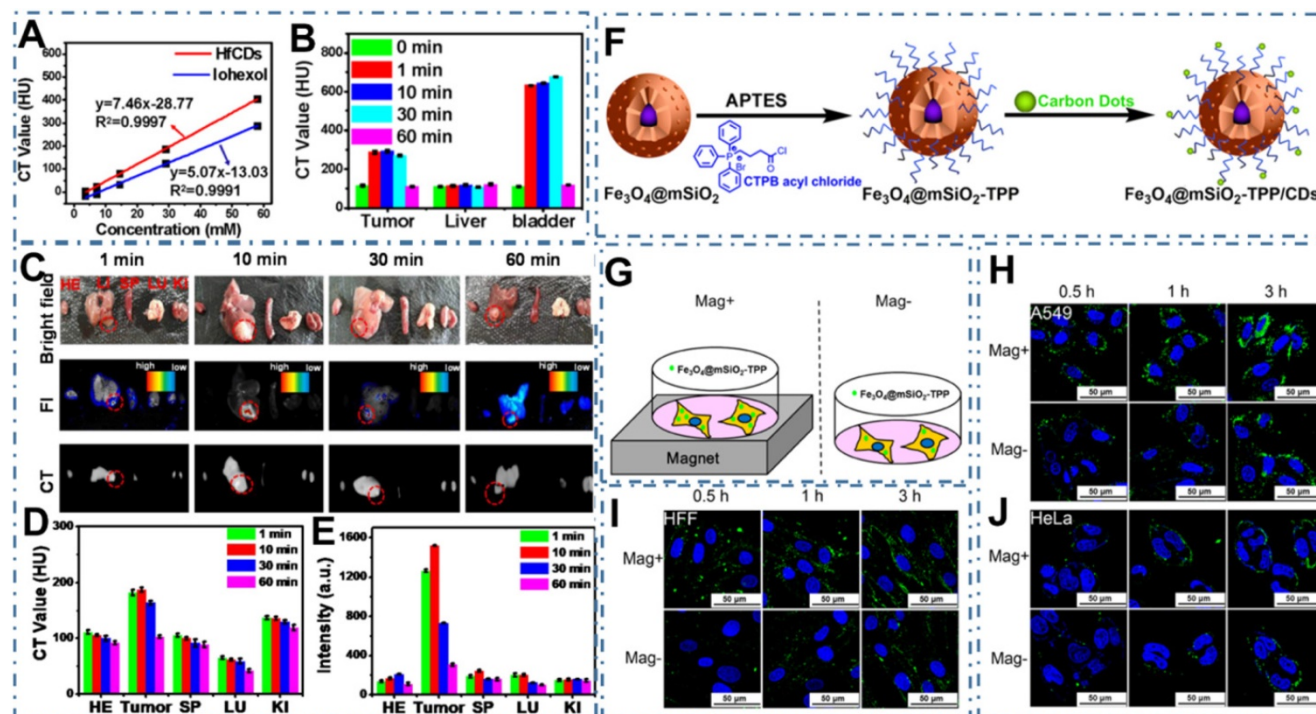


Figure 4. CDs-based targeted bioimaging through uptake accumulation. (A) CT value of Hf-CDs/iohexol aqueous solution at different concentrations. (B) CT values of major organs collected at different times after intravenous injection of Hf-CDs. (C) Ex vivo bright field, FI and CT images of major organs collected at different intervals post tail vein injection of Hf-CDs. (D) Quantitative analysis of the CT values. (E) Quantitative analysis of the FI intensity. Adapted with permission from [184], copyright 2020 Elsevier Ltd. (F) Schematic route of the synthesis of Fe₃O₄@mSiO₂-TPP/CDs nanoplatform. (G) Illustration of the cells exposed to the Fe₃O₄@mSiO₂-TPP NPs while positioned or not in a static magnetic field. (H-J) CLSM images of the A549 (H), HFF (I), and HeLa (K) cell lines treated with the Fe₃O₄@mSiO₂-TPP NPs for different time under Mag+ or Mag-. Adapted with permission from [185], copyright 2015 American Chemical Society.

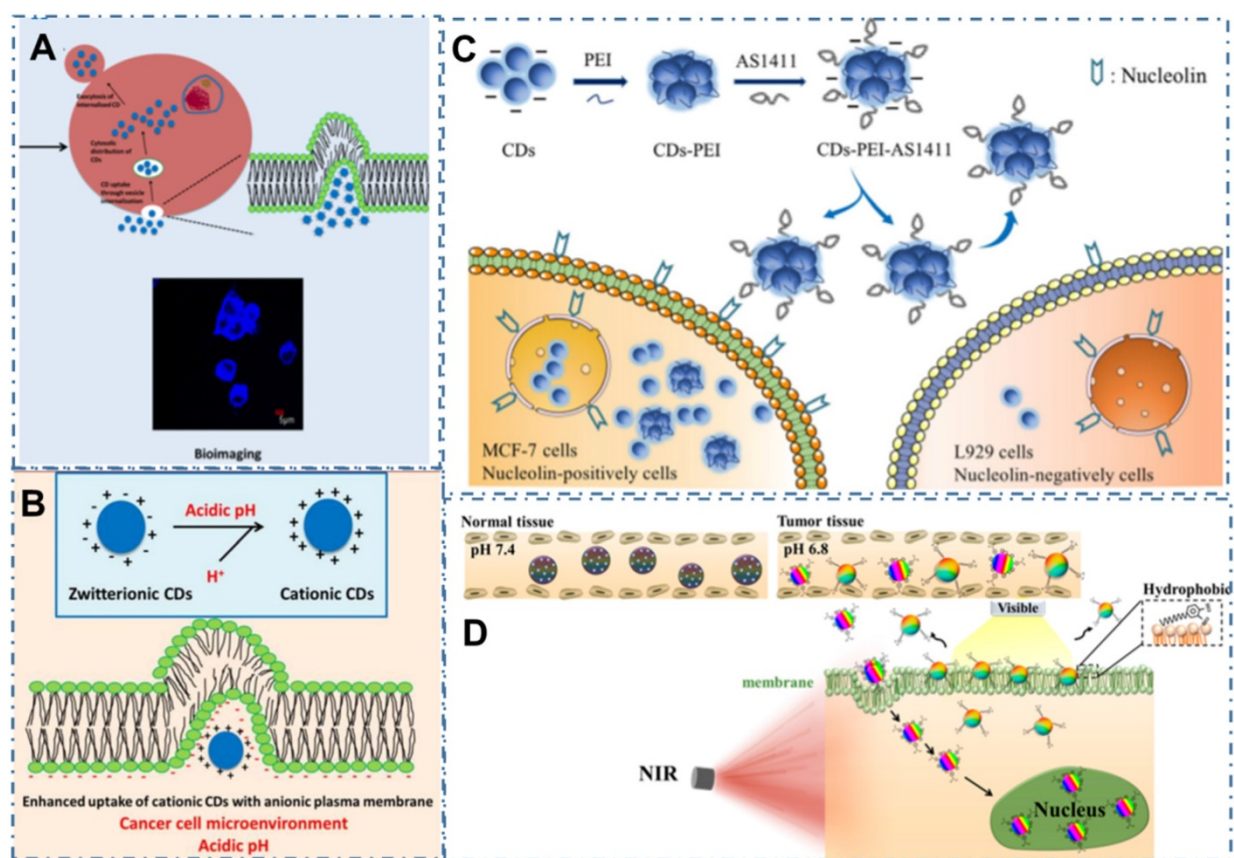


Figure 5. CDs-based targeted bioimaging through charge or pH interaction. (A) Scheme of the synthesis of CDs and its bio-imaging in oral cancer cell lines. (B) Mechanism underlying uptake of zwitterionic CDs. Adapted with permission from [189], copyright 2018 American Chemical Society. (C) Predicted mechanism of the different cellular uptake behaviour of CDs-PEI-AS1411 with the nucleolin-positive MCF-7 cancer cells and nucleolin-negative L929 fibroblast cells. Adapted with permission from [190], copyright 2019 John Wiley & Sons Ltd. (D) Scheme of the design and application of pH-responsive C-CD/TiO₂ for targeted bioimaging via cellular membrane-nucleus translocation in response to visible-light irradiation. Adapted with permission from [139], copyright 2020 American Chemical Society.

3.3. Targeting biomarker

Beyond the direct targeted imaging of cancer cells, the strategy to *in vivo* image the biomarkers in tumors is another approach to the diagnosis of cancer [191–193]. For example, Shen et al. reported one approach to bioimaging Cathepsin B (CTSB), which were one of the most promising biomarkers for numerous malignant tumors, enabling efficient diagnosis of cancers at an early stage [194]. In the work, researchers developed one kind of amine-rich CDs and further covalently assembled the nucleolin-targeting recognition nucleic acid aptamer AS1411 and a CTSB-cleavable peptide substrate that tethered with chlorin e6 (Ce6), enabling a cancer-targeting and CTSB stimulus-responsive ratiometric nanoprobe of AS1411-Ce6-CQDs (Figure 6A). With the quenching of blue fluorescence from CDs and NIR fluorescence enhancement from the Ce6 by the efficient fluorescence resonance energy transfer (FRET), the overexpressed CTSB in lysosome could cleave Ce6-Pep and trigger the Ce6 moiety dissociation from AS1411-Ce6-CQDs after selective accumulation in cancer cells, thus leading to the

termination of FRET and achieving the ratiometric fluorescence response to CTSB (Figure 6B). Thereby, a vigorous ratiometric fluorescent method could be achieved by integrating a cancer-targeting recognition moiety to report CTSB activity. Meanwhile, Qian et al. prepared one kind of CDs (AA-CDs) and proved that the AA-CDs could selectively recognize folic acid (FA), resulting in fluorescence quenching (Figure 6C) [195]. In their work, researchers developed a sensitive approach to FA analysis with a detection limit of 40 nM and further developed one kind of fluorescent nanoprobe (FA-AA-CDs) via the conjugated interaction between FA and AA-CDs, enabling them as a fluorescence turn-on nanoprobe for targeted imaging of cancer cells. In the models of cancer cells with different levels of folate receptors (FRs) expression (Hela, SMMC-7721, and A549 cells), FA-AA-CDs exhibited specially targeted imaging of cancer cells with the accordant relationship between the corresponding PL intensity of these cells and their FRs expression levels. Similarly, Das et al. reported the ACD-GNP nanohybrid which comprised the anionic CDs (ACD) protected gold nanoparticle (GNP) as nanoprobe for imaging glutathione (GSH)

[196]. These researchers indicated the selective GSH sensing of ACD-GNP nanohybrid based on the GSH-triggered variation between fluorescent indicator ACD and the GNP (Figure 6D). With higher selectivity and sensitivity to GSH than other biothiols, the ACD-GNP hybrid achieved selective imaging of cancer cells. In addition, Li et al. developed one kind of dual-emission CDs and approved their ability of ratiometric GSH sensing in cancer cells [197]. With the intrinsic ratiometric fluorescence displacement of as-prepared CDs for GSH sensing (Figure 6E-F), these CDs could be employed as an effective tool to achieve targeted imaging of cancer cells.

As similar as these common strategies to directly sense the biomarker, the approaches to selective recognizing the substance such as antibody or metabolites of cancer cells are also developed. For example, Gao et al. designed one kind of turn-on fluorescent nanoprobes of P-CDs/HA-Dox by electrostatic assembly of PEI-modified CDs (P-CDs) and Hyaluronic acid (HA)-conjugated doxorubicin

(Dox) to selectively sense and image hyaluronidase (HAase) (Figure 7A) [198]. In their work, the P-CDs/HADox illustrated low PL emission in a physiological environment and were capable to selectively penetrate into cancer cells due to the activation of HAase by utilizing their overexpressed HA to CD44 receptors, resulting in effectively distinguish of cancer cells and sensitive assay of HAase. In addition, Demir et al. coupled one kind of CDs with molecularly imprinted polymers (MIPs) to prepare biocompatible nanoprobes for cancer cells (Figure 7B) [199]. In their work, researchers designed a MIP shell round the CDs by the CDs' emission as an internal light source for photopolymerization to specific recognize the glucuronic acid (GlcA), which was a substructure (epitope) of hyaluronan and a biomarker for certain cancers (Figure 7C-D). Their work proved the targeting imaging of hyaluronan and selectively recognized human cervical cancer with the CD-based nanocomposites.

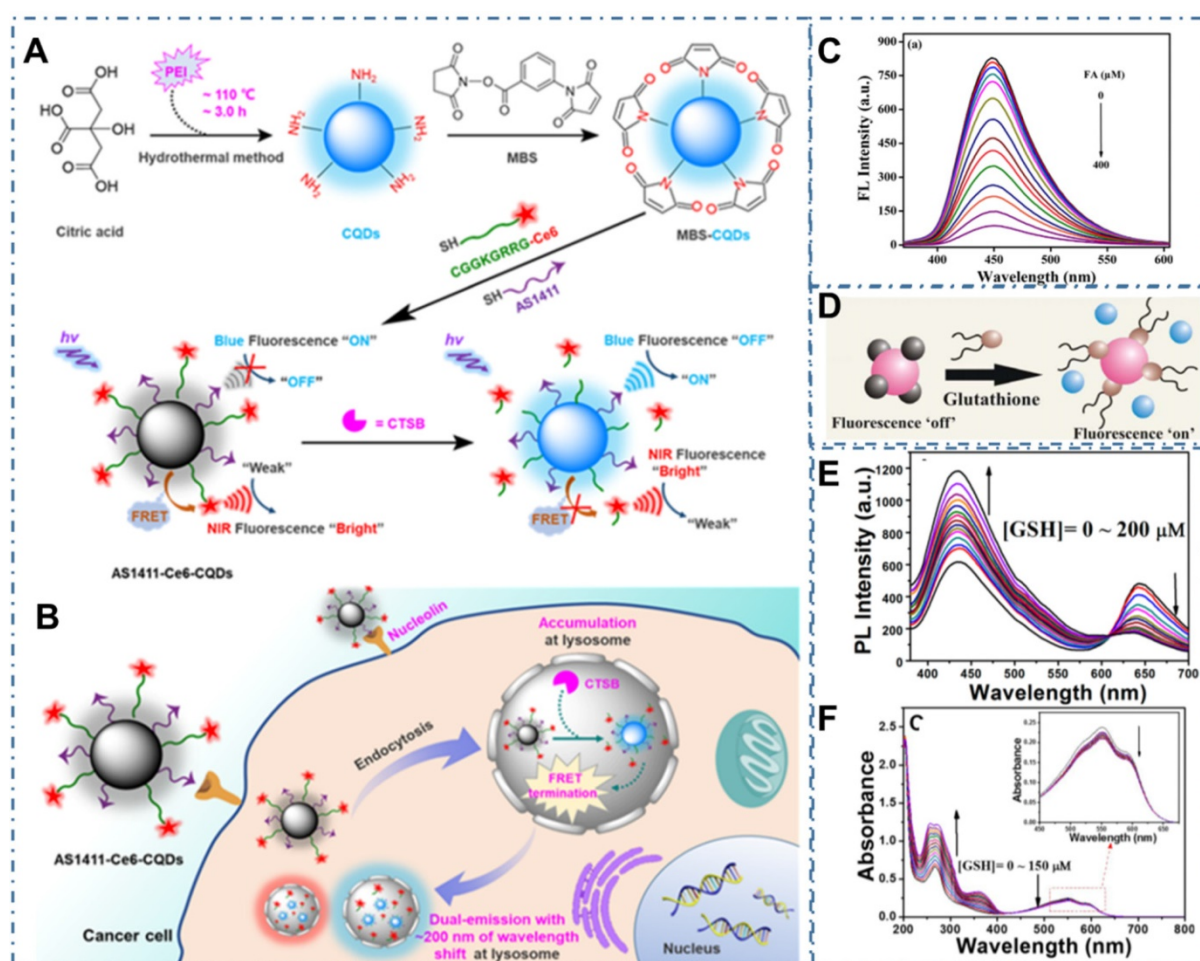


Figure 6. CDs-based targeted biomaging through targeting biomarker sensor. (A-B) Schematic diagram of the engineering of nucleolin-targeted ratiometric fluorescent nanoprobe AS1411-CQDs-Ce6 for endogenous CTSB imaging with a remarkably large emission wavelength shift in living cancer cells. Adapted with permission from [194], copyright 2020 American Chemical Society. (C) Fluorescence emission spectra of AA-CDs upon gradual addition of FA. Adapted with permission from [195], copyright 2018 Elsevier B.V. (D) Schematic of the glutathione triggered Fluorescence "Turn On" of ACD. Reproduced with permission [196], copyright 2016 American Chemical Society. (E) Fluorescence spectrum of CDs in the presence of various concentrations of GSH. (F) UV-vis spectrum of CDs in the presence of various concentrations of GSH. Adapted with permission from [197], copyright 2020 American Chemical Society.

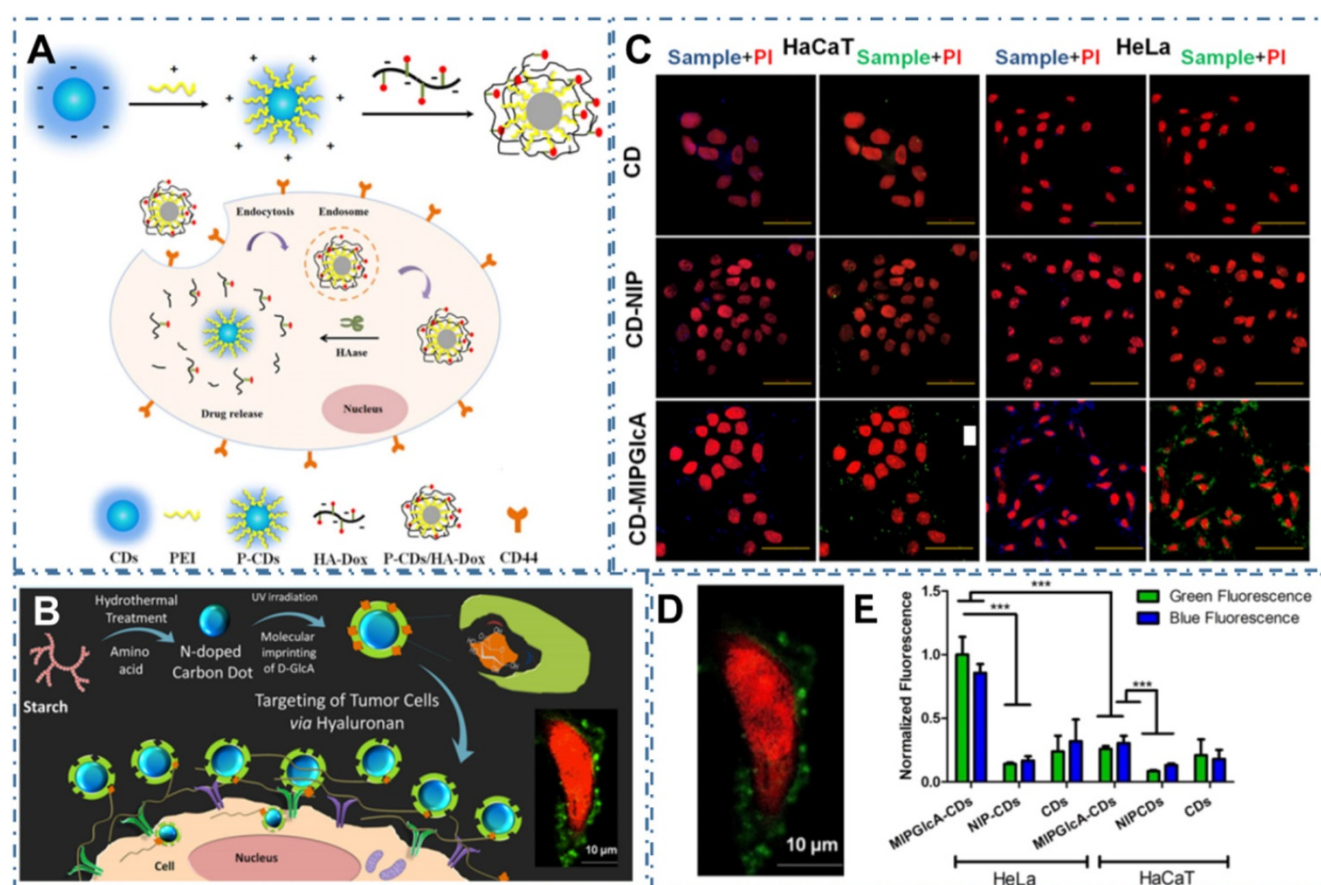


Figure 7. CDs-based targeted bioimaging through selective recognition. (A) Schematic illustration of the formation of PEI-CDs/HA-Dox, and the nanoprobe used for targeted cancer cell imaging and drug delivery. Adapted with permission from [198], copyright 2017 Elsevier B.V. (B) Schematic of molecularly imprinted polymer coated CDs for cancer cell targeting bioimaging. (C) Confocal microscope images of fixed HaCaT and HeLa cells treated with CDs, CD-NIP, and CD-MIPGlcA. (D) Confocal micrographs showing labeling of GlcA on a single HeLa cell by CD-MIPGlcA (green) and nuclear staining with PI (red). (E) Analysis of labeled cells with CD-MIPGlcA, CDNIP, and CD as obtained from Image J by measuring the normalized fluorescence of each single cell area from five different images. Adapted with permission from [199], copyright 2018 American Chemical Society.

3.4. Self-Targeting

Since the CDs were proved a powerful targeted imaging agent to achieve diagnosis of cancer, these strategies still remain a great challenge to achieve clinic application due to their complex chemical route and potential toxicity. Recently, several kinds of CDs are proved distinctive self-targeting for cancer cells, enabling their promising application in various fields. For example, Zheng *et al.* designed the self-targeted CDs (CD-Asp) with targeting capability to brain cancer glioma through a direct pyrolysis approach with D-glucose and L-aspartic acid [200]. The as-prepared CD-Asp with tunable PL emission exhibited selective targeted function toward C6 glioma cells without the requirement of another targeting molecular. In their work, the *in vivo* bioimaging with CD-Asp as fluorescent imaging agent exhibited high-contrast targeted distribution and the higher fluorescent intensity obtained in the glioma site than that in normal brain, enabling the capability of CD-Asp for free penetration in the blood-brain barrier and precise self-targeting of

glioma tissue (Figure 8A-D). Generally, there are two major mechanisms by which various agents can cross the BBB: transporter- and receptor-mediated transports. Glucose transporter (GLUT-1) is a brain-tumor-targeting property through facilitative glucose metabolism by the glucose transporters. ASCT2 is an important L-isomer-selective transporter across the BBB through L-glutamine (L-Glu) and L-asparagine (L-Asp) as high-affinity substrates. In the work, researchers observed that the CDs synthesized with glucose, L-Asp, and/or L-Glu and containing the reactant functional groups (glucose, L-Asp, L-Glu) could help them cross the BBB through the GLUT-1 and ASCT2 transporters. Therefore, RGD, a tripeptide composed of L-arginine, glycine, and L-aspartic acid, was a common glioma-targeting agent that binding to RV β 3 integrin on immature endothelial cells. Thereupon, researchers deduced that the targeting function of CD-Asp originated from the formation of RGD-like functional groups on the CDs' edge, which were prepared and derived from D-glucose and L-Asp. Similarly, Li *et al.* developed a series of self-targeted CDs (LAAM TC-CQDs) which

functionalized with multiple paired α -carboxyl and amino groups and indicated their selective accumulation in tumor [201]. In their work, the LAAM TC-CQDs showed bright PL emission with a NIR PL emission peak around 700 nm (Figure 9A-B). With the treatment of the excess of Leu, Phe or Gly before adding LAAM TC-CQDs for HeLa cells, researchers found that the cell uptake of LAAM TC-CQDs was significantly inhibited by Leu and Phe but not by Gly (Figure 9C). On the basis of different experiments, researchers indicated that the LAAM TC-CQDs could penetrate into cancer cells via the interaction with LAT1 and approved this hypothetical mechanism with six lines. First, the pretreatment with the LAT1 inhibitor BCH reduced the uptake of LAAM TC-CQDs (Figure 9D). Second, LAT1 knockout

reduced the uptake of LAAM TC-CQDs (Figure 9E-F). Third, overexpressing LAT1 of HeLa cells via lentiviral transduction increased the cellular uptake of LAAM TC-CQDs. Fourth, the expression level of LAT1 correlated with the amount of LAAM TC-CQDs in diverse cell lines and the level of LAT1 expression in cancer cells was higher than that in normal cells. Fifth, the overexpression of LAT1 in tumors increased the uptake LAAM TC-CQDs *in vivo*. Sixth, the pretreatment with Leu decreased the accumulation of LAAM TC-CQDs in tumors. With the functionalized CDs which could load aromatic drugs through π - π stacking interactions, researchers further achieved the NIR fluorescence and photoacoustic imaging for various tumors and the targeted drug delivery for the chemotherapeutics to the tumors.

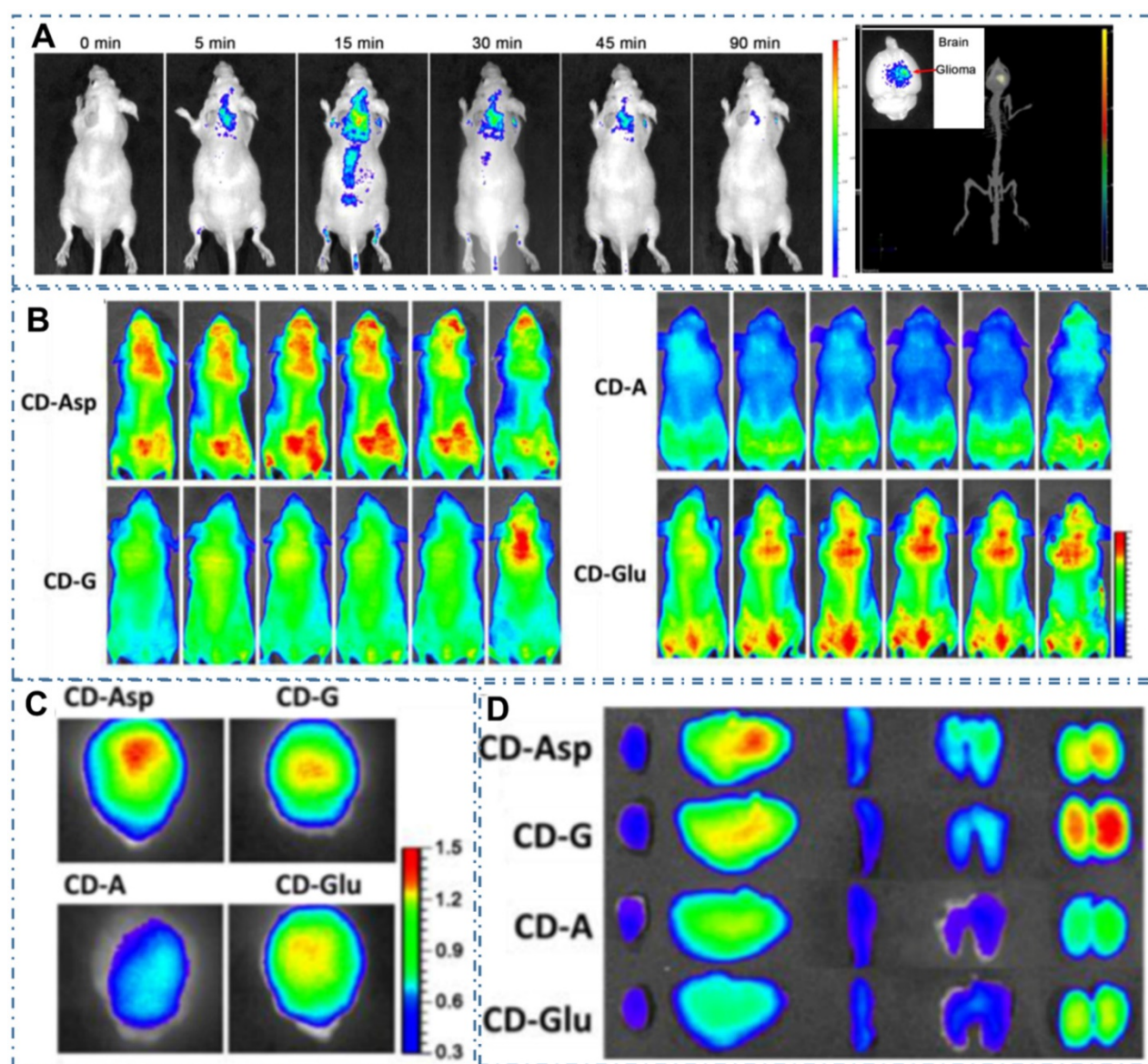


Figure 8. CDs-based targeted bioimaging by self-targeting. (A) *In vivo* and *ex vivo* imaging of glioma-bearing mice after tail intravenous injection of CD-Asp. (B) *In vivo* imaging of glioma-bearing mice at different time points after injection with CD-Asp, CD-G, CD-A, and CD-Glu. (C) *Ex vivo* imaging of glioma-bearing brain of brain and glioma. (D) *Ex vivo* imaging after the injection of CD-Asp, CD-G, CD-A, and CD-Glu of heart, liver, spleen, lung, and kidney. Adapted with permission from [200], copyright 2015 American Chemical Society.

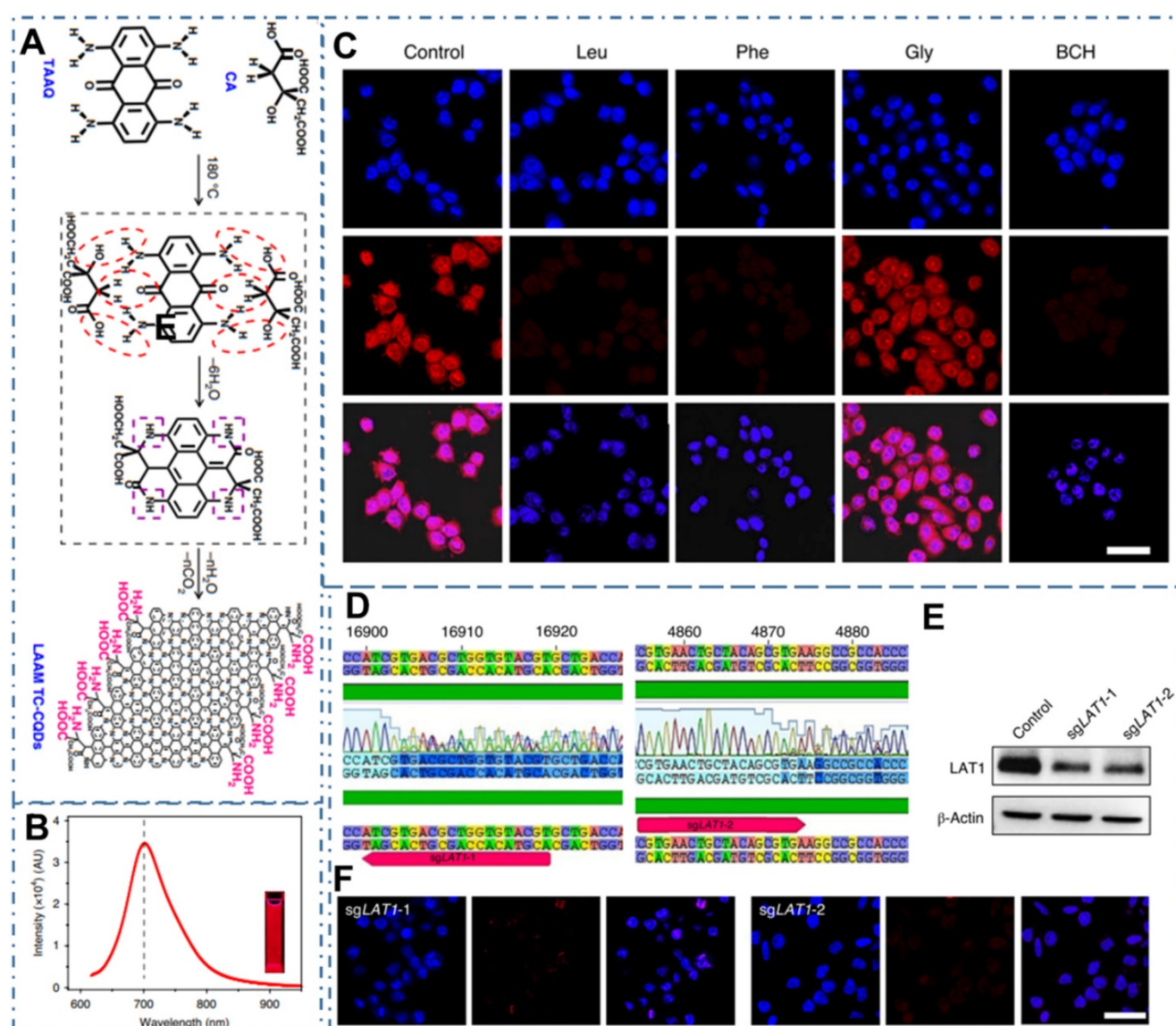


Figure 9. CDs-based targeted bioimaging by self-targeting. (A) Schematic and hypothetical steps of LAAM TC-CQD synthesis. (B) Fluorescence emission spectrum with an excitation wavelength of 600 nm. (C) LCM images of HeLa cells that were pretreated with Leu, Phe, Gly or BCH. (D)-(F) Downregulation of LAT1 expression by CRISPR-Cas9 in HeLa cells reduced the cellular uptake of LAAM TC-CQDs (F). The red arrows in b indicate the sgRNA-targeting sequences. Successful targeting of LAT1 was confirmed using Sanger sequencing (D) and western-blot analysis (E). Adapted with permission from [201], copyright 2020 Springer Nature.

With these excellent performances in bioimaging, CDs exhibit great potentials for the diagnosis of cancer in clinic [173, 174]. In practical, Wang *et al.* have employed CDs in the clinical application and demonstrated their excellent performance for guiding the precision surgery of papillary thyroid carcinoma [173]. In their reports, researchers evaluated the application of CDs as lymphatic tracer in total thyroidectomy and bilateral Central District's thyroidectomy for papillary thyroid carcinoma. The related results confirmed the CDs can distinguish the thyroid tissue from the surrounding lymphoid adipose tissue and clearly mark the Central District lymph nodes, resulting in the decrease for the risk of parathyroid gland injury during the thyroid cancer. Therefore, the relevant research has confirmed

the capability of CDs for targeted cancer bioimaging and approved their great potentials of CDs for clinic applications in future.

4. Targeted Cancer Therapy

As CDs accumulate specifically in tumors, they are ideal for further use in targeted cancer therapy [17, 202-235]. Meanwhile, with CDs' excellent performance in various bioimaging techniques, it is possible to develop nanotheranostic strategies that can reveal simultaneous diagnosis and treatment of various cancers. At an early stage, CDs are demonstrated to be excellent nanocarriers to reunite with different drugs to enhance targeted therapeutic effect. As nanomaterials develop, CDs have also been used as a new class of nanocarriers for creating

nanocomposites with a series of functional nanoparticles such as Au NPs, Fe₃O₄ NPs, and some inorganic quantum dots, endowing them with additional characteristics, such as oxidative stress amplifier, magnetic functions and radioactivity, for advanced therapeutic applications. In addition, the special photophysical properties, such as strong absorbance of NIR light and/or excellent photothermal/photodynamic character, endow various CDs for light-active nanotheranostic of cancer. Compared with the traditional chemotherapy, the light-active nanotheranostic have received more and more attention due to its noninvasive and stimuli-responsive features and the promising characters to over drug-fast. In addition, several kinds of CDs have been observed distinctive cytotoxicity with novel metabolic pathway in cell growth and death, enabling their direct application for cancer therapy as nanomedicines. Finally, with the development of nanotechnologies, CDs also play important role in various advanced technologies and exhibit excellent applications in several kinds of cancer to overcome the limitation of common medicine.

4.1. Drug delivery

Chemotherapy is the most common strategy for diverse cancers. Nevertheless, the limitation such as potential drug resistance and ineffectiveness against metastatic disease and lack of an effective targeting of the classical drug for cancer therapy seriously restrict their therapeutic effect in living body. Thereupon, different nanotechnologies are developed to achieve enhanced targeted therapy for tumors. In the field, CDs also are employed as nanocarriers to achieve precise drug delivery through their novel surface structures to load drugs or distinctive targeted release capability triggered by tumor microenvironment. Meanwhile, besides both excellent optical imaging quality and drug delivery efficiency, these CDs used for nanocarriers are demonstrated few or nontoxic effects with *in vitro* and *in vivo* studies. And these CDs-based nanomedicines illustrate excellent therapeutic effect (Table 2). The maximal drug loading capability of the CDs approach 96% with no noticeable cell growth inhibition, morphological damage or inflammatory injury. For example, Feng *et al.* designed a drug nanocarriers with the responsivity of tumor extracellular microenvironment based on the cisplatin(IV) prodrug-loaded CDs (CDs-Pt(IV)@PEG-(PAH/DMMA)) for bioimaging-guided drug delivery (Figure 10A-B) [207]. In their work, the anionic polymer of dimethylmaleic acid (PEG-(PAH/DMMA)) on the CDs-Pt(IV)@PEG-(PAH/DMMA) could pass through charge conversion to the cationic

polymer in the tumor extracellular microenvironment (pH~6.8), enabling the strong electrostatic repulsion and release of positive CDs-Pt(IV). In addition, the nanocarrier with positive charge displayed high affinity to cancer cell membrane with negative charge, which resulted in the increase of internalization and effective activation of cisplatin (IV) prodrug. The *in vitro* experiments indicated that this promising exhibited the better therapeutic efficiency of the charge-convertible nanocarriers under tumor extracellular microenvironment than the normal physiological condition and the noncharge-convertible nanocarriers. The *in vivo* experiments further approved the high tumor-inhibition efficacy and low side effects of these charge-convertible CDs, implying their capability as promising drug nanocarriers in practical clinical application. On the condition, Feng *et al.* further developed the pH/redox dual-responsive CDs (CDsRGD-Pt(IV)-PEG) for tumor extracellular microenvironment responsive targeted bioimaging and enhanced anticancer drug delivery (Figure 10C-D) [208]. In their work, the CDsRGD-Pt(IV)-PEG were constructed with fluorescent CDs as drug nanocarriers, cisplatin(IV) as prodrug, and RGD peptide as active targeting ligand by the cover of monomethoxypolyethylene glycol (mPEG) via the pH responsive benzoic-imine bond in tumor extracellular microenvironment (6.5~6.8). The drug nanocarriers could be tracked by the fluorescence of CDs and illustrated effective uptake in cancer cells via RGD-integrin $\alpha\beta_3$ (ligand-receptor) interaction after the hydrolysis of benzoic-imine bond in the tumor extracellular microenvironment to release the inner RGD peptide. Although these nanocarriers were promising to overcome the biological barriers in the process of drug delivery, the fibrosis in tumor sites could cause hypoxia, immunosuppression and limited immunocytes infiltration, thus reducing the antitumor curative effect of various nanosystems. Thereupon, Hou *et al.* designed one kind of honeycomb-like nanoassemblies of CDs with cancer associated fibroblasts (CAFs) responsivity to spatially program the delivery of therapeutics for enhanced antitumor efficiency (Figure 11A-B) [219]. In their work, the doxorubicin (DOX) and immunotherapeutic enhancer (Feions) were attached on the CDs, and the tumor microenvironment modifier (losartan, LOS) was encapsulated within the mesopores. Their experiments indicated the drug-loaded nanoassemblies could be disunited to release LOS to mitigate stroma and hypoxia with the responsivity to CAFs, and the individual CDs with DOX and Fe ion could efficiently penetrate into tumor sites to enhance immune responses. The *in vitro* and *in vivo*

experiments indicated that the nanoassemblies exhibited effective T-cells infiltration, tumor growth inhibition and lung metastasis prevention. These

works provided the new therapeutic nanoplatforms for diverse tumors.

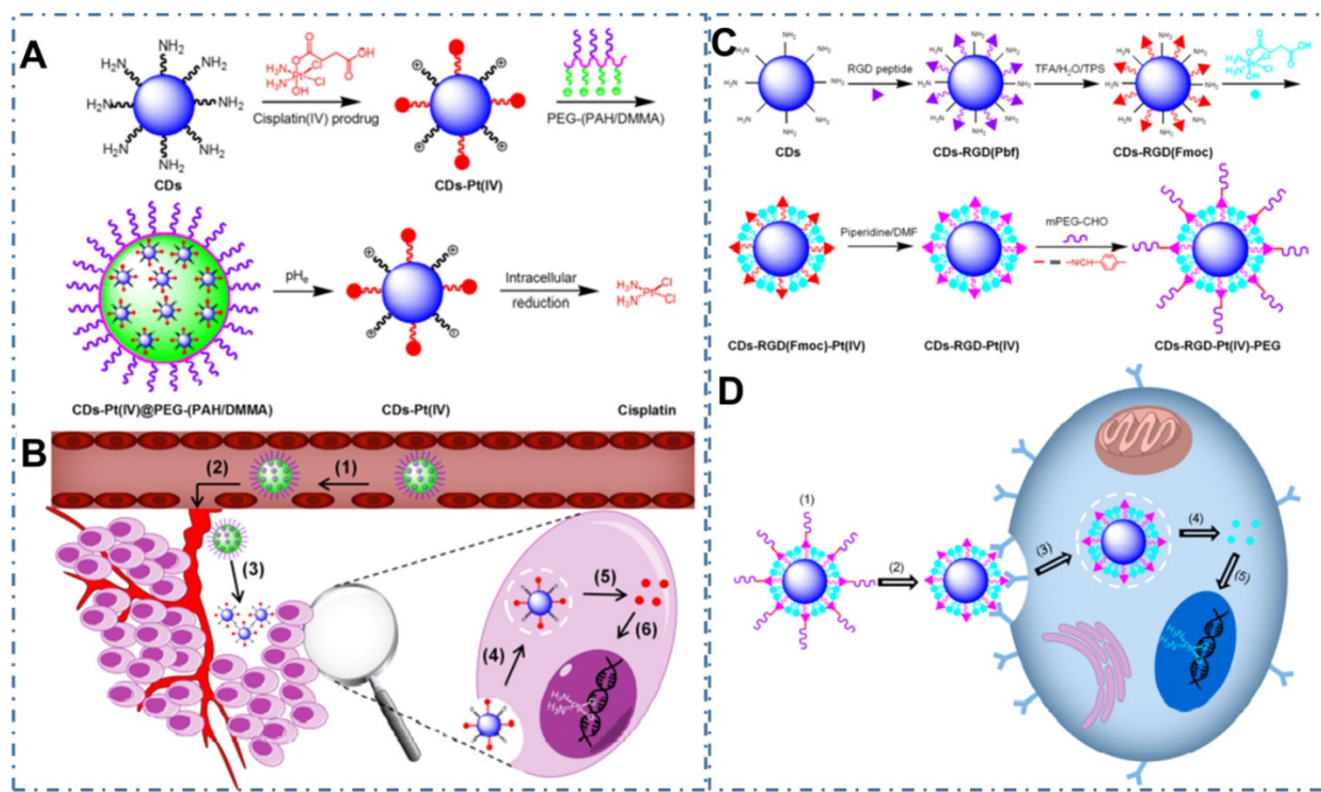


Figure 10. CDs-based cancer therapy via drug delivery. (A) Schematic illustration for the preparation of charge-convertible CDs-based drug nanocarrier CD_s-Pt(IV)@PEG-(PAH/DMMA). (B) Schematic illustration for the drug delivery process of CD_s-Pt(IV)@PEG-(PAH/DMMA). Adapted with permission from [207], copyright 2016, American Chemical Society. (C) Schematic illustration for the preparation of CD-based drug nanocarrier CD_s-RGD-Pt(IV)-PEG with tumor-triggered targeting property. (D) Schematic illustration of the drug delivery process using CD_s-RGD-Pt(IV)-PEG. Adapted with permission from [208], copyright 2016 American Chemical Society.

Similarly, CDs may be used as nanocomposites, composited with other nanomaterials, so as to provide additional characteristics. For example, Gong *et al.* reported a mitochondrial oxidative stress amplifier of MitoCAT-g with CDs and indicated that the MitoCAT-g particles could selectively target mitochondria and deplete mitochondrial GSH with atomic economy, thus amplifying the ROS damage and resulting in apoptosis of cancer cells (Figure 12A) [221]. In their work, the MitoCAT-g was designed by CDs-supported atomically dispersed gold (CAT-g) with further surface modifications of triphenylphosphine (TPP) and cinnamaldehyde (CA) (Figure 12B). With the *in vivo* experiments, the capability and mechanism of MitoCAT-g to suppress tumor growth in a subcutaneous tumor model were proposed (Figure 12C-D). With the *in vivo* tumor-bearing mice models, all the group showed a significant change in body weight (Figure 12E) and the MitoCAT-g group exhibited a significant inhibited tumor growth compared with the saline, CDs, TPP and CDs-TPP treated groups. Meanwhile, the MitoCAT-d-treated group showed 87.5% survival and

the antitumor effect was reversed in HepG-2 (SOD2-mito-CAT) tumors. These results confirmed the effectiveness of CDs-based nanocomposites for antitumor application and represent a promising medicine for clinical anticancer applications.

With these excellent optical properties and low toxicity (Table 2), CDs exhibit promising potential application in the nanotheranostics. Though most of CDs exhibit low toxicity, there are still widespread concerns about the risk of CDs for therapy applications. On the one hand, there have been various animal studies revealing that other carbon family nanomaterials like CNTs, can be internalized by macrophages and induce inflammation and injury in the respiratory system. So far, reports of CDs for therapy applications have employed in different tissues. There still are no reports about the inflammatory response or neoplastic lesions known about whether CDs exposure may eventually affect cancer progression via possible systemic effects on non-adjacent organs. On the other hand, there have been several reports about the novel cytotoxicity in some kinds of CDs, such as their ROS-generation

toxicity, dose-dependent toxicity, etc. Thereby, the risk of CDs for clinic therapy applications still needs more concerns and studies.

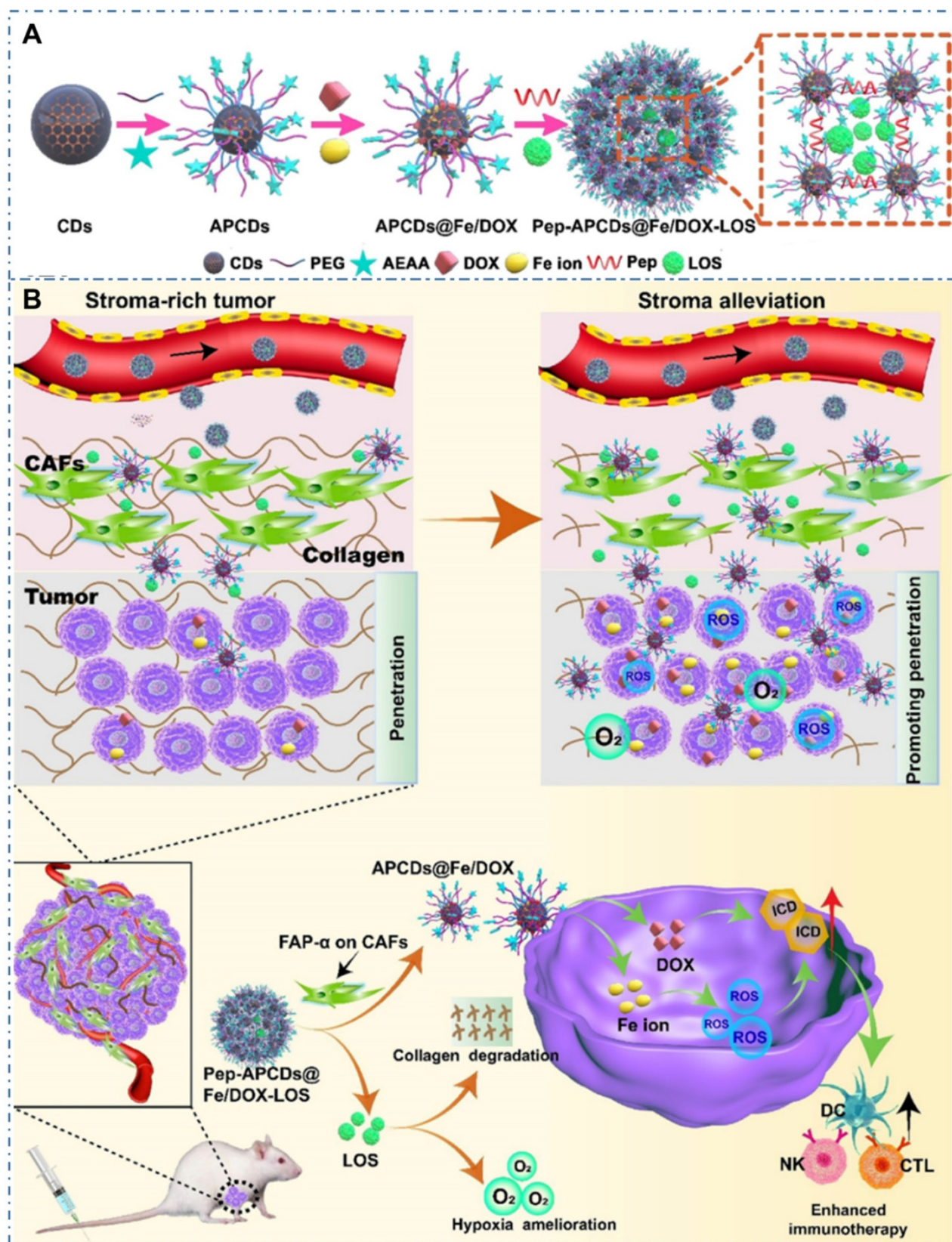


Figure 11. CDs-based cancer therapy via drug delivery. (A) Schematic illustration for the preparation of drugs-loaded nanoassemblies of Pep-APCDs@Fe/DOX-LOS. (B) The transformation and enhanced antitumor immunity mechanism of Pep-APCDs@Fe/DOX-LOS. Adapted with permission from [219], copyright 2020 Wiley-VCH GmbH.

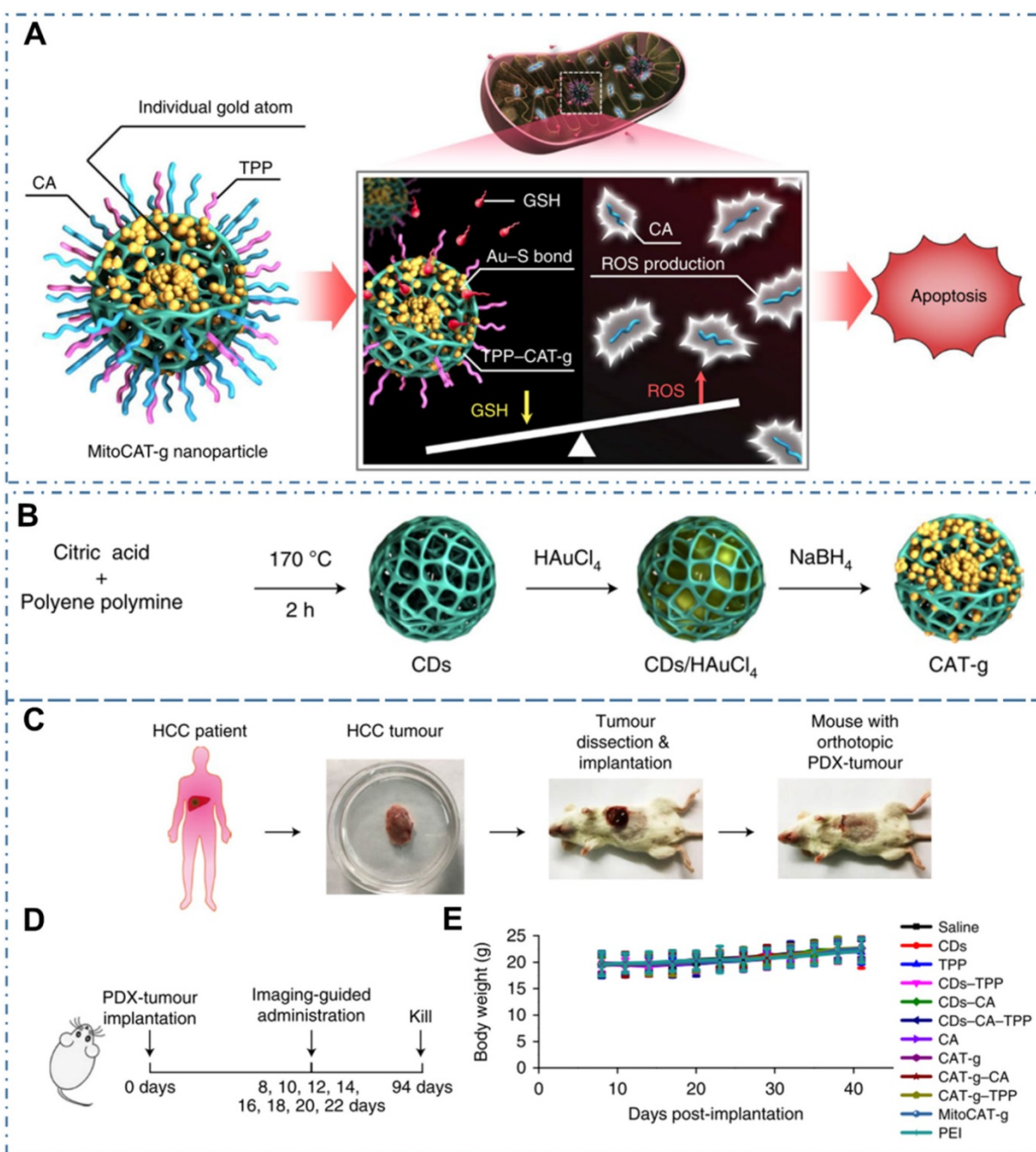


Figure 12. CDs-based cancer therapy via drug delivery. (A) Design and mechanism of MitoCAT-g to amplify oxidative stress in mitochondria and cause apoptotic cell death. (B) Schematic illustration of the synthesis process of CAT-g. (C) Schematic illustration of the establishment of the orthotopic PDX tumour model in NOD-SCID mice. (D) Scheme of the treatment schedule. (E) Effect of the different formulations on animal body weight. Adapted with permission from [221], copyright 2019 Springer Nature.

Table 2. Summary of the types of CDs and their toxicity and drug loading capacity.

Type	Size of CDs	Size of nanocarriers	Surface Engineering	Drug	DLC, (wt%)	Cell lines, Animal models	Observation	Ref
Qucbl-CDs	5-7 nm	60-80 nm	Covalently anchored	Qucbl	N/A	Hela	Qucbl-CDs: 0-50 µM, cellviability >90%	[203]
DOX-CDs	6.8±1.3 nm (D) 8 (H)	N/A	Physisorbed through interactions such as π-π stacking, hydrophobic and van der Waals interactions	DOX	6.0	A549	DOX-CDs: 400 µg mL ⁻¹ , no growth inhibition	[204]
CA-CD	N/A	220 ± 25.99 µm	Hydrogen bonding	b-TC	77	N/A	N/A	[205]
CDs-Oxa	2.28±0.42 nm (D) 0.34-1.4 nm (H)	2.71 ± 0.43 nm (D) 2.5-4.2 nm (H)	Condensation reaction between the amino group and the carboxyl group	Oxa(IV)-COOH	4.2	L929; HepG2	CDs: 0.5 mg mL ⁻¹ , survival rates > 75%; CD-Oxa: cytotoxic as oxaliplatin(II) (IC ₅₀ = 3.4 µg mL ⁻¹)	[206]

Type	Size of CDs	Size of nanocarriers	Surface Engineering	Drug	DLC, (wt%)	Cell lines, Animal models	Observation	Ref
CDs-Pt(IV)@PEG-(PAH/DMMA)	7 nm	125 nm	Intriguing charge conversion to a cationic polymer	Pt(IV)	6.7	A2780	CDs: 3.125-400 $\mu\text{g mL}^{-1}$, no toxicity (A2780); CDs-Pt(IV)@PEG-(PAH/SA): 0.18-11.44 μM , no toxicity to cancer cells at pH 6.8 or 7.4	[207]
CDsRGD-Pt(IV)-PEG	5-8 nm	31 nm	Intriguing charge conversion to a cationic polymer	Pt(IV)	4.1	MDA-MB-231, MCF-7 cells	CDs: 200 $\mu\text{g mL}^{-1}$, negligible toxicity, CDs-RGD-Pt(IV)-PEG: at pH 6.8, much higher cytotoxicity	[208]
PNHCDS-DOX	5.8 \pm 0.1 nm (D) 3.8 nm (H)	N/A	Interactions such as electrostatic attraction, π - π stacking, van der Waals force, and hydrophobic interaction	DOX	35.43	HepG2, SiHa, MCF-7	PNHCDS: no affect to cell survival; PNHCDS-DOX: 400 $\mu\text{g mL}^{-1}$, 65-70%	[209]
CD-DOX conjugates	2-6 nm	N/A	Amines bind with the carboxylic acid via electrostatic interactions or hydrogen bonding.	DOX	N/A	HepG2 cells HL-7702 cells	CD: 1.5625-100 mg mL^{-1} , no influence; CD-DOX: dose-dependent death	[210]
P-CDs/HA-Dox	1.4-3.2 nm	15-30 nm	Electrostatic self-assembly	DOX	6.3	HeLa, NIH-3T3	PCDs/HA-Dox: 50 $\mu\text{g/mL}$, 90% of NIH-3T3 cells survive	[198]
IL-OCDS/Cur	7.2 nm	N/A	Hydrophobic interaction	Cur	69.2	HeLa cells.	IL-HCDs: 50 $\mu\text{g mL}^{-1}$, cell viability of >80%,	[211]
DOX@ACD	119 \pm 207 nm	131 \pm 3.7 nm	Amphiphilic interaction	DOX	14.2 \pm 0.003 wt%	A549	ACD@DOX: higher cell viability at low concentrations and lower viability at higher than DOX.	[212]
FA-Gd@CQDs/DOX	4.0 \pm 0.7 nm	N/A	π - π stacking and hydrophobic interactions.	DOX	74.5 \pm 3.96	HeLa, HepG2, and HeLung cell	FA-Gd@CQDs: low cytotoxicity, FA-Gd@CQDs/DOX: greater cell growth inhibition toward HeLa cells than DOX	[213]
pCBMA(CD-D/DOX)	3 nm	183 \pm 27 nm (D) 200 nm (H)	Electrostatic interactions and π - π stacking	DOX HCl	96.9	4T1 and HepG2 cells	CDs: 0.01-5 $\mu\text{g/mL}$, survival rates ~100%; pCBMA(CD-D/DOX): at low DOX dose (0.01, 0.1 $\mu\text{g/mL}$), 4T1 cells incubation rates ~100%	[214]
CDs-epi	1.5 (D) 1.7(H)	2.6 (D) 3.5 (H)	Conjugated	Epirubicin	N/A	SJGBM2, CHLA200, CHLA266, U87	CDs-epi: 10 μM , 17-30% survival rates	[215]
p(CAT2-CD-BA1)	2.72 nm	3.79 nm	Noninvasive adsorption	DOX	84.28	HeLa	p(CAT2-CD-BA1): 100 $\mu\text{g mL}^{-1}$, cell viability unchanged	[216]
CD-PEI-DOX	2-8 nm (D), 2-10 nm (H)	222.5 \pm 20.1 nm	Electrostatic interactions	DOX	35.88	L02, MHCC-97L, Hep3B	CD-PEI-DOX: (<10 $\mu\text{g mL}^{-1}$, effective inhibition, far less cytotoxic to L02 than to cancer cells	[217]
DS-NA	5 nm	7235 \pm 2.9 nm	Hydrophobicity interaction	DOX	23.5	MDA-MB-435S, 4T1	DS-NA: higher cytotoxicity to MDA-MB-435S cells (IC_{50} = 4.841 $\mu\text{g mL}^{-1}$) than 4T1 cells (IC_{50} =16.08 $\mu\text{g mL}^{-1}$)	[218]
APCDs@Fe/DOX-LOS	9.4 \pm 0.62 nm	106 \pm 1.5 nm	π - π stacking interaction with large p-conjugated structure of APCDs	DOX	30.3 \pm 1.3	4T1 tumorbearing mice	Blood biochemical parameters: levels remained normal ranges, H&E staining: no noticeable morphological damage or inflammatory injury	[219]

Abbreviations: D – diameter; H – height; DLC – Drug loading capability

4.2. Light-activated theranostic

Beyond traditional drug delivery, light-activated nanotheranostics are considered as the most promising cancer therapy strategy in clinic [53, 118, 222, 223]. As the important modalities of light-triggered treatment such as photothermal therapy (PTT) and photodynamic therapy (PDT), utilizing photoabsorbing molecules or nanoparticles to convert absorbed light energy to heat or generate reactive oxygen species (ROS), consequently achieving local hyperthermia for efficient cancer therapy. In the last ten years, the CDs and their composites are skillfully designed to satisfy the requirement of practical treatment, such high NIR absorbance, excellent biocompatibility and low nephrotoxicity. In the process, the intrinsic characters of CDs or the obtained properties of CDs-based nanocomposites combined with other assembled materials are gradually improved and perfected with various technologies. In these strategies, PTT is one kind of promising therapeutic strategy for diverse cancer while it is still a critical challenge in the rational design of photothermal agent with effective

photothermal conversion for the therapeutic outcome. In general, the main differences of PTT properties from photothermal agents are based on the following three parameters: the photothermal conversion efficiency (PCT), absorption cross section and selectivity of light absorption. In these concepts, the PCT is the ratio of converted thermal power to excited light power, which directly decides the treatment performance of PTT materials under same condition. The absorption cross section is based on the particles' geometric cross section and light absorption efficiency, which determines the absorption capability of materials under the same powerful light. The selectivity of light absorption refers to the light absorption efficiency for different lights. Due to the scatter of tissues, the therapeutic window in the near infrared region from 650 to 1000 nm has a high tissue penetration depth in comparison to the visible light, which is benefited in the application of light-active treatment. The photothermal properties of CDs with different sizes have been summarized in Table 1. The maximum PCT of CDs can reach 78% under the excitation of 808 nm near-infrared light. And the

effective light absorption range has been extended to NIR-II region with the light absorption greater than 1000 nm. For the CDs with photothermal capability, researchers have designed and tuned the intrinsic photothermal conversion property by rational raw materials and chemical route for the preparation. For example, Ge *et al.* designed the CDs with intrinsic photothermal conversion by choosing precursor molecules of polythiophene derivatives (PT2) and then further carbonized the polymer of polythiophene phenylpropionic acid (PPA) (Figure 13A-B) [116]. The as-prepared CDs exhibited a broad absorption band from the visible to NIR region with a red emission (Figure 13C) and efficient photothermal conversion efficiency (Figure 13D-E). With the novel ability, researchers employed the CDs as simultaneous fluorescence, PA and thermal theranostics for cancer diagnosis and therapy in living mice and achieved excellent performance. In addition to the intrinsic PTT, CDs also are employed as nanoplatfoms to assemble with other materials to enhance photothermal conversion. For example, Yu *et al.* rationally designed one kind of hollow-structured CuS nanoparticles composited with CDs to form CuSCDs and proved their high photothermal conversion efficiency with excellent biocompatibility and low toxicity (Figure 13F) [129]. With the coating of a macrophage membrane hybridized with T7 peptide on the surface of the proteasome inhibitor loaded CuSCD, the obtained CuSCDB@MMT7 illustrated selective specificity to cancer cells with the characteristics of immunity escaping and increased transferrin receptor-mediated endocytosis (Figure 13G). Meanwhile, the CuSCDB@MMT7-triggered PTT showed the accumulation of the polyubiquitinated tumor suppressor protein that was heat stabilized under NIR induced hyperthermia, facilitating augmented tumor cell apoptosis and the attenuated metastasis.

Compared with PTT, the PDT, which employ CDs as photosensitizers (PSs) to generate reactive oxygen species (ROS) and consequently ablate cancer cells or diseased tissue, is another light-activate nanotheranostic strategy with unique advantages. Under light excitation, part of the excited-state electrons in CDs can transfer to the ambient H₂O or dissolved oxygen and in turn lead to the type I, type II and type III photochemical ROS production of hydroxyl radicals or singlet oxygen. On the one hand, these ROS can fervently react with the protein, lipid, polysaccharide as well as other constituting members of bacteria membrane, leading to bacterial perforation and death. On the other hand, the *in vivo* generated ROS in cells can endow the apoptosis of tumor cells,

thus enabling their application for cancer therapy. Therefore, the scope of PDT treatment with CDs can be extended from tumor treatment to other application fields, such as antibacterial treatment, wound healing, inflammatory treatment, plant preservation and so on. For example, Pang *et al.* designed one kind of CDs with both intrinsic nucleolus-targeting and ROS generation capability (Figure 14A) [224]. With more efficient tumor treatment induced by the ROS located within nucleolus and nucleolus from the CDs, the enhanced *in vitro* and *in vivo* PDT at a low dose of CDs and light irradiation were achieved. On the condition, various strategies such as functionalized CDs to targeted specific sub-cellular organelles were developed to further enhance the PDT effect of CDs. For example, owing to the limit therapeutic effects of oxygen-dependent PDT induced by the hypoxic tumor microenvironment and rapid consumption of oxygen in the PDT process, Jia *et al.* developed a novel CD as an in-situ tumor oxygenerator to overcome hypoxia and substantially enhance the PDT efficacy (Figure 14B) [225]. In their work, researchers firstly prepared magnetofluorescent Mn-CDs with manganese(II) phthalocyanine as a precursor. With the self-assembly of DSPE-PEG, the obtained Mn-CD nanoassemblies with both NIR fluorescence and T1-weighted magnetic resonance (MR) could effectively produce ¹O₂ and highly catalyze H₂O₂ to generate oxygen, enabling them as an acidic H₂O₂-driven oxygenerator to improve the oxygen concentration in hypoxic solid tumors for enhanced PDT.

Similarly, Zheng *et al.* designed a carbon nitride (C₃N₄)-based multifunctional nanocomposites (PCCN) for light-driven water splitting to decrease the remarkably restriction of hypoxia in solid tumors for PDT (Figure 15) [226]. In their work, researchers developed CDs-doped C₃N₄ to enhance absorption ranged in red region for the process of *in vivo* water splitting, and then induced a polymer with the protoporphyrin photosensitizer, polyethylene glycol segment, and targeting Arg-Gly-Asp motif into the obtained CDs-doped C₃N₄, successfully achieving the PCCN. With the *in vitro* study, the nanocomposites of PCCN were indicated the capability to improve the intracellular O₂ concentration and increase the generated ROS in the hypoxic and normoxic microenvironments upon light irradiation. The experiment of cell viability approved that the PCCN could reverse the hypoxia-triggered PDT resistance, enabling a excellent growth inhibition of cancer sites in an O₂ concentration of 1% and exhibiting superior capability to overcome the hypoxia of cancer.

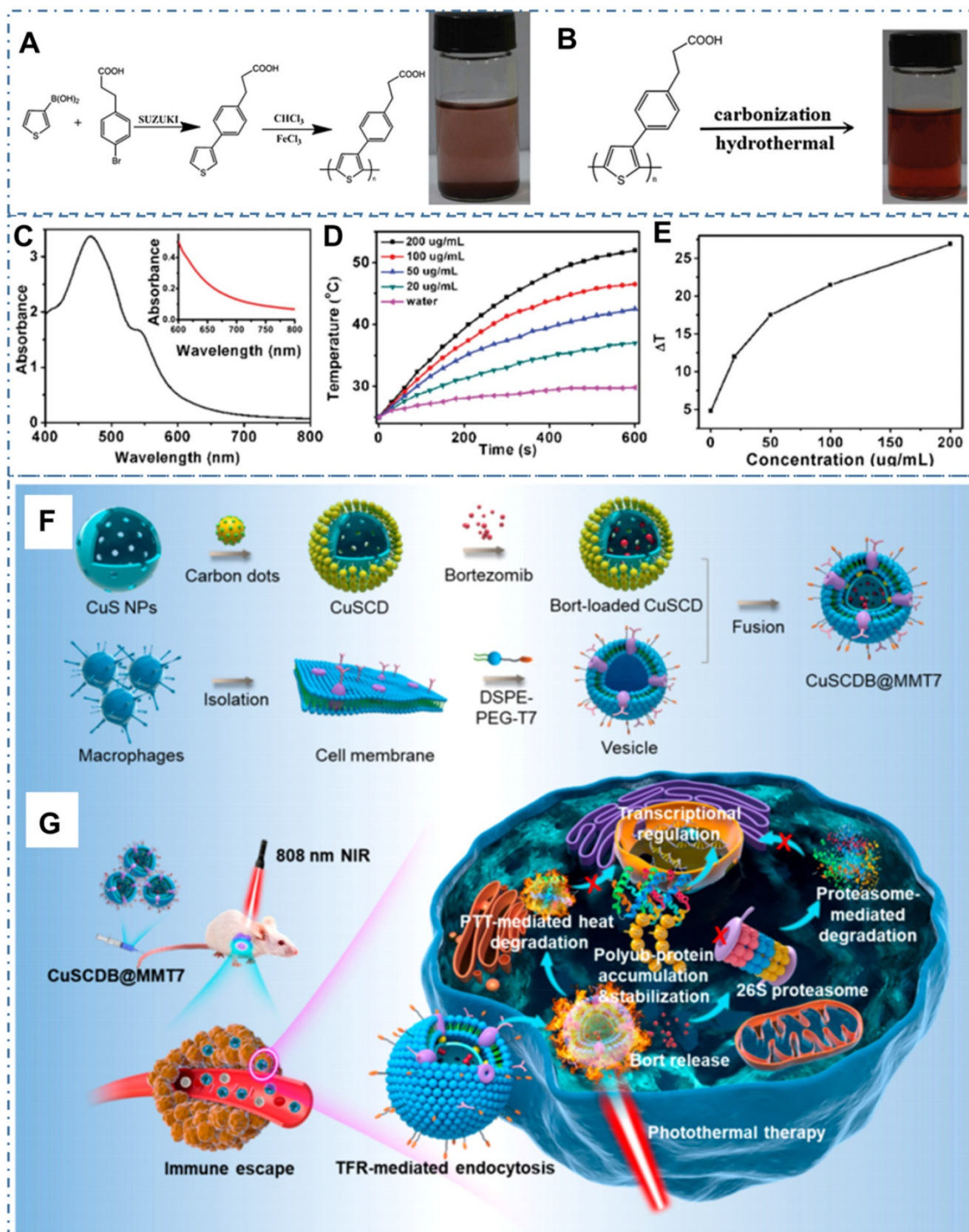


Figure 13. CDs-based cancer therapy by PTT. (A) Synthetic route of PPA. (B) Synthetic route of CDs. (C) The absorption of water-dispersible CDs. (D) Temperature elevation of pure water and the aqueous dispersion of CDs with different concentrations under laser irradiation. (E) Plot of temperature change over a period of 600 s versus the aqueous dispersion of CDs with different concentrations. Adapted with permission from [116], copyright 2015 WILEY-VCH Verlag GmbH & Co. KGaA, Weinheim. (F) Schematic illustration of the generation of proteasome inhibitor-encapsulated CuS/carbon dots nanocomposites (CuSCDB@MMT7). (G) Schematic illustration of the application of CuSCDB@MMT7 for enhanced PTT via heat-stabilization of various substrates in the ubiquitin-dependent proteasomal degradation pathway. Adapted with permission from [129], copyright 2020, American Chemical Society.

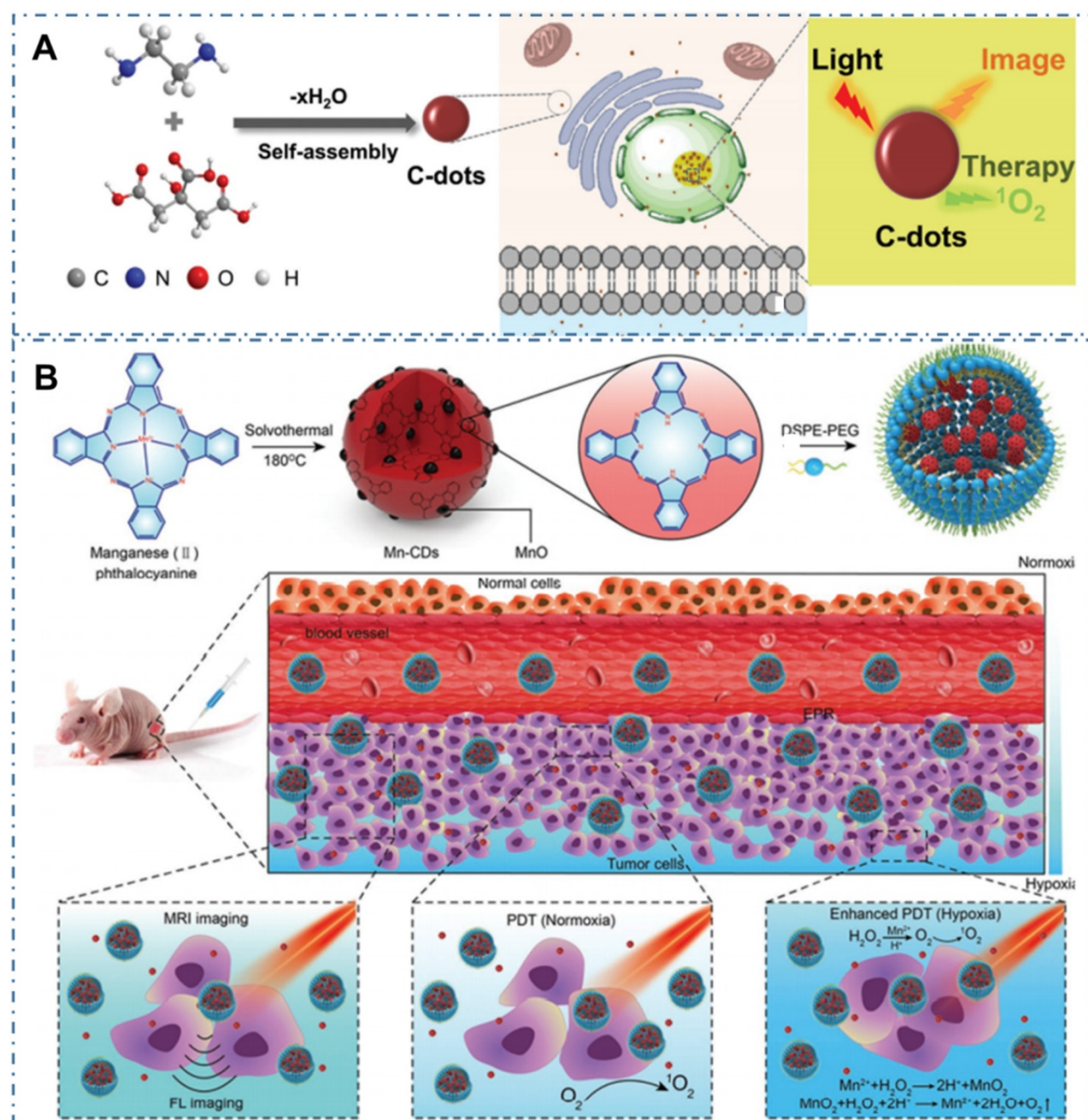


Figure 14. CDs-based cancer therapy by PDT. (A) Schematics of synthetic procedure of CDs and corresponding nucleolus-targeted photodynamic anticancer therapy. Adapted with permission from [224], copyright 2020 WILEY-VCH Verlag GmbH & Co. KGaA, Weinheim. (B) Schematic illustration of the Mn-CD assembly as an acidic H_2O_2 -driven oxygen generator to enhance the anticancer efficiency of PDT in a solid tumor. Adapted with permission from [225], copyright 2018 American Chemical Society.

In addition, due to limitation of PSs' side effects and singlet oxygen's short half-life, Wu *et al.* designed a mitochondria-targeted nanosystem to improve the PDT efficacy by releasing a bioprecursor of PSs under two-photon irradiation [227]. In their work, researchers synthesized a phototriggerable coumarin derivative by linking 5-aminolevulinic acid (5-ALA, the bioprecursor) to coumarin; and then prepared the nanosystem (CD-ALA-TPP) by incorporating the coumarin derivative and mitochondria-targeting compound TPP on CDs (Figure 16A). With cellular

internalization, the nanosystem exhibited selective accumulation in mitochondria; and could release 5-ALA molecules to metabolize into protoporphyrin IX in mitochondria via the biosynthesis process under one- or two-photon irradiation. With the generated singlet oxygen induced by endogenously synthesized photosensitizer under light irradiation, the CD-ALA-TPP could cause oxidant damage to mitochondria and then induce the apoptosis of the cells. Similarly, due to the major obstacles of the current PSs and the tissue penetration limit of the

outer light source in PDT, Yang *et al.* developed the CL emission as an inner light source for the intracellular activation of CDs-based PDT (Figure 16B-C) [228]. In their work, researchers carefully selected the nanocarriers of CDs, the inner light of CL from the reaction of luminol-H₂O₂-horseradish peroxidase, and the PDT agent of Ce6 to design an efficient and united system for the full use of light and enhancement of the overall PDT yield. With the observations of proliferating cell nuclear antigen (PCNA) and platelet/endothelial cell adhesion molecule-1 (PECAM-1 or CD31) results, researchers indicated the excellent performance of CL-induced γ -CDs-Ce6 system in cancer therapy, providing a promising approach to achieve the selective PDT therapy (Figure 16D).

As CDs exhibit excellent intrinsic PTT and PDT properties, simultaneous PTT and PDT therapy in a single nanoplatform may provide the best therapeutic impact. Generally, the photosensitizers (PS) functioning as PDT agent in tumor under light can generate different ROS, thereby achieving effective treatment. Generally, the ideal PS are employed with the following characters: (1) efficient energy transfer with high quantum yield of ROS, (2) low toxicity in dark, (3) excellent photostability, (4) water solubility, and (5) broad light absorption ranging in the therapeutic window. Nevertheless, current PS from CDs are always limited by their poor water solubility, low photostability, suboptimal excitation wavelengths, or low efficiency of ROS generation. Thereupon, the combination therapy of PDT with other therapies, such as PTT, can provide the unique advantages. On the one hand, the local hypoxia in tumor can seriously limit the therapeutic effect of PDT owing to the exhaustion of tissue oxygen and fracture of tumor blood flow. Thereupon, the combination therapy can resolve the hypoxia problem to achieve enhanced anticancer efficacy. On the other hand, the combination therapy can also solve the respective limitations of common PS based on the only PDT or PTT, such as low efficacy of ROS generation, and the requirement of high photoactive power density. Thereby, considerable efforts have been exerted to develop light-triggered combination therapy. For example, Ge *et al.* prepared one kind of CDs with intrinsic PTT and PDT properties with polythiophene benzoic acid as carbon source (Figure 17A) [119]. In their work, the obtained CDs with bright red fluorescence exhibited photodynamic capability with a singlet oxygen generation efficiency of 27% and photothermal effects with a photothermal conversion efficiency of 36.2%. On the condition, the CDs were successfully employed in the red-light-triggered photodynamic-photothermal simultaneous therapy *in*

vitro and *in vivo* within the therapeutic window in the region from 600 to 1000 nm. Similarly, Zhang *et al.* combined the action of starving therapy/PDT/PTT and checkpoint-blockade immunotherapy to improve cancer therapy [177]. In detail, the immunoadjuvant nanoagents (γ PGA@GOx@Mn, Cu-CDs) were designed by integrating the gamma-glutamyl transferase (GGT) enzyme-induced cellular uptake polymer-poly (γ -glutamic acid) (γ -PGA), the glucose-metabolic reaction agent-glucose oxidase (GOx), the Mn, Cu-doped CDs as PSs and self-supplied oxygenator nanodots (Figure 17B). The obtained γ PGA@GOx@Mn, Cu-CDs NPs illustrated long retention time at the tumor acidic microenvironment and targeted capability for cancer cells with both photothermal and photodynamic effects under laser irradiation of 730 nm. With the endogenous generation of H₂O₂ caused by the nanoreactors, tumor hypoxia and further the enhancement of *in vivo* PDT were significantly relieved, enabling the improvement of therapeutic effect. Moreover, Sun *et al.* developed another method to design one kind of nanoplatform for fluorescence imaging and synergistic cancer therapy with tumor microenvironment stimuli-responsivity [229]. With the assembling of Ce6 modified CDs (CDs-Ce6) and Cu²⁺ (Figure 17C), the as-obtained nanoassemblies (Cu/CC NPs) exhibited quenched fluorescence/PDT due to the aggregation of CDs-Ce6 and recovered fluorescence /PDT functions triggered by the stimulation of tumor microenvironment (Figure 17D). With the extra chemodynamic therapy (CDT) function through reaction with H₂O₂ and depletes GSH in tumors by aredox reaction introduced by Cu²⁺ in the Cu/CC NPs, the amplifier of the intracellular oxidative stress and enhanced PDT were achieved.

As well as the common PDT generated by ROS under light excitation, nitric oxide (NO) is another gaseous signal molecule with multiple physiological functions in cancer therapy [230]. Due to the unsatisfactory anticancer effect of the O₂-dependent production of NO, Fang *et al.* reported a NO-based phototherapeutic strategy mediated by photogenerated holes for hypoxic tumors (Figure 18A) [231]. In their work, the phototherapeutic strategy was achieved with the NO generated by the poly-L-arginine modified CDs-doped graphitic carbon nitride nanomaterial (ArgCCN) under light excitation (Figure 18B-D). Mechanically, the holes generated by CCN could oxidize the arginine residues on poly-L-arginine to generate NO with the irradiation of 660 nm laser, thus subsequently resulting in tumor cell apoptosis. Meanwhile, regarding the large size distribution and conjugating with active tumor targeting ligands could improve the

enrichment of the phototherapy nanoplatform at tumor sites (Figure 18E-F). Thereupon, the capability of ArgCCN to generate NO without O₂ consumption could overcome the therapeutic challenges of the hypoxic microenvironment in tumor sites, paving the new approaches to cancer therapy.

4.3. Metabolism Effect

Despite their low systemic toxicity in mice, CDs' metabolic pathway is unclear in both normal and tumor cell growth and apoptosis. In several recent reports, researchers have observed the novel cytotoxicity of some carbon-based nanomaterials, such as carbon nanotubes, graphene, and graphene oxide, which can cause DNA and lysosomal damage and mitochondrial dysfunction, resulting in the apoptosis or necrosis. With the similar chemical structure and physical property, several kinds of CDs have been observed the similar effect on the cell metabolism. For example, Li *et al.* synthesized one kind of cysteine-based chiral optically active CDs and indicated their influences to cellular energy metabolism, which was vital for essential cellular functions [232]. In their work, researchers developed a green and effective synthesis strategy for the chiral N-S-doped CDs (L-CDs and D-CDs) by hydrothermal treatment of L- or D-cysteine (Figure 19A-C). With more characterizations and experiments, the

chirality-dependent enhancement of L-CDs in cellular glycolysis were observed while there were no influences on the cellular ATP levels of T24 cells (Figure 19D-E). The novel cellular energy metabolism performances indicated the potential applications of CDs in promising biomedicine for cancer therapy. In addition, Ding *et al.* observed the novel dose-dependent cytotoxicity of CDs (Figure 19F) [233]. In their work, researchers demonstrated the CDs-induced dose-dependent increase of ROS levels in Uveal melanoma (UM) cell metabolism, tumorigenicity of zebrafish and nude mouse xenograft model. In practice, the effect of CDs-induced ROS could promote the growth, invasiveness and tumorigenicity of UM cells at low concentration and result in the apoptosis of UM cells of at high concentration. More experiments indicated that the CDs at 25~100 μg mL⁻¹ could activate Akt/mammalian target of rapamycin (mTOR) signaling and induced glutamine metabolism, providing a cascade that promotes UM cell growth (Figure 19G). With these novel cytotoxicity capabilities in the metabolism pathway of cells, CDs could be employed one kind of potential nanomaterials for the rational design of various promising nanomedicines in cancer therapy.

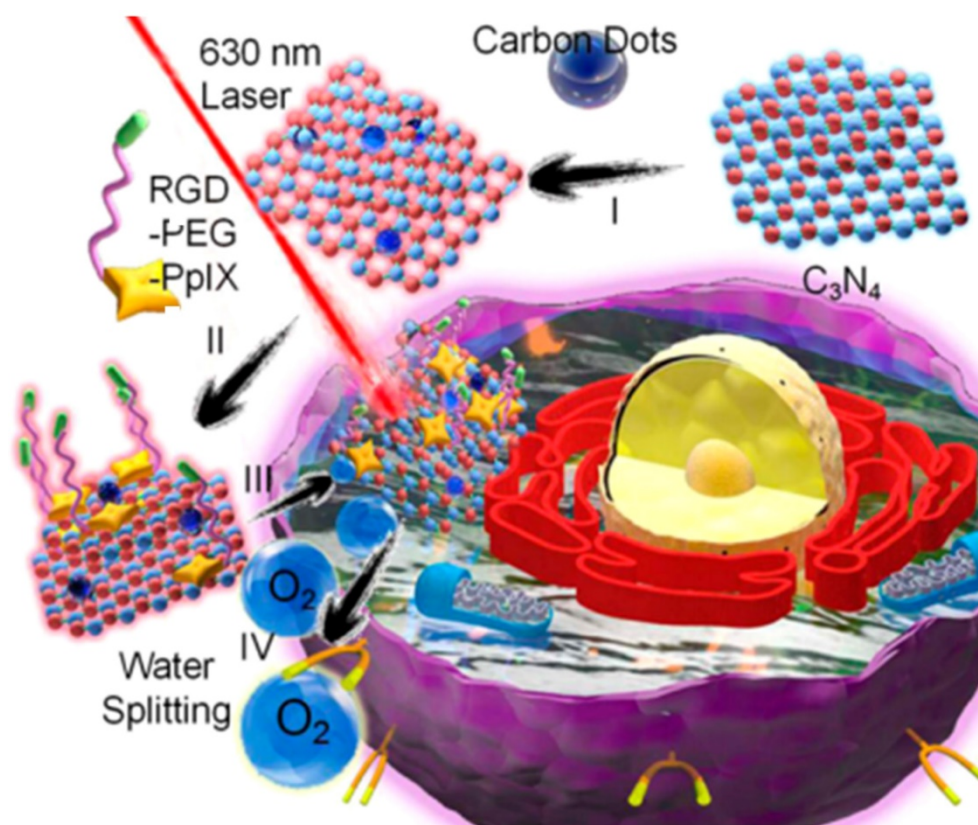


Figure 15. Structure of PCCN and schematic diagram of 630 nm light-driven water splitting enhanced PDT. Adapted with permission from [226], copyright 2016 American Chemical Society.

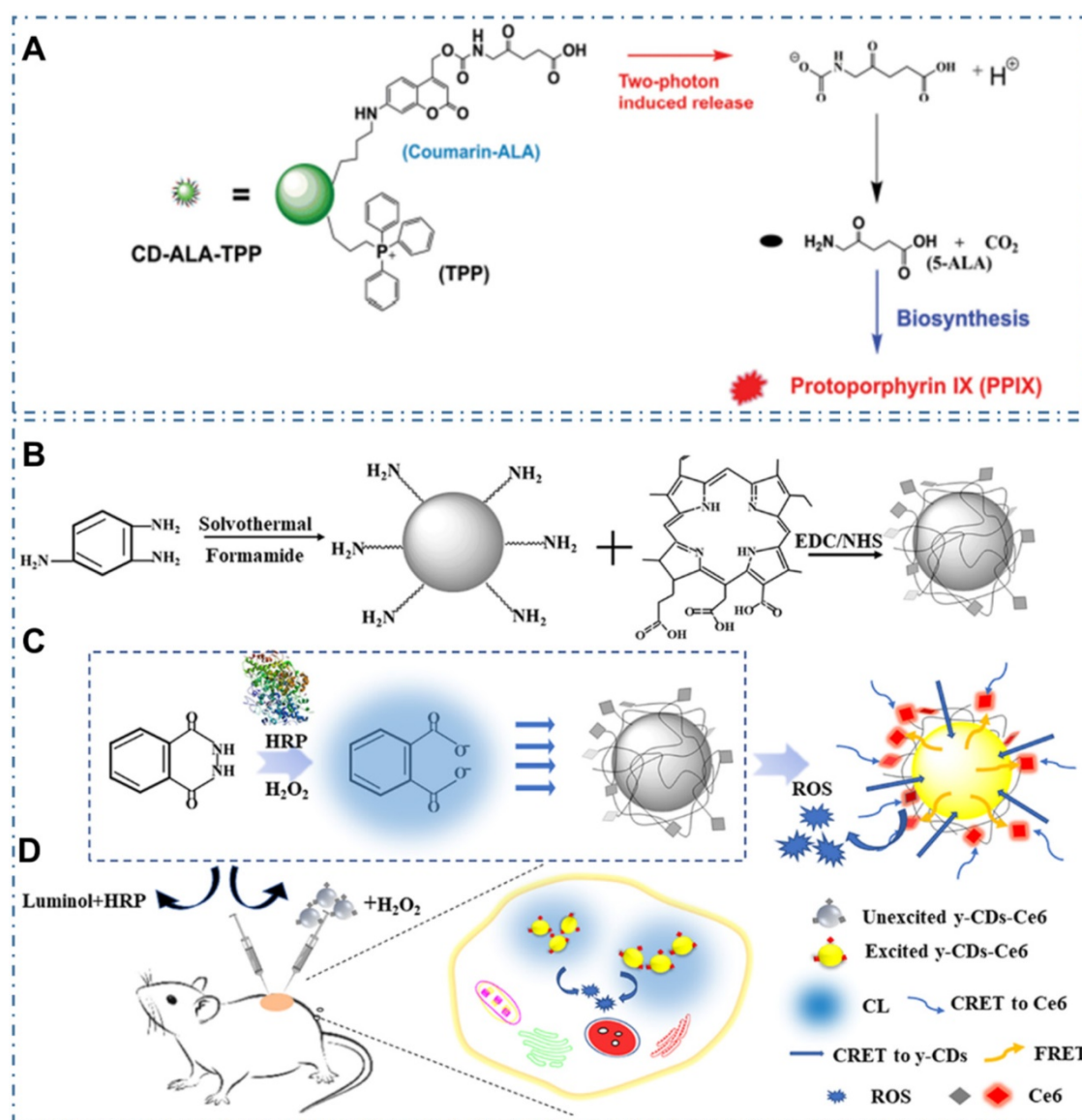


Figure 16. CDs-based cancer therapy by PDT with two-photon irradiation or CL. (A) Schematic illustration for the photo-triggered release of ALA from CD-ALA-TTP and the subsequent proapoptotic action on a cancer cell. Adapted with permission from [227], copyright 2015 WILEY-VCH Verlag GmbH & Co. KGaA, Weinheim. (B) Synthesis process of γ -CDs and γ -CDs-Ce6 conjugate. (C) Enhancement of therapeutic effect by optimization of CRET step to the PS in CL-induced γ -CDs-Ce6 system. (D) Illustration of the PDT system *in vivo*. Adapted with permission from [228], copyright 2019 American Chemical Society.

4.4. Advanced technology

Except the above strategy to achieve cancer therapy, there are still other advanced nanotechnology to be developed with CDs for diverse cancer. For example, boron neutron capture therapy (BNCT) was a noninvasive radiation therapeutic modality for cancer therapy and Li et al. designed one kind of novel boron-containing carbon dots (BCDs) for the BNCT by tracking ¹⁰B *in vitro* and *in vivo* [234]. With the encapsulation of BCDs by exosomes (Exos), researchers designed the BCD-Exos which could internalize and distribute around the nuclei of U-87-MG glioma cells (Figure 20A-B). With the ability to cross the blood-brain barrier and significant accumulation in tumor sites of the orthotopic

U-87-MG glioma tumor-bearing mice model (Figure 20C), the BCD-Exos exhibited a prominent BNCT effect for the brain glioma in the mice model (Figure 20D-E). The excellent curative effect of BNCT with BCD-Exos in the application of brain glioma therapy exhibited promising potential of CDs in various neutron capture therapy.

Meanwhile, due to the scaffolds of DNA nanostructures for drug delivery, biosensing, and bioimaging by their vulnerability in physiological settings, less favorable of incorporating arbitrary guest molecules and other desirable functionalities, Wu et al. designed a DNA nanostructure self-assembly strategy mediated by nitrogen-rich CDs (NCDs) with the excellent PL and photodynamic properties and indicated the great potential of the

obtained DNA/NCDs nanocomplex in anticancer therapy (Figure 21A-B) [235]. In their work, researchers demonstrated the NCDs could mediate DNA nanoprism (NP^{NCD}) self-assembly isothermally at a large temperature and pH range in a magnesium-free manner by polyacrylamide gel electrophoresis (PAGE) (Figure 21C-I). With excellent biocompatibility and high cellular uptake efficiency of

NP^{NCD}, the designed NP^{NCD} with KRAS siRNA (NP^{NCDK}) was further conjugated for KRAS-mutated non-small cell lung cancer therapy (NSCLC), illustrating excellent gene knockdown efficiency and anticancer effect *in vitro*. These advanced technologies could greatly expand the applications of CDs in an increasing range of significant precise cancer therapy.

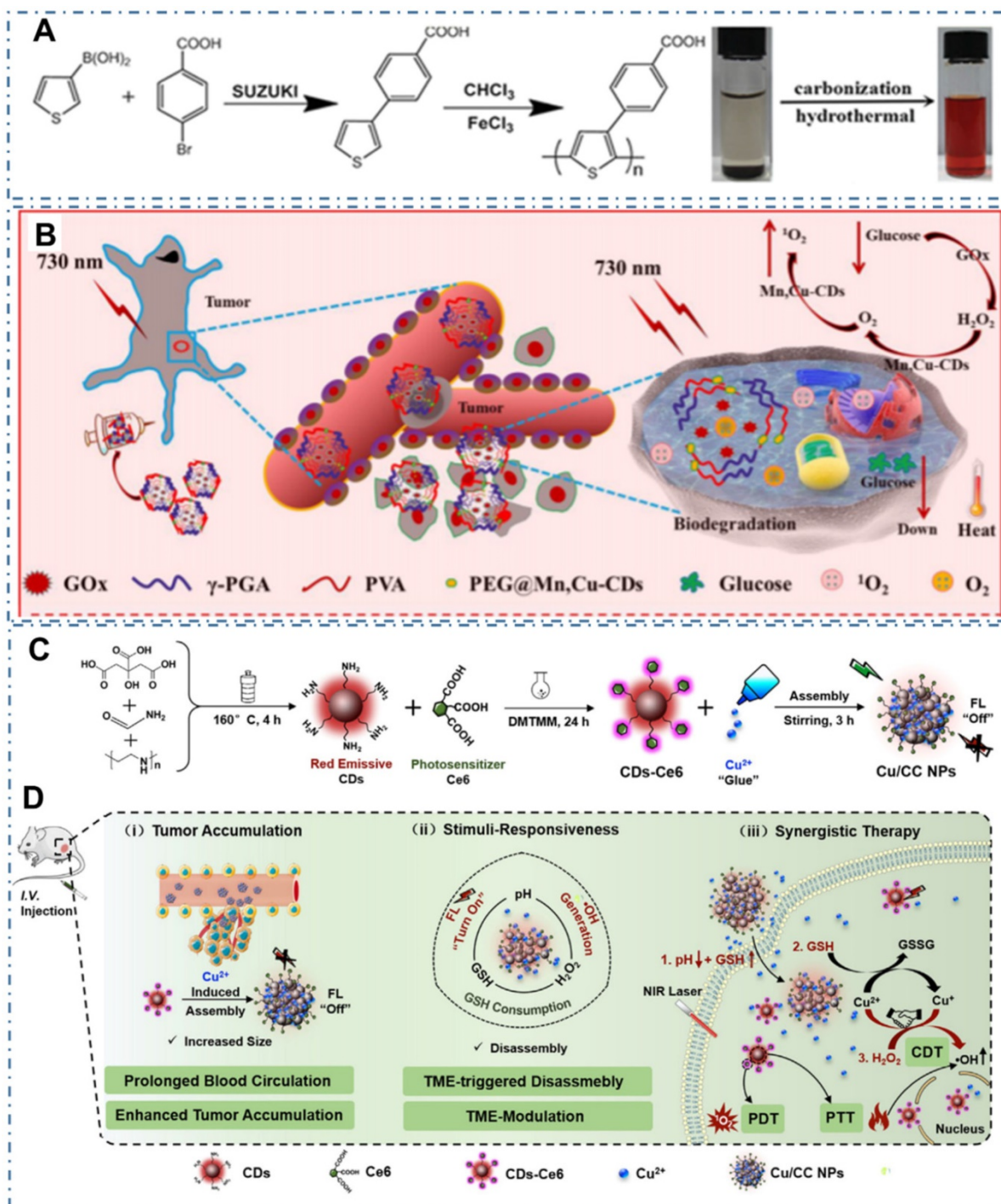


Figure 17. CDs-based cancer therapy by simultaneous PTT and PDT. (A) Synthetic route of PBA and CDs WITH simultaneous PTT and PDT capability by polymerization to carbonization. Adapted with permission from [119], copyright 2015 WILEY-VCH Verlag GmbH & Co. KGaA, Weinheim. (B) Schematic illustration of starving and phototherapy mediated by γ -PGA@GOx@Mn,Cu-CDs NPs. Adapted with permission from [177], copyright 2020 Elsevier Ltd. (C) Illustration of the synthesis process of Cu/CC nanoassemblies. (D) Illustration of the features for enhancing tumor accumulation, TME stimuli-responses and synergistic therapy. Adapted with permission from [229], copyright 2020 Wiley-VCH GmbH.

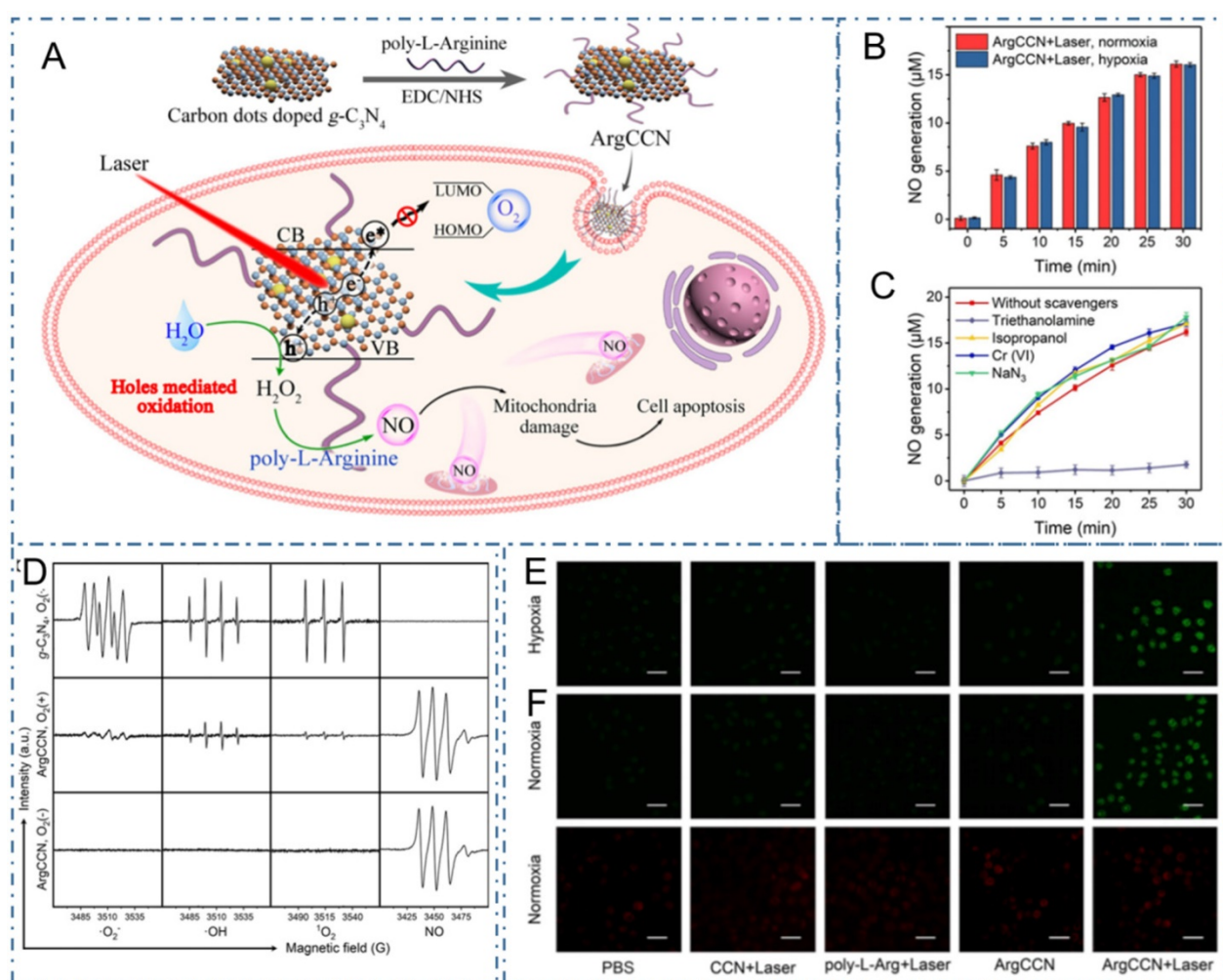


Figure 18. CDs-based cancer therapy by NO-based phototherapeutic. (A) The schematic diagram of microenvironment-independent NO-based phototherapeutic nanoplatform. (B) NO generation in hypoxia and normoxia; (C) ESR spectra of g-C₃N₄ (with O₂) and ArgCCN (with or without O₂) under irradiation. (D) NO generation in the presence of various scavengers. (E) CLSM images of intracellular NO generation. (F) Fluorescence images of intracellular O₂ content probe in MCF-7 cells treated with PBS only or CCN+laser, poly-L-arginine+laser, ArgCCN and ArgCCN+laser. Adapted with permission from [231], copyright 2020 Wiley-VCH GmbH.

5. Discussion and Conclusion

In this paper, we have summarized and highlighted the current progress of CDs-involved nanotheranostic application in targeted bioimaging and cancer therapy. These results imply the various advantages to employ CDs as nanoplatforms to achieve targeted imaging and therapeutic functions for tumors. Through the diverse biodistribution in tumor sites and normal organism, charge and pH effect of CDs in tumor microenvironment, biomarker sensor and the self-targeting for some tumor, CDs illustrate excellent capability of *in vivo* targeted tumor cells or sites. Meanwhile, with the capability as nanocarriers for drug delivery, as agent for light-active theranostic, as interference to affect cell metabolism and as nanoplatforms for achieving advanced technology, CDs are employed to achieve precise cancer therapy. These recent progress of CDs in targeted bioimaging and cancer therapy approved

the promising potential of CDs for the clinic diagnose and treatment for cancer in future.

6. Future prospect and outlook

In this paper, the recent progress of CDs-based nanotheranostic in targeted bioimaging and cancer therapy has been summarized. Although there have been various progresses in the nanotheranostic of CDs, there still remains various challenges to be resolved for the future biological applications.

Firstly, the structures of CDs remain to be analyzed. Compared with the molecular probes, the structures of CDs and their corresponding luminescence mechanism are not clear, thereby restricting the improvement of structure and luminescent properties for the clinic requirement.

Secondly, the metabolism of CDs in living body remains to be further analyzed. Compared with the classical medicine, the circulation of CDs in living body and organs is not clear and the interaction

between CDs and living molecular is complex, leading to the limitation of CDs in clinic applications.

Thirdly, the risk of CDs for clinic therapy applications remains more studies. Though most of CDs exhibit low toxicity, there are still widespread concerns about the risk of CDs for therapy applications. On the one hand, there have been various animal studies revealing that other carbon family nanomaterials like CNTs, can be internalized by macrophages and induce inflammation and injury in the respiratory system. So far, reports of CDs for

therapy applications have employed in different tissues. There still are no reports about the inflammatory response or neoplastic lesions known about whether CDs exposure may eventually affect cancer progression via possible systemic effects on non-adjacent organs. On the other hand, there have been several reports about the novel cytotoxicity in some kinds of CDs, such as their ROS-generation toxicity, dose-dependent toxicity, etc. Thereby, the risk of CDs for clinic therapy applications still needs more concerns and studies.

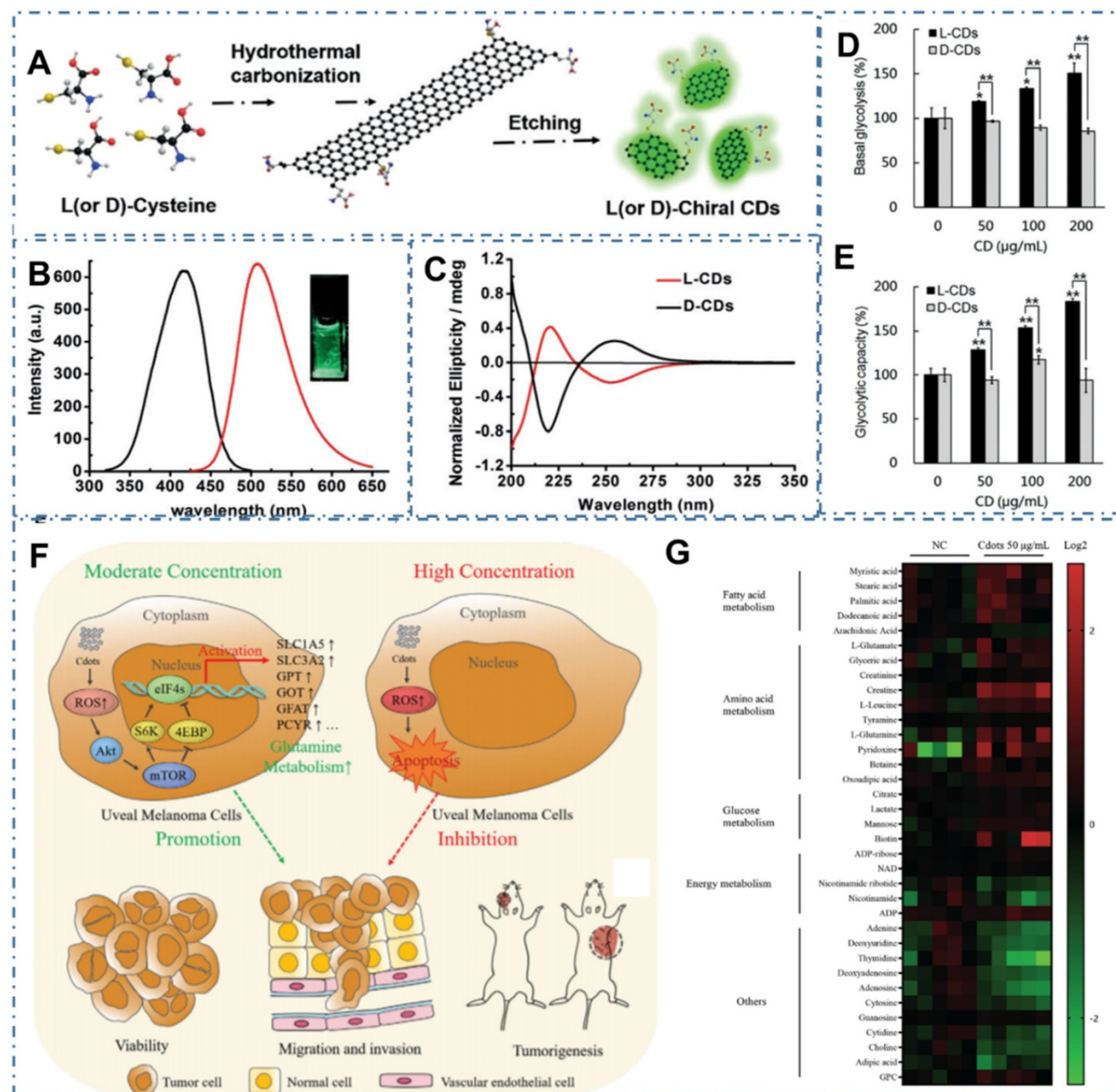


Figure 19. CDs-based cancer therapy by cell metabolism effect. (A) Synthesis of chiral CDs by hydrothermal treatment of chiral cysteines. (B) PL excitation and emission spectrum of the L-CDs. (C) Circular dichroism spectra of the L- and D-CDs. (D) Basal Glycolysis from the extracellular acidification rate curves. (E) Glycolytic capacity. Adapted with permission from [232], copyright 2018Wiley-VCH Verlag GmbH & Co. KGaA, Weinheim. (F) Schematic of the opposing CDs-concentration-dependent effects on tumor cell progression and metastasis. (g) Heatmap depicting changes in metabolite concentration between control and 50 µg mL⁻¹ CDs-treated Mum2B cells (p < 0.05). Adapted with permission from [233], copyright 2021 Wiley-VCH GmbH.

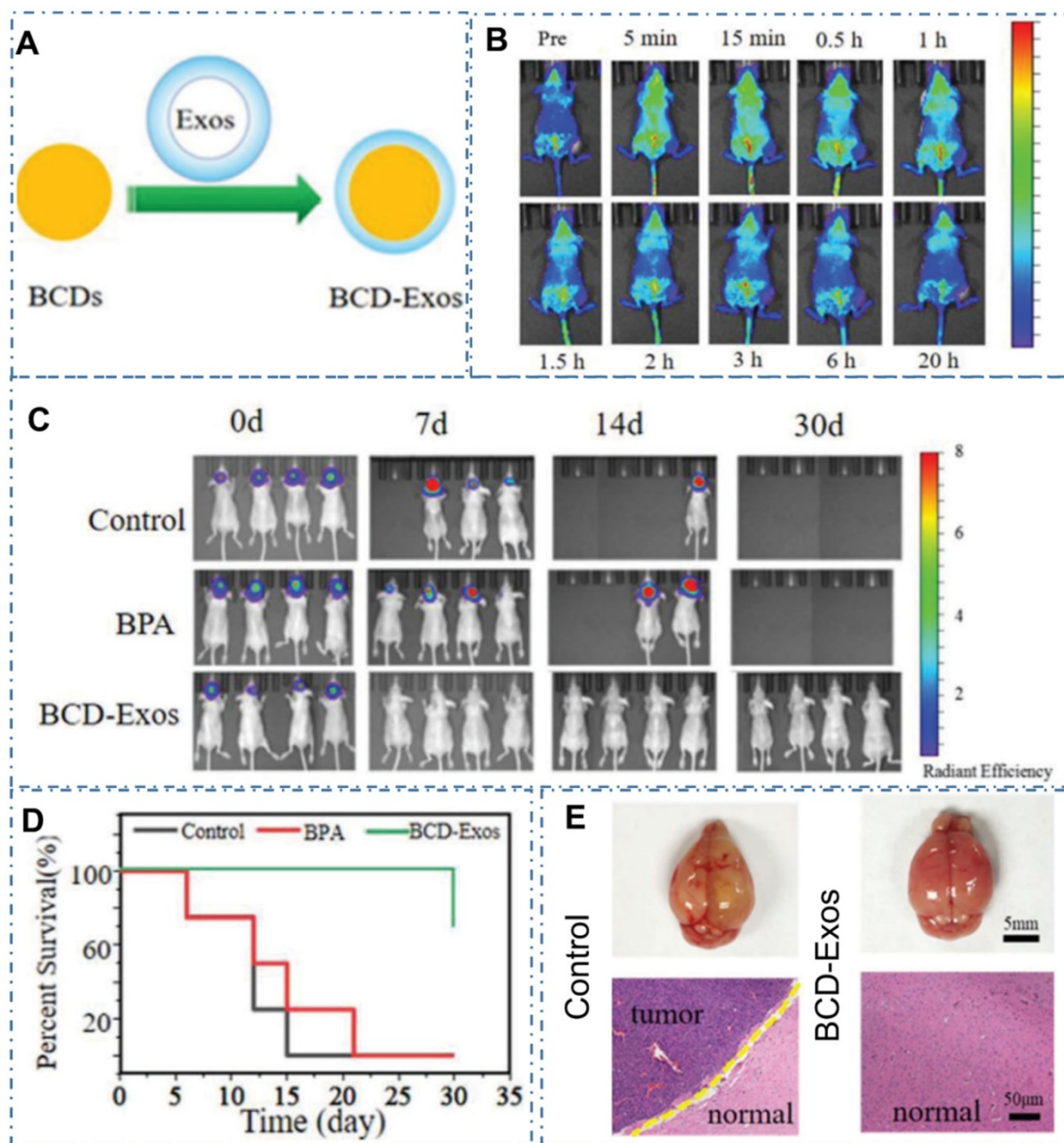


Figure 20. CDs-based cancer therapy by boron neutron capture therapy. (A) The preparation of BCD-Exos. (B) The ability of BCDs for bioimaging in the normal mice model. (C) The *in vivo* bioimaging of U87-Luc transplanted mice model treated with saline as the control, BPA, and BCD-Exos after BNCT. (D) Survival curves after BNCT. (E) Gross images of mice brains and microscopic images of H&E-stained tumor sections in each group. Adapted with permission from [234], copyright 2021 Wiley-VCH GmbH.

Fourthly, the principle and mechanism about the novel properties of CDs, such as self-targeting, metabolism effect, etc. still remain to be further analyzed and developed for more applications.

At last, more advanced nanotechnologies about CDs and their nanocomposites remain to be employed for overcoming the practical limitations in classical diagnosis and therapy.

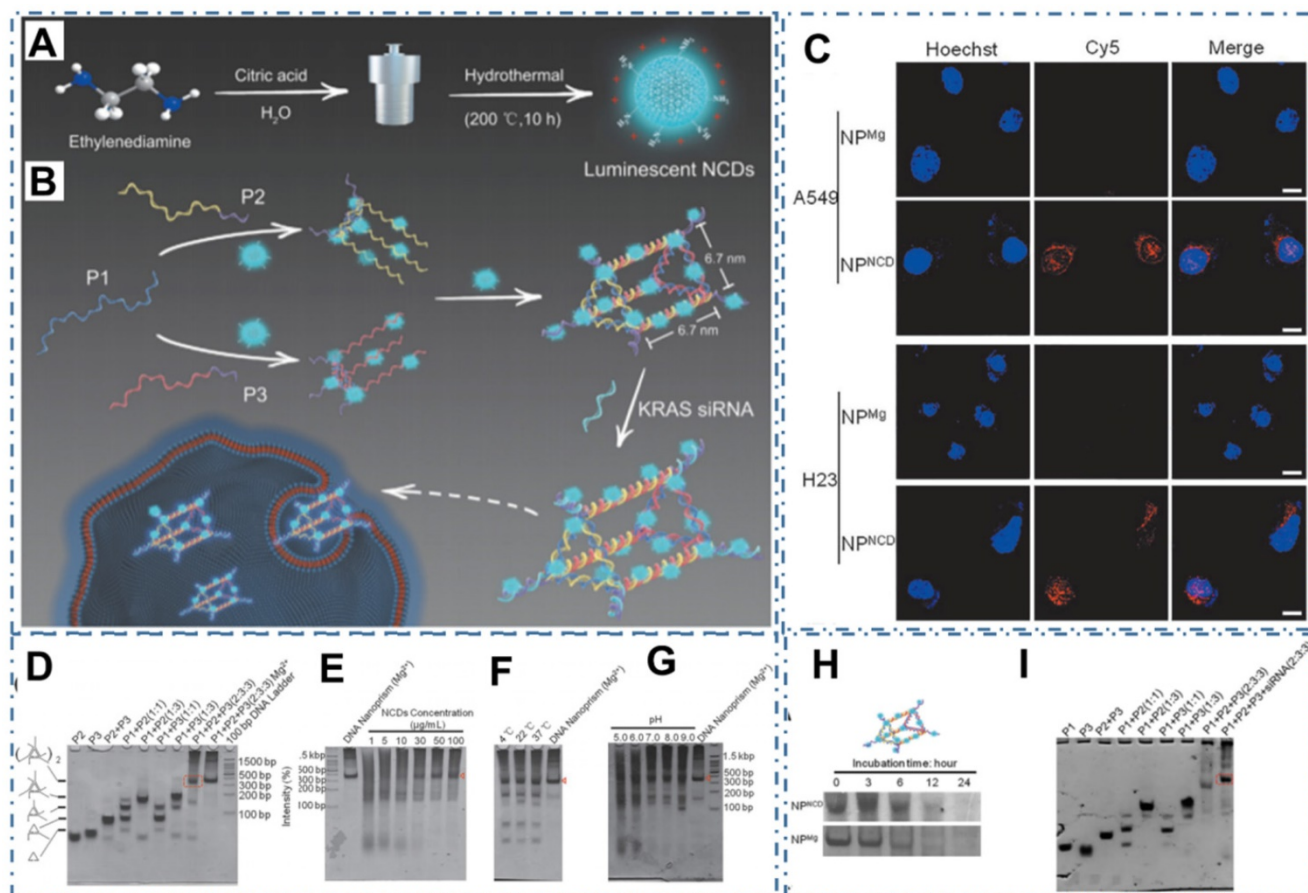


Figure 21. CDs-based cancer therapy by DNA nanostructure. (A) The chemical route to synthesize NCDs. (B) NCDs-assisted DNA NP self-assembly. (C) Cellular uptake evaluation of NPNCD on KRAS-mutated NSCLC cell lines and CLSM imaging of NPNCD internalized by A549 and H23. (D) The formation of NPNCD showed by PAGE. (E) Self-assembly of NPNCD at various NCDs concentration. (F) NCDs-induced isothermal DNA NP self-assembly and corresponding formation of DNA NP at different temperature. (G) PAGE analysis of NPNCD formation under different pH values. (H) PAGE electrophoresis showing the serum stability of NPNCD and magnesium-assembled NP (NPMg). (I) PAGE analysis of the formation of CDs/NP conjugating with KRAS siRNA. Adapted with permission from [235], copyright 2020 WILEY-VCH Verlag GmbH & Co. KGaA, Weinheim.

Acknowledgements

We gratefully acknowledge the support of this research by the National Natural Science Foundation of China (12074348 and U2004168, and U21A2070), the China Postdoctoral Science Foundation (2020M6 82310), the Natural Science Foundation of Henan Province (212300410078).

Competing Interests

The authors have declared that no competing interest exists.

References

- Tricoli JV, Blair DG, Anders CK, Bleyer WA, Boardman LA, Khan J, et al. Biologic and clinical characteristics of adolescent and young adult cancers: Acute lymphoblastic leukemia, colorectal cancer, breast cancer, melanoma, and sarcoma. *Cancer*. 2016; 122: 1017-28.
- Bray F, Ferlay J, Soerjomataram I, Siegel RL, Torre LA, Jemal A. Global cancer statistics 2018: GLOBOCAN estimates of incidence and mortality worldwide for 36 cancers in 185 countries. *CA: a cancer journal for clinicians*. 2018; 68: 394-424.
- Hanahan D, Weinberg RA. Hallmarks of cancer: the next generation. *Cell*. 2011; 144: 646-74.
- Ferrara N, Adams AP. Ten years of anti-vascular endothelial growth factor therapy. *Nat Rev Drug Discov*. 2016; 15: 385-403.
- De Palma M, Biziato D, Petrova TV. Microenvironmental regulation of tumour angiogenesis. *Nat Rev Cancer*. 2017; 17: 457-74.
- Ferrara N. VEGF and the quest for tumour angiogenesis factors. *Nat Rev Cancer*. 2002; 2: 795-803.
- Motz GT, Santoro SP, Wang LP, Garrabrant T, Lastra RR, Hagemann IS, et al. Tumor endothelium FasL establishes a selective immune barrier promoting tolerance in tumors. *Nat Med*. 2014; 20: 607-15.
- Folkman, Judah. Angiogenesis in cancer, vascular, rheumatoid and other disease. *Nat Med*. 1995; 1: 27-31.
- Folkman J. Tumor angiogenesis: therapeutic implications. *New Eng J Med*. 1971; 285: 1182.
- Jayson GC, Kerbel R, Ellis LM, Harris AL. Antiangiogenic therapy in oncology: current status and future directions. *Lancet*. 2016; 388: 518-29.
- Páez-Ribes M, Allen E, Hudock J, Takeda T, Okuyama H, Vinals F, et al. Antiangiogenic therapy elicits malignant progression of tumors to increased local invasion and distant metastasis. *Cancer Cell*. 2009; 15: 220-31.
- Liu S, Qin T, Liu Z, Wang J, Jia Y, Feng Y, et al. anlotinib alters tumor immune microenvironment by downregulating PD-L1 expression on vascular endothelial cells. *Cell Death & Disease*. 2020; 11: 309.
- Miao Q, Xie C, Zhen X, Lyu Y, Duan H, Liu X, et al. Molecular afterglow imaging with bright, biodegradable polymer nanoparticles. *Nat Biotechnol*. 2017; 35: 1102-10.
- Wang Y, Zhou K, Huang G, Hensley C, Huang X, Ma X, et al. A nanoparticle-based strategy for the imaging of a broad range of tumours by nonlinear amplification of microenvironment signals. *Nat Mater*. 2014; 13: 204-12.
- Hong G, Antaris AL, Dai H. Near-infrared fluorophores for biomedical imaging. *Nat Biomed Eng*. 2017; 1: 0010.
- Peng B, Almqadadi M, Laroche F, Palantavida S, Dokukin M, Roper J, et al. Ultrabright fluorescent cellulose acetate nanoparticles for imaging tumors through systemic and topical applications. *Mater Today*. 2019; 23: 16-25.
- Biju V. Chemical modifications and bioconjugate reactions of nanomaterials for sensing, imaging, drug delivery and therapy. *Chem Soc Rev*. 2014; 43: 744-64.

18. Meng HM, Liu H, Kuai H, Peng R, Mo L, Zhang XB. Aptamer-integrated DNA nanostructures for biosensing, bioimaging and cancer therapy. *Chem Soc Rev*. 2016; 45: 2583-602.
19. Huang J, Li J, Lyu Y, Miao Q, Pu K. Molecular optical imaging probes for early diagnosis of drug-induced acute kidney injury. *Nat Mater*. 2019; 18: 1133-43.
20. Lee D, Khaja S, Velasquez-Castano JC, Dasari M, Sun C, Petros J, et al. *In vivo* imaging of hydrogen peroxide with chemiluminescent nanoparticles. *Nat Mater*. 2007; 6: 765-9.
21. Pu K, Shuhendler AJ, Jokerst JV, Mei J, Gambhir SS, Bao Z, et al. Semiconducting polymer nanoparticles as photoacoustic molecular imaging probes in living mice. *Nat Nanotechnol*. 2014; 9: 233-9.
22. Shuhendler AJ, Pu K, Cui L, Utrecht JP, Rao J. Real-time imaging of oxidative and nitrosative stress in the liver of live animals for drug-toxicity testing. *Nat Biotechnol*. 2014; 32: 373-80.
23. Xu X, An H, Zhang D, Tao H, Dou Y, Li X, et al. A self-illuminating nanoparticle for inflammation imaging and cancer therapy. *Sci Adv*. 2019; 5: eaat2953.
24. Liang L, Chen N, Jia Y, Ma Q, Wang J, Yuan Q, et al. Recent progress in engineering near-infrared persistent luminescence nanoprobes for time-resolved biosensing/bioimaging. *Nano Res*. 2019; 12: 1279-92.
25. Wang Y, Shi L, Ye Z, Guan K, Teng L, Wu J, et al. Reactive Oxygen Correlated Chemiluminescent Imaging of a Semiconducting Polymer Nanoparticle for Monitoring Chemodynamic Therapy. *Nano Lett*. 2020; 20: 176-83.
26. Wang H, Chen Q, Zhou S. Carbon-based hybrid nanogels: a synergistic nanoparticle platform for combined biosensing, bioimaging, and responsive drug delivery. *Chem Soc Rev*. 2018; 47: 4198-232.
27. Li J, Pu K. Development of organic semiconducting materials for deep-tissue optical imaging, phototherapy and photoactivation. *Chem Soc Rev*. 2019; 48: 38-71.
28. Haupt K, Medina Rangel PX, Bui BTS. Molecularly Imprinted Polymers: Antibody Mimics for Bioimaging and Therapy. *Chem Rev*. 2020; 120: 9554-82.
29. Pennathur A, Gibson MK, Jobe BA, Luketich JD. Oesophageal carcinoma. *Lancet*. 2013; 381: 400-12.
30. Arnold M, Soerjomataram I, Ferlay J, Forman D. Global incidence of oesophageal cancer by histological subtype in 2012. *Gut*. 2015; 64: 381-7.
31. Folkman J. Angiogenesis in cancer, vascular, rheumatoid and other disease. *Nat Med*. 1995; 1: 27-31.
32. Jain RK. Normalizing tumor vasculature with anti-angiogenic therapy: a new paradigm for combination therapy. *Nat Med*. 2001; 7: 987-9.
33. Gong N, Sheppard NC, Billingsley MM, June CH, Mitchell MJ. Nanomaterials for T-cell cancer immunotherapy. *Nat Nanotechnol*. 2021; 16: 25-36.
34. Tang L, Zheng Y, Melo MB, Mabardi L, Castano AP, Xie YQ, et al. Enhancing T cell therapy through TCR-signaling-responsive nanoparticle drug delivery. *Nat Biotechnol*. 2018; 36: 707-16.
35. Irvine DJ, Dane EL. Enhancing cancer immunotherapy with nanomedicine. *Nat Rev Immunol*. 2020; 20: 321-34.
36. Kievit FM, Zhang M. Cancer nanotheranostics: improving imaging and therapy by targeted delivery across biological barriers. *Adv Mater*. 2011; 23: H217-H47.
37. Huang X, Zhang W, Guan G, Song G, Zou R, Hu J. Design and functionalization of the NIR-responsive photothermal semiconductor nanomaterials for cancer theranostics. *Acc Chem Res*. 2017; 50: 2529-38.
38. Melancon MP, Zhou M, Li C. Cancer Theranostics with near-infrared light-activatable multimodal nanoparticles. *Acc Chem Res*. 2011; 44: 947-56.
39. Bao X, Yuan Y, Chen J, Zhang B, Li D, Zhou D, et al. *In vivo* theranostics with near-infrared-emitting carbon dots-highly efficient photothermal therapy based on passive targeting after intravenous administration. *Light Sci Appl*. 2018; 7: 91.
40. Hassan M, Gomes VG, Dehghani A, Ardekani SM. Engineering carbon quantum dots for photomediated theranostics. *Nano Res*. 2017; 11: 1-41.
41. Cho MH, Li Y, Lo PC, Lee H, Choi Y. Fucoidan-based theranostic nanogel for enhancing imaging and photodynamic therapy of cancer. *Nano-Micro Lett*. 2020; 12: 47.
42. Chen Q, Liu Z. Albumin carriers for cancer theranostics: a conventional platform with new promise. *Adv Mater*. 2016; 28: 10557-66.
43. Chen W, Zhang S, Yu Y, Zhang H, He Q. Structural-engineering rationales of gold nanoparticles for cancer theranostics. *Adv Mater*. 2016; 28: 8567-85.
44. Cheng L, Wang X, Gong F, Liu T, Liu Z. 2D nanomaterials for cancer theranostic applications. *Adv Mater*. 2020; 32: 1902333.
45. Fan W, Tang W, Lau J, Shen Z, Xie J, Shi J, et al. Breaking the depth dependence by nanotechnology-enhanced X-ray-excited deep cancer theranostics. *Adv Mater*. 2019; 31: 1806381.
46. Huang J, He B, Zhang Z, Li Y, Kang M, Wang Y, et al. Aggregation-induced emission luminogens married to 2D black phosphorus nanosheets for highly efficient multimodal theranostics. *Adv Mater*. 2020; 32: 2003382.
47. Peng L, Mei X, He J, Xu J, Zhang W, Liang R, et al. Monolayer nanosheets with an extremely high drug loading toward controlled delivery and cancer theranostics. *Adv Mater*. 2018; 30: 1707389.
48. Tang W, Fan W, Zhang W, Yang Z, Li L, Wang Z, et al. Wet/Sono-chemical synthesis of enzymatic two-dimensional MnO₂ nanosheets for synergistic catalysis-enhanced phototheranostics. *Adv Mater*. 2019; 31: 1900401.
49. Tao W, Ji X, Zhu X, Li L, Wang J, Zhang Y, et al. Two-dimensional antimonene-based photonic nanomedicine for cancer theranostics. *Adv Mater*. 2018; 30: 1802061.
50. Tao W, Zhu X, Yu X, Zeng X, Xiao Q, Zhang X, et al. Black phosphorus nanosheets as a robust delivery platform for cancer theranostics. *Adv Mater*. 2017; 29: 1603276.
51. Vankayala R, Hwang KC. Near-infrared-light-activatable nanomaterial-mediated phototheranostic nanomedicines: an emerging paradigm for cancer treatment. *Adv Mater*. 2018; 30: 1706320.
52. Xing R, Zou Q, Yuan C, Zhao L, Chang R, Yan X. Self-assembling endogenous biliverdin as a versatile near-infrared photothermal nanoagent for cancer theranostics. *Adv Mater*. 2019; 31: 1900822.
53. Lyu Y, Fang Y, Miao Q, Zhen X, Ding D, Pu K. Intraparticle molecular orbital engineering of semiconducting polymer nanoparticles as amplified theranostics for *in vivo* photoacoustic imaging and photothermal therapy. *ACS Nano*. 2016; 10: 4472-81.
54. Gu X, Tang BZ. No UV irradiation needed! chemiexcited AIE dots for cancer theranostics. *Chem*. 2017; 3: 922-4.
55. Ding S, Khan AI, Cai X, Song Y, Lyu Z, Du D, et al. Overcoming blood-brain barrier transport: Advances in nanoparticle-based drug delivery strategies. *Mater Today*. 2020; 37: 112-25.
56. Cai Y, Wei Z, Song C, Tang C, Han W, Dong X. Optical nano-agents in the second near-infrared window for biomedical applications. *Chem Soc Rev*. 2019; 48: 22-37.
57. Karimi M, Ghasemi A, Sahandi Zangabad P, Rahighi R, Moosavi Basri SM, Mirshekari H, et al. Smart micro/nanoparticles in stimulus-responsive drug/gene delivery systems. *Chem Soc Rev*. 2016; 45: 1457-501.
58. Molina M, Asadian-Birjand M, Balach J, Bergueiro J, Miceli E, Calderon M. Stimuli-responsive nanogel composites and their application in nanomedicine. *Chem Soc Rev*. 2015; 44: 6161-86.
59. Zeng L, Gupta P, Chen Y, Wang E, Ji L, Chao H, et al. The development of anticancer ruthenium(II) complexes: from single molecule compounds to nanomaterials. *Chem Soc Rev*. 2017; 46: 5771-804.
60. Zhang X, Malhotra S, Molina M, Haag R. Micro- and nanogels with labile crosslinks - from synthesis to biomedical applications. *Chem Soc Rev*. 2015; 44: 1948-73.
61. Xu X, Ray R, Gu Y, Ploehn HJ, Gearheart L, Raker K, et al. Electrophoretic analysis and purification of fluorescent single-walled carbon nanotube fragments. *J Am Chem Soc*. 2004; 126: 12736-7.
62. Lu S, Sui L, Liu J, Zhu S, Chen A, Jin M, et al. Near-infrared photoluminescent polymer-carbon nanodots with two-photon fluorescence. *Adv Mater*. 2017; 29: 1603443.
63. Hofmann MS, Gluckert JT, Noe J, Bourjau C, Dehmel R, Hoge A. Bright, long-lived and coherent excitons in carbon nanotube quantum dots. *Nat Nanotechnol*. 2013; 8: 502-5.
64. Choi H, Ko S-J, Choi Y, Joo P, Kim T, Lee BR, et al. Versatile surface plasmon resonance of carbon-dot-supported silver nanoparticles in polymer optoelectronic devices. *Nat Photon*. 2013; 7: 732-8.
65. Jiang L, Ding H, Lu S, Geng T, Xiao G, Zou B, et al. Photoactivated fluorescence enhancement in F, N-doped carbon dots with piezochromic behavior. *Angew Chem Int Ed*. 2020; 59: 9986-91.
66. Ru Y, Sui L, Song H, Liu X, Tang Z, Zang SQ, et al. Rational design of multicolor-emitting chiral carbonized polymer dots for full-color and white circularly polarized luminescence. *Angew Chem Int Ed*. 2021; 60: 14091-9.
67. Song H, Wu M, Tang Z, Tse JS, Yang B, Lu S. Single atom ruthenium-doped CoP/CDs nanosheets via splicing of carbon-dots for robust hydrogen production. *Angew Chem Int Ed*. 2021; 60: 7234-44.
68. Meng T, Wang Z, Yuan T, Li X, Li Y, Zhang Y, et al. Gram-scale synthesis of highly efficient rare-earth element-free red/green/blue solid-state bandgap fluorescent carbon quantum rings for white light-emitting diodes. *Angew Chem Int Ed*. 2021; 60: 16343.
69. Liang YC, Gou SS, Liu KK, Wu WJ, Guo CZ, Lu SY, et al. Ultralong and efficient phosphorescence from silica confined carbon nanodots in aqueous solution. *Nano Today*. 2020; 34: 100900.
70. Shen CL, Zheng GS, Wu MY, Wei JY, Lou Q, Ye YL, et al. Chemiluminescent carbon nanodots as sensors for hydrogen peroxide and glucose. *Nanophotonics*. 2020; 9: 3597-604.
71. Ai L, Yang Y, Wang B, Chang J, Tang Z, Yang B, et al. Insights into photoluminescence mechanisms of carbon dots: advances and perspectives. *Sci Bull*. 2021; 66: 839-56.
72. Hola K, Sudolska M, Kalytchuk S, Nachtigallova D, Rogach AL, Otyepka M, et al. Graphitic nitrogen triggers red fluorescence in carbon dots. *ACS Nano*. 2017; 11: 12402-10.
73. Liang YC, Liu KK, Wu XY, Lou Q, Sui LZ, Dong L, et al. Lifetime-engineered carbon nanodots for time division duplexing. *Adv Sci*. 2021; 8: 2003433.
74. Wang B, Song H, Qu X, Chang J, Yang B, Lu S. Carbon dots as a new class of nanomedicines: opportunities and challenges. *Coord Chem Rev*. 2021; 442: 214010.
75. Song H, Liu X, Wang B, Tang Z, Lu S. High production-yield solid-state carbon dots with tunable photoluminescence for white/multi-color light-emitting diodes. *Sci Bull*. 2019; 64: 1788-94.
76. Liu Y, Huang X, Niu Z, Wang D, Gou H, Liao Q, et al. Photo-induced ultralong phosphorescence of carbon dots for thermally sensitive dynamic patterning. *Chem Sci*. 2021; 12: 8199-8206.
77. Shen CL, Lou Q, Liu KK, Dong L, Shan CX. Chemiluminescent carbon dots: synthesis, properties, and applications. *Nano Today*. 2020; 35: 100954.

78. Wu J, Xin W, Wu Y, Zhan Y, Li J, Wang J, et al. Solid-state photoluminescent silicone-carbon dots/dendrimer composites for highly efficient luminescent solar concentrators. *Chem Eng J*. 2021; 422: 130158.
79. Liu H, Ye T, Mao C. Fluorescent carbon nanoparticles derived from candle soot. *Angew Chem Int Ed*. 2007; 46: 6473-5.
80. Yang S, Cao L, Luo PG, Lu F, Wang X, Wang H, et al. Carbon dots for optical imaging *in vivo*. *J Am Chem Soc*. 2009; 131: 11308-9.
81. Liu R, Wu D, Liu S, Koynov K, Knoll W, Li Q. An aqueous route to multicolor photoluminescent carbon dots using silica spheres as carriers. *Angew Chem Int Ed*. 2009; 48: 4598-601.
82. Qu S, Wang X, Lu Q, Liu X, Wang L. A biocompatible fluorescent ink based on water-soluble luminescent carbon nanodots. *Angew Chem Int Ed*. 2012; 51: 12215-8.
83. Zhu S, Meng Q, Wang L, Zhang J, Song Y, Jin H, et al. Highly photoluminescent carbon dots for multicolor patterning, sensors, and bioimaging. *Angew Chem Int Ed*. 2013; 52: 3953-7.
84. Jia Q, Zhao Z, Liang K, Nan F, Li Y, Wang J, et al. Recent advances and prospects of carbon dots in cancer nanotheranostics. *Mater Chem Front*. 2020; 4: 449-71.
85. Lu S, Sui L, Wu M, Zhu S, Yong X, Yang B. Graphitic nitrogen and high-crystalline triggered strong photoluminescence and room-temperature ferromagnetism in carbonized polymer dots. *Adv Sci*. 2019; 6: 1801192.
86. Shen CL, Lou Q, Lv CF, Zang JH, Qu SN, Dong L, et al. Bright and multicolor chemiluminescent carbon nanodots for advanced information encryption. *Adv Sci*. 2019; 6: 1802331.
87. Wang B, Lu S. The light of carbon dots: From mechanism to applications. *Matter*. 2022; 5:110-149.
88. Zhang C, Liu X, Li Z, Zhang C, Chen Z, Pan D, et al. Nitrogen-doped accordion-like soft carbon anodes with exposed hierarchical pores for advanced potassium-ion hybrid capacitors. *Adv Funct Mater*. 2021; 31: 2101470.
89. Arcudi F, Đorđević L, Rebecani S, Cacioppo M, Zanut A, Valenti G, et al. Lighting up the electrochemiluminescence of carbon dots through pre- and post-synthetic design. *Adv Sci*. 2021; 8: 2100125.
90. Liu KK, Song SY, Sui LZ, Wu SX, Jing PT, Wang RQ, et al. Efficient red/near-infrared-emissive carbon nanodots with multiphoton excited upconversion fluorescence. *Adv Sci*. 2019; 6: 1900766.
91. Shen CL, Zang JH, Lou Q, Su LX, Li Z, Liu ZY, et al. In-situ embedding of carbon dots in a trisodium citrate crystal matrix for tunable solid-state fluorescence. *Carbon*. 2018; 136: 359-68.
92. Xia C, Zhu S, Feng T, Yang M, Yang B. Evolution and synthesis of carbon dots: from carbon dots to carbonized polymer dots. *Adv Sci*. 2019; 6: 1901316.
93. Du J, Xu N, Fan J, Sun W, Peng X. Carbon dots for *in vivo* bioimaging and theranostics. *Small*. 2019; 15: 1805087.
94. Anilkumar P, Cao L, Yu JJ, Tackett KN, 2nd, Wang P, Meziani MJ, et al. Crosslinked carbon dots as ultra-bright fluorescence probes. *Small*. 2013; 9: 545-51.
95. Shi X, Meng H, Sun Y, Qu L, Lin Y, Li Z, et al. Far-red to near-infrared carbon dots: preparation and applications in biotechnology. *Small*. 2019; 15: 1901507.
96. Zhang L, Wei H, Gao F, Su Y, Su Y, Zhang J, et al. Controllable synthesis of fluorescent carbon dots and their detection application as nanoprobe. *Nano-Micro Lett*. 2013; 5: 247-259.
97. Yuan F, Yuan T, Sui L, Wang Z, Xi Z, Li Y, et al. Engineering triangular carbon quantum dots with unprecedented narrow bandwidth emission for multicolored LEDs. *Nat Commun*. 2018; 9: 2249.
98. Vallan L, Urriolabeitia EP, Ruipérez F, Matxain JM, Canton-Vitoria R, Tagmatarchis N, et al. Supramolecular-enhanced charge transfer within entangled polyamide chains as the origin of the universal blue fluorescence of polymer carbon dots. *J Am Chem Soc*. 2018; 140: 12862-9.
99. Meng W, Wang B, Ai L, Song H, Lu S. Engineering white light-emitting diodes with high color rendering index from biomass carbonized polymer dots. *J Colloid Interface Sci*. 2021; 598: 274-82.
100. Shen CL, Lou Q, Lv CF, Zheng GS, Zang JH, Jiang TC, et al. Trigonal nitrogen activates high-brightness chemiluminescent carbon nanodots. *ACS Mater Lett*. 2021; 3: 826-37.
101. Shen CL, Zang JH, Lou Q, Zheng GS, Wu MY, Ye YL, et al. Surface chemical engineering towards efficient and bright chemiluminescent carbon nanodots. *Appl Surf Sci*. 2021; 559: 149947.
102. Chen S, Xing C, Huang D, Zhou C, Ding B, Guo Z, et al. Eradication of tumor growth by delivering novel photothermal selenium-coated tellurium nanoheterojunctions. *Sci Adv*. 2020; 6: eaay6825.
103. Ji X, Kong N, Wang J, Li W, Xiao Y, Gan ST, et al. A novel top-down synthesis of ultrathin 2D boron nanosheets for multimodal imaging-guided cancer therapy. *Adv Mater*. 2018; 30: 1803031.
104. Tao W, Ji X, Zhu X, Li L, Wang J, Zhang Y, et al. Two-dimensional antimonene-based photonic nanomedicine for cancer theranostics. *Adv Mater*. 2018; 30: 1802061.
105. Xing C, Chen S, Liang X, Liu Q, Qu M, Zou Q, et al. Two-dimensional MXene (Ti₃C₂)-integrated cellulose hydrogels: toward smart three-dimensional network nanoplateforms exhibiting light-induced swelling and bimodal photothermal/chemotherapy anticancer activity. *ACS Appl Mater Interfaces*. 2018; 10: 27631-43.
106. Xing C, Chen S, Qiu M, Liang X, Liu Q, Zou Q, et al. Conceptually novel black phosphorus/cellulose hydrogels as promising photothermal agents for effective cancer therapy. *Adv Healthcare Mater*. 2018; 7: 1701510.
107. Tao W, Ji X, Xu X, Islam MA, Li Z, Chen S, et al. Antimonene Quantum Dots: synthesis and application as near-infrared photothermal agents for effective cancer therapy. *Angew Chem Int Ed*. 2017; 56: 11896-900.
108. Rosenkrans ZT, Sun T, Jiang D, Chen W, Barnhart TE, Zhang Z, et al. Selenium-doped carbon quantum dots act as broad-spectrum antioxidants for acute kidney injury management. *Adv Sci*. 2020; 7: 2000420.
109. Kim D, Yoo JM, Hwang H, Lee J, Lee SH, Yun SP, et al. Graphene quantum dots prevent alpha-synucleinopathy in Parkinson's disease. *Nat Nanotechnol*. 2018; 13: 812-8.
110. Pandey S, Bodas D. High-quality quantum dots for multiplexed bioimaging: A critical review. *Adv Colloid Interface Sci*. 2020; 278: 102137.
111. Fu Y, Zeng G, Lai C, Huang D, Qin L, Yi H, et al. Hybrid architectures based on noble metals and carbon-based dots nanomaterials: A review of recent progress in synthesis and applications. *Chem Eng J*. 2020; 399: 125743.
112. Zhu Y, Xie Z, Li J, Liu Y, Li C, Liang W, et al. From phosphorus to phosphorene: Applications in disease theranostics. *Coord Chem Rev*. 2021; 446: 214110.
113. Wang Y, Qiu M, Won M, Jung E, Fan T, Xie N, et al. Emerging 2D material-based nanocarrier for cancer therapy beyond graphene. *Coord Chem Rev*. 2019; 400: 213041.
114. Xie J, Wang Y, Choi W, Jangili P, Ge Y, Xu Y, et al. Overcoming barriers in photodynamic therapy harnessing nano-formulation strategies. *Chem Soc Rev*. 2021; 50: 9152-201.
115. Xie Z, Zhang B, Ge Y, Zhu Y, Nie G, Song Y, et al. Chemistry, functionalization, and applications of recent monoelemental two-dimensional materials and their heterostructures. *Chem Rev*. 2022; 122: 1127-207.
116. Ge J, Jia Q, Liu W, Guo L, Liu Q, Lan M, et al. Red-emissive carbon dots for fluorescent, photoacoustic, and thermal theranostics in living mice. *Adv Mater*. 2015; 27: 4169-77.
117. Li D, Han D, Qu SN, Liu L, Jing PT, Zhou D, et al. Supra-(carbon nanodots) with a strong visible to near-infrared absorption band and efficient photothermal conversion. *Light Sci Appl*. 2016; 5: e16120.
118. Zheng M, Li Y, Liu S, Wang W, Xie Z, Jing X. One-pot to synthesize multifunctional carbon dots for near infrared fluorescence imaging and photothermal cancer therapy. *ACS Appl Mater Interfaces*. 2016; 8: 23533-41.
119. Ge J, Jia Q, Liu W, Lan M, Zhou B, Guo L, et al. Carbon dots with intrinsic theranostic properties for bioimaging, red-light-triggered photodynamic/photothermal simultaneous therapy *in vitro* and *in vivo*. *Adv Healthcare Mater*. 2016; 5: 665-75.
120. Sun S, Zhang L, Jiang K, Wu A, Lin H. Toward high-efficient red emissive carbon dots: facile preparation, unique properties, and applications as multifunctional theranostic agents. *Chem Mater*. 2016; 28: 8659-68.
121. Lu S, Sui L, Liu J, Zhu S, Chen A, Jin M, et al. Near-infrared photoluminescent polymer-carbon nanodots with two-photon fluorescence. *Adv Mater*. 2017; 29: 1603443.
122. Lan M, Zhao S, Zhang Z, Yan L, Guo L, Niu G, et al. Two-photon-excited near-infrared emissive carbon dots as multifunctional agents for fluorescence imaging and photothermal therapy. *Nano Res*. 2017; 10: 3113-23.
123. Ding H, Wei JS, Zhang P, Zhou ZY, Gao QY, Xiong HM. Solvent-controlled synthesis of highly luminescent carbon dots with a wide color gamut and narrowed emission peak widths. *Small*. 2018; 14: 1800612.
124. Zhang J, Lu X, Tang D, Wu S, Hou X, Liu J, et al. Phosphorescent carbon dots for highly efficient oxygen photosensitization and as photo-oxidative nanozymes. *ACS Appl Mater Interfaces*. 2018; 10: 40808-14.
125. Geng B, Yang D, Pan D, Wang L, Zheng F, Shen W, et al. NIR-responsive carbon dots for efficient photothermal cancer therapy at low power densities. *Carbon*. 2018; 134: 153-62.
126. Permatasari FA, Fukazawa H, Ogi T, Iskandar F, Okuyama K. Design of pyrrolic-N-rich carbon dots with absorption in the first near-infrared window for photothermal therapy. *ACS Appl Nano Mater*. 2018; 1: 2368-75.
127. He H, Zheng X, Liu S, Zheng M, Xie Z, Wang Y, et al. Diketopyrrolopyrrole-based carbon dots for photodynamic therapy. *Nanoscale*. 2018; 10: 10991-8.
128. Bao YW, Hua XW, Li YH, Jia HR, Wu FG. Hyperthermia-promoted cytosolic and nuclear delivery of copper/carbon quantum dot-crosslinked nanosheets: multimodal imaging-guided photothermal cancer therapy. *ACS Appl Mater Interfaces*. 2018; 10: 1544-55.
129. Yu Y, Song M, Chen C, Du Y, Li C, Han Y, et al. Bortezomib-encapsulated CuS/carbon dot nanocomposites for enhanced photothermal therapy via stabilization of polyubiquitinated substrates in the proteasomal degradation pathway. *ACS Nano*. 2020; 14: 10688-703.
130. Hua XW, Bao YW, Zeng J, Wu FG. Ultrasmall all-in-one nanodots formed via carbon dot-mediated and albumin-based synthesis: multimodal imaging-guided and mild laser-enhanced cancer therapy. *ACS Appl Mater Interfaces*. 2018; 10: 42077-87.
131. Wang B, Li J, Tang Z, Yang B, Lu S. Near-infrared emissive carbon dots with 33.96% emission in aqueous solution for cellular sensing and light-emitting diodes. *Sci Bull*. 2019; 64: 1285-92.
132. Ye X, Xiang Y, Wang Q, Li Z, Liu Z. A red emissive two-photon fluorescence probe based on carbon dots for intracellular pH detection. *Small*. 2019; 15: 1901673.
133. Li D, Liang C, Ushakova EV, Sun M, Huang X, Zhang X, et al. Thermally activated upconversion near-infrared photoluminescence from carbon dots synthesized via microwave assisted exfoliation. *Small*. 2019; 15: 1905050.

134. Sun S, Chen J, Jiang K, Tang Z, Wang Y, Li Z, et al. Ce6-modified carbon dots for multimodal-imaging-guided and single-NIR-laser-triggered photothermal/photodynamic synergistic cancer therapy by reduced irradiation power. *ACS Appl Mater Interfaces*. 2019; 11: 5791-803.
135. Wu S, Li W, Sun Y, Zhang X, Zhuang J, Hu H, et al. Synthesis of dual-emissive carbon dots with a unique solvatochromism phenomenon. *J Colloid Interface Sci*. 2019; 555: 607-14.
136. Geng B, Qin H, Zheng F, Shen W, Li P, Wu K, et al. Carbon dot-sensitized MoS₂ nanosheet heterojunctions as highly efficient NIR photothermal agents for complete tumor ablation at an ultralow laser exposure. *Nanoscale*. 2019; 11: 7209-20.
137. Zhang M, Zheng T, Sheng B, Wu F, Zhang Q, Wang W, et al. Mn²⁺ complex-modified polydopamine- and dual emissive carbon dots based nanoparticles for *in vitro* and *in vivo* trimodality fluorescent, photothermal, and magnetic resonance imaging. *Chem Eng J*. 2019; 373: 1054-63.
138. Wang L, Li W, Yin L, Liu Y, Guo H, Lai J, et al. Full-color fluorescent carbon quantum dots. *Sci Adv*. 2020; 6: eabb6772.
139. Phuong PTM, Won HJ, Robby AI, Kim SG, Im GB, Bhang SH, et al. NIR-vis-induced pH-sensitive TiO₂ immobilized carbon dot for controllable membrane-nuclei targeting and photothermal therapy of cancer cells. *ACS Appl Mater Interfaces*. 2020; 12: 37929-42.
140. Zhao S, Yan L, Cao M, Huang L, Yang K, Wu S, et al. Near-infrared light-triggered lysosome-targetable carbon dots for photothermal therapy of cancer. *ACS Appl Mater Interfaces*. 2021; 13: 53610-7.
141. Shen Y, Zhang X, Liang L, Yue J, Huang D, Xu W, et al. Mitochondria-targeting supra-carbon dots: enhanced photothermal therapy selective to cancer cells and their hyperthermia molecular actions. *Carbon*. 2020; 156: 558-67.
142. Jiang L, Ding H, Xu M, Hu X, Li S, Zhang M, et al. UV-vis-NIR full-range responsive carbon dots with large multiphoton absorption cross sections and deep-red fluorescence at nucleoli and *in vivo*. *Small*. 2020; 16: 2000680.
143. Shen CL, Lou Q, Zang JH, Liu KK, Qu SN, Dong L, et al. Near-infrared chemiluminescent carbon nanodots and their application in reactive oxygen species bioimaging. *Adv Sci*. 2020; 7: 1903525.
144. Wei S-M, Feng K, Li C, Xie N, Wang Y, Yang X-L, et al. ZnCl₂ enabled synthesis of highly crystalline and emissive carbon dots with exceptional capability to generate O₂⁻. *Matter*. 2020; 2: 495-506.
145. Xu N, Du J, Yao Q, Ge H, Li H, Xu F, et al. Precise photodynamic therapy: Penetrating the nuclear envelope with photosensitive carbon dots. *Carbon*. 2020; 159: 74-82.
146. Chen S, Sun T, Zheng M, Xie Z. Carbon dots based nanoscale covalent organic frameworks for photodynamic therapy. *Adv Funct Mater*. 2020; 30: 2004680.
147. Chen T, Yao T, Peng H, Whittaker AK, Li Y, Zhu S, et al. An injectable hydrogel for simultaneous photothermal therapy and photodynamic therapy with ultrahigh efficiency based on carbon dots and modified cellulose nanocrystals. *Adv Funct Mater*. 2021; 31: 2106079.
148. Kim D, Jo G, Chae Y, Subramani S, Lee BY, Kim EJ, et al. Bioinspired camellia japonica carbon dots with high near-infrared absorbance for efficient photothermal cancer therapy. *Nanoscale*. 2021; 13: 14426-34.
149. Tian B, Liu S, Feng L, Liu S, Gai S, Dai Y, et al. Renal-clearable nickel-doped carbon dots with boosted photothermal conversion efficiency for multimodal imaging-guided cancer therapy in the second near-infrared biowindow. *Adv Funct Mater*. 2021; 31: 2100549.
150. Bai Y, Zhao J, Wang S, Lin T, Ye F, Zhao S. Carbon dots with absorption red-shifting for two-photon fluorescence imaging of tumor tissue pH and synergistic phototherapy. *ACS Appl Mater Interfaces*. 2021; 13: 35365-75.
151. Yi S, Deng S, Guo X, Pang C, Zeng J, Ji S, et al. Red emissive two-photon carbon dots: Photodynamic therapy in combination with real-time dynamic monitoring for the nucleolus. *Carbon*. 2021; 182: 155-66.
152. Hasan MT, Lee BH, Lin C-W, McDonald-Boyer A, Gonzalez-Rodriguez R, Vasireddy S, et al. Near-infrared emitting graphene quantum dots synthesized from reduced graphene oxide for *in vitro/in vivo/ex vivo* bioimaging applications. *2D Materials*. 2021; 8: 035013.
153. Yue J, Li L, Jiang C, Mei Q, Dong WF, Yan R. Riboflavin-based carbon dots with high singlet oxygen generation for photodynamic therapy. *J Mater Chem B*. 2021; 9: 7972-8.
154. Wu J, Lei JH, He B, Deng CX, Tang Z, Qu S. Generating long-wavelength absorption bands with enhanced deep red fluorescence and photothermal performance in fused carbon dots aggregates. *Aggregate*. 2021; 2: e139.
155. Kim TE, Jang HJ, Park SW, Wei J, Cho S, Park WI, et al. Folic acid functionalized carbon dot/polypropylene nanoparticles for specific bioimaging and photothermal therapy. *ACS Appl Bio Mater*. 2021; 4: 3453-61.
156. Chang Q, Shen Z, Guo Z, Xue C, Li N, Yang J, et al. Hydroxypropylmethyl cellulose modified with carbon dots exhibits light-responsive and reversible optical switching. *ACS Appl Mater Interfaces*. 2021; 13: 12375-82.
157. Li Z, Ni J, Liu L, Gu L, Wu Z, Li T, et al. Imaging-guided chemo-photothermal polydopamine carbon dots for EpCAM-targeted delivery toward liver tumor. *ACS Appl Mater Interfaces*. 2021; 13: 29340-8.
158. Zhu Z, Cheng R, Ling L, Li Q, Chen S. Rapid and large-scale production of multi-fluorescence carbon dots by a magnetic hyperthermia method. *Angew Chem Int Ed*. 2020; 59: 3099-105.
159. Baker SN, Baker GA. Luminescent carbon nanodots: emergent nanolights. *Angew Chem Int Ed*. 2010; 49: 6726-44.
160. Dong Y, Pang H, Yang HB, Guo C, Shao J, Chi Y, et al. Carbon-based dots co-doped with nitrogen and sulfur for high quantum yield and excitation-independent emission. *Angew Chem Int Ed*. 2013; 52: 7800-4.
161. Jiang K, Wang Y, Gao X, Cai C, Lin H. Facile, Quick, and Gram-scale synthesis of ultralong-lifetime room-temperature-phosphorescent carbon dots by microwave irradiation. *Angew Chem Int Ed*. 2018; 57: 6216-20.
162. Li H, He X, Kang Z, Huang H, Liu Y, Liu J, et al. Water-soluble fluorescent carbon quantum dots and photocatalyst design. *Angew Chem Int Ed*. 2010; 49: 4430-4.
163. Sekiya R, Uemura Y, Murakami H, Haino T. White-light-emitting edge-functionalized graphene quantum dots. *Angew Chem Int Ed*. 2014; 53: 5619-23.
164. Xiong R, Zhang X, Krecker M, Kang S, Smith MJ, Tsukruk VV. Large and emissive crystals from carbon quantum dots onto interfacial organized templates. *Angew Chem Int Ed*. 2020; 59: 20167-73.
165. Shakeel A, Bhattacharya R, Jeevanandham S, Kochhar D, Singh A, Mehra L, et al. Graphene quantum dots in the game of directing polymer self-assembly to exotic kagome lattice and janus nanostructures. *ACS Nano*. 2019; 13: 9397-407.
166. Kalytchuk S, Polakova K, Wang Y, Froning JP, Cepe K, Rogach AL, et al. Carbon dot nanothermometry: intracellular photoluminescence lifetime thermal sensing. *ACS Nano*. 2017; 11: 1432-42.
167. Zhi B, Cui Y, Wang S, Frank BP, Williams DN, Brown RP, et al. Malic acid carbon dots: from super-resolution live-cell imaging to highly efficient separation. *ACS Nano*. 2018; 12: 5741-52.
168. He H, Chen X, Feng Z, Liu L, Wang Q, Bi S. Nanoscopic imaging of nucleolar stress enabled by protein-mimicking carbon dots. *Nano Lett*. 2021; 21: 5689-96.
169. Ye Z, Wei L, Geng X, Wang X, Li Z, Xiao L. Mitochondrion-specific blinking fluorescent bioprobe for nanoscopic monitoring of mitophagy. *ACS Nano*. 2019; 13: 11593-602.
170. Wang H, Wang K, Tian B, Revia R, Mu Q, Jeon M, et al. Preloading of hydrophobic anticancer drug into multifunctional nanocarrier for multimodal imaging, NIR-responsive drug release, and synergistic therapy. *Small*. 2016; 12: 6388-97.
171. Shen J, Zhu Y, Yang X, Li C. Graphene quantum dots: emergent nanolights for bioimaging, sensors, catalysis and photovoltaic devices. *Chem Commun*. 2012; 48: 3686-99.
172. Liu C, Zhang P, Zhai X, Tian F, Li W, Yang J, et al. Nano-carrier for gene delivery and bioimaging based on carbon dots with PEI-passivation enhanced fluorescence. *Biomaterials*. 2012; 33: 3604-13.
173. Wang C, Wang X, Liu L. Clinical application of carbon nanoparticles suspension in operation of papillary thyroid carcinoma. *Journal of clinical otorhinolaryngology, head, and neck surgery*. 2020; 34: 165-9.
174. Wu G, Cai L, Hu J, Zhao R, Ge J, Zhao Y, et al. Role of carbon nanoparticles in patients with thyroid carcinoma undergoing total thyroidectomy plus bilateral central neck dissection. *Zhonghua yi xue za zhi*. 2015; 95: 912-6.
175. Wang L, Zhou HS. Green synthesis of luminescent nitrogen-doped carbon dots from milk and its imaging application. *Anal Chem*. 2014; 86: 8902-5.
176. Ni P, Li Q, Xu C, Lai H, Bai Y, Chen T. Optical properties of nitrogen and sulfur co-doped carbon dots and their applicability as fluorescent probes for living cell imaging. *Appl Surf Sci*. 2019; 494: 377-83.
177. Zhang M, Wang W, Wu F, Zheng T, Ashley J, Mohammadniaei M, et al. Biodegradable poly(gamma-glutamic acid)/glucose oxidase@carbon dot nanoparticles for simultaneous multimodal imaging and synergetic cancer therapy. *Biomaterials*. 2020; 252: 120106.
178. Pan L, Sun S, Zhang A, Jiang K, Zhang L, Dong C, et al. Truly fluorescent excitation-dependent carbon dots and their applications in multicolor cellular imaging and multidimensional sensing. *Adv Mater*. 2015; 27: 7782-7.
179. Kong B, Zhu A, Ding C, Zhao X, Li B, Tian Y. Carbon dot-based inorganic-organic nanosystem for two-photon imaging and biosensing of pH variation in living cells and tissues. *Adv Mater*. 2012; 24: 5844-8.
180. Liu X, Jiang H, Ye J, Zhao C, Gao S, Wu C, et al. Nitrogen-doped carbon quantum dot stabilized magnetic iron oxide nanoprobe for fluorescence, magnetic resonance, and computed tomography triple-modal *in vivo* bioimaging. *Adv Funct Mater*. 2016; 26: 8694-706.
181. Jiang K, Sun S, Zhang L, Lu Y, Wu A, Cai C, et al. Red, green, and blue luminescence by carbon dots: full-color emission tuning and multicolor cellular imaging. *Angew Chem Int Ed*. 2015; 54: 5360-3.
182. Ko HY, Chang YW, Paramasivam G, Jeong MS, Cho S, Kim S. *In vivo* imaging of tumour bearing near-infrared fluorescence-emitting carbon nanodots derived from tire soot. *Chem Commun*. 2013; 49: 10290-2.
183. Nurunnabi M, Khatun Z, Reeck GR, Lee DY, Lee YK. Near infrared photoluminescent graphene nanoparticles greatly expand their use in noninvasive biomedical imaging. *Chem Commun*. 2013; 49: 5079-81.
184. Su Y, Liu S, Guan Y, Xie Z, Zheng M, Jing X. Renal clearable Hafnium-doped carbon dots for CT/fluorescence imaging of orthotopic liver cancer. *Biomaterials*. 2020; 255: 120110.
185. Zhang Y, Shen Y, Teng X, Yan M, Bi H, Morais PC. Mitochondria-targeting nanoplateform with fluorescent carbon dots for long time imaging and magnetic field-enhanced cellular uptake. *ACS Appl Mater Interfaces*. 2015; 7: 10201-12.
186. Yang Z, Hou B, Yang Y, Jiang L, Xie A, Shen Y, et al. A pH-induced charge convertible nanocomposite as novel targeted phototherapy agent and gene carrier. *Chem Eng J*. 2018; 353: 350-60.

187. Li W, Liu Q, Zhang P, Liu L. Zwitterionic nanogels crosslinked by fluorescent carbon dots for targeted drug delivery and simultaneous bioimaging. *Acta Biomater.* 2016; 40: 254-62.
188. Peng S, Wang H, Zhao W, Xin Y, Liu Y, Yu X, et al. Zwitterionic polysulfamide drug nanogels with microwave augmented tumor accumulation and on-demand drug release for enhanced cancer therapy. *Adv Funct Mater.* 2020; 30: 2001832.
189. Sri S, Kumar R, Panda AK, Solanki PR. Highly biocompatible, fluorescence, and zwitterionic carbon dots as a novel approach for bioimaging applications in cancerous cells. *ACS Appl Mater Interfaces.* 2018; 10: 37835-45.
190. Kong T, Zhou R, Zhang Y, Hao L, Cai X, Zhu B. AS1411 aptamer modified carbon dots via polyethylenimine-assisted strategy for efficient targeted cancer cell imaging. *Cell Prolif.* 2020; 53: 12713.
191. Gong P, Sun L, Wang F, Liu X, Yan Z, Wang M, et al. Highly fluorescent N-doped carbon dots with two-photon emission for ultrasensitive detection of tumor marker and visual monitor anticancer drug loading and delivery. *Chem Eng J.* 2019; 356: 994-1002.
192. Gu C, Guo C, Li Z, Wang M, Zhou N, He L, et al. Bimetallic ZrHf-based metal-organic framework embedded with carbon dots: ultra-sensitive platform for early diagnosis of HER2 and HER2-overexpressed living cancer cells. *Biosens Bioelectron.* 2019; 134: 8-15.
193. Hamd-Ghadareh S, Salimi A, Fathi F, Bahrami S. An amplified comparative fluorescence resonance energy transfer immunosensing of CA125 tumor marker and ovarian cancer cells using green and economic carbon dots for bio-applications in labeling, imaging and sensing. *Biosens Bioelectron.* 2017; 96: 308-16.
194. Shen Y, Wu T, Wang Y, Zhang SL, Zhao X, Chen HY, et al. Nucleolin-targeted ratiometric fluorescent carbon dots with a remarkably large emission wavelength shift for precise imaging of cathepsin B in living cancer cells. *Anal Chem.* 2021; 93: 4042-50.
195. Qian J, Quan F, Zhao F, Wu C, Wang Z, Zhou L. Aconitic acid derived carbon dots: conjugated interaction for the detection of folic acid and fluorescence targeted imaging of folate receptor overexpressed cancer cells. *Sensors Actuat B-Chem.* 2018; 262: 444-51.
196. Das K, Sarkar S, Das PK. Fluorescent indicator displacement assay: ultrasensitive detection of glutathione and selective cancer cell imaging. *ACS Appl Mater Interfaces.* 2016; 8: 25691-701.
197. Li L, Shi L, Jia J, Eltayeb O, Lu W, Tang Y, et al. Dual photoluminescence emission carbon dots for ratiometric fluorescent GSH sensing and cancer cell recognition. *ACS Appl Mater Interfaces.* 2020; 12: 18250-7.
198. Gao N, Yang W, Nie H, Gong Y, Jing J, Gao L, et al. Turn-on theranostic fluorescent nanoprobe by electrostatic self-assembly of carbon dots with doxorubicin for targeted cancer cell imaging, *in vivo* hyaluronidase analysis, and targeted drug delivery. *Biosens Bioelectron.* 2017; 96: 300-7.
199. Demir B, Lemberger MM, Panagiotopoulou M, Medina Rangel PX, Timur S, Hirsch T, et al. Tracking hyaluronan: molecularly imprinted polymer coated carbon dots for cancer cell targeting and imaging. *ACS Appl Mater Interfaces.* 2018; 10: 3305-13.
200. Zheng M, Ruan S, Liu S, Sun T, Qu D, Zhao H, et al. Self-targeting fluorescent carbon dots for diagnosis of brain cancer cells. *ACS Nano.* 2015; 9: 11455-61.
201. Li S, Su W, Wu H, Yuan T, Yuan C, Liu J, et al. Targeted tumour theranostics in mice via carbon quantum dots structurally mimicking large amino acids. *Nat Biomed Eng.* 2020; 4: 704-16.
202. Luo GF, Chen WH, Zeng X, Zhang XZ. Cell primitive-based biomimetic functional materials for enhanced cancer therapy. *Chem Soc Rev.* 2021; 50: 945-85.
203. Karthik S, Saha B, Ghosh SK, Pradeep Singh ND. Photoresponsive quinoline tethered fluorescent carbon dots for regulated anticancer drug delivery. *Chem Commun.* 2013; 49: 10471-3.
204. Wang Q, Huang X, Long Y, Wang X, Zhang H, Zhu R, et al. Hollow luminescent carbon dots for drug delivery. *Carbon.* 2013; 59: 192-9.
205. Gogoi N, Chowdhury D. Novel carbon dot coated alginate beads with superior stability, swelling and pH responsive drug delivery. *J Mater Chem B.* 2014; 2: 4089-99.
206. Zheng M, Liu S, Li J, Qu D, Zhao H, Guan X, et al. Integrating oxaliplatin with highly luminescent carbon dots: an unprecedented theranostic agent for personalized medicine. *Adv Mater.* 2014; 26: 3554-60.
207. Feng T, Ai X, An G, Yang P, Zhao Y. Charge-convertible carbon dots for imaging-guided drug delivery with enhanced *in vivo* cancer therapeutic efficiency. *ACS Nano.* 2016; 10: 4410-20.
208. Feng T, Ai X, Ong H, Zhao Y. Dual-responsive carbon dots for tumor extracellular microenvironment triggered targeting and enhanced anticancer drug delivery. *ACS Appl Mater Interfaces.* 2016; 8: 18732-40.
209. Gong X, Zhang Q, Gao Y, Shuang S, Choi MM, Dong C. Phosphorus and nitrogen dual-doped hollow carbon dot as a nanocarrier for doxorubicin delivery and biological imaging. *ACS Appl Mater Interfaces.* 2016; 8: 11288-97.
210. Zeng Q, Shao D, He X, Ren Z, Ji W, Shan C, et al. Carbon dots as a trackable drug delivery carrier for localized cancer therapy *in vivo*. *J Mater Chem B.* 2016; 4: 5119-26.
211. Shu Y, Lu J, Mao QX, Song RS, Wang XY, Chen XW, et al. Ionic liquid mediated organophilic carbon dots for drug delivery and bioimaging. *Carbon.* 2017; 114: 324-33.
212. Wang HJ, He X, Luo TY, Zhang J, Liu YH, Yu XQ. Amphiphilic carbon dots as versatile vectors for nucleic acid and drug delivery. *Nanoscale.* 2017; 9: 5935-47.
213. Yao YY, Gedda G, Girma WM, Yen CL, Ling YC, Chang JY. Magnetofluorescent carbon dots derived from crab shell for targeted dual-modality bioimaging and drug delivery. *ACS Appl Mater Interfaces.* 2017; 9: 13887-99.
214. Ma J, Kang K, Zhang Y, Yi Q, Gu Z. Detachable polyzwitterion-coated ternary nanoparticles based on peptide dendritic carbon dots for efficient drug delivery in cancer therapy. *ACS Appl Mater Interfaces.* 2018; 10: 43923-35.
215. Hettiarachchi SD, Graham RM, Mintz KJ, Zhou Y, Vanni S, Peng Z, et al. Triple conjugated carbon dots as a nano-drug delivery model for glioblastoma brain tumors. *Nanoscale.* 2019; 11: 6192-205.
216. Wu R, Liu J, Chen D, Pan J. Carbon nanodots modified with catechol-borane moieties for pH-stimulated doxorubicin delivery: toward nuclear targeting. *ACS Appl Nano Mater.* 2019; 2: 4333-41.
217. Hailing Y, Xiufang L, Lili W, Baoqiang L, Kaichen H, Yongquan H, et al. Doxorubicin-loaded fluorescent carbon dots with PEI passivation as a drug delivery system for cancer therapy. *Nanoscale.* 2020; 12: 17222-37.
218. Liang YC, Gou S-S, Liu K-K, Wu W-J, Guo C-Z, Lu S-Y, et al. Ultralong and efficient phosphorescence from silica confined carbon nanodots in aqueous solution. *Nano Today.* 2020; 34: 100900.
219. Hou L, Chen D, Wang R, Wang R, Zhang H, Zhang Z, et al. Transformable honeycomb-like nanoassemblies of carbon dots for regulated multisite delivery and enhanced antitumor chemoimmunotherapy. *Angew Chem Int Ed.* 2021; 60: 6581-92.
220. Kong T, Hao L, Wei Y, Cai X, Zhu B. Doxorubicin conjugated carbon dots as a drug delivery system for human breast cancer therapy. *Cell Prolif.* 2018; 51: 12488.
221. Gong N, Ma X, Ye X, Zhou Q, Chen X, Tan X, et al. Carbon-dot-supported atomically dispersed gold as a mitochondrial oxidative stress amplifier for cancer treatment. *Nat Nanotechnol.* 2019; 14: 379-87.
222. Zhao S, Wu S, Jia Q, Huang L, Lan M, Wang P, et al. Lysosome-targetable carbon dots for highly efficient photothermal/photodynamic synergistic cancer therapy and photoacoustic/two-photon excited fluorescence imaging. *Chem Eng J.* 2020; 388: 124212.
223. Li Y, Bai G, Zeng S, Hao J. Theranostic carbon dots with innovative NIR-II emission for *in vivo* renal-excreted optical imaging and photothermal therapy. *ACS Appl Mater Interfaces.* 2019; 11: 4737-44.
224. Pang W, Jiang P, Ding S, Bao Z, Wang N, Wang H, et al. Nucleolus-targeted photodynamic anticancer therapy using renal-clearable carbon dots. *Adv Healthcare Mater.* 2020; 9: 2000607.
225. Jia Q, Ge J, Liu W, Zheng X, Chen S, Wen Y, et al. A magnetofluorescent carbon dot assembly as an acidic H₂O₂-driven oxygenator to regulate tumor hypoxia for simultaneous bimodal imaging and enhanced photodynamic therapy. *Adv Mater.* 2018; 30: 1706909.
226. Zheng DW, Li B, Li CX, Fan JX, Lei Q, Li C, et al. Carbon-dot-decorated carbon nitride nanoparticles for enhanced photodynamic therapy against hypoxic tumor via water splitting. *ACS Nano.* 2016; 10: 8715-22.
227. Wu H, Zeng F, Zhang H, Xu J, Qiu J, Wu S. A nanosystem capable of releasing a photosensitizer bioprecursor under two-photon irradiation for photodynamic therapy. *Adv Sci.* 2016; 3: 1500254.
228. Yang K, Wang C, Wei X, Ding S, Liu C, Tian F, et al. Self-illuminating photodynamic therapy with enhanced therapeutic effect by optimization of the chemiluminescence resonance energy transfer step to the photosensitizer. *Bioconjug Chem.* 2020; 31: 595-604.
229. Sun S, Chen Q, Tang Z, Liu C, Li Z, Wu A, et al. Tumor microenvironment stimuli-responsive fluorescence imaging and synergistic cancer therapy by carbon-dot-Cu(2+) nanoassemblies. *Angew Chem Int Ed.* 2020; 59: 21041-8.
230. Xu J, Zeng F, Wu H, Hu C, Yu C, Wu S. Preparation of a mitochondria-targeted and NO-releasing nanoplateform and its enhanced pro-apoptotic effect on cancer cells. *Small.* 2014; 10: 3750-60.
231. Fang X, Cai S, Wang M, Chen Z, Lu C, Yang H. Photogenerated holes mediated nitric oxide production for hypoxic tumor treatment. *Angew Chem Int Ed.* 2021; 60: 7046-50.
232. Li F, Li Y, Yang X, Han X, Jiao Y, Wei T, et al. Highly fluorescent chiral N-S-doped carbon dots from cysteine: affecting cellular energy metabolism. *Angew Chem Int Ed.* 2018; 57: 2377-82.
233. Ding Y, Yu J, Chen X, Wang S, Tu Z, Shen G, et al. Dose-dependent carbon-dot-induced ROS promote uveal melanoma cell tumorigenicity via activation of mTOR signaling and glutamine metabolism. *Adv Sci.* 2021; 8: 2002404.
234. Li J, Kong J, Ma S, Li J, Mao M, Chen K, et al. Exosome-coated 10B carbon dots for precise boron neutron capture therapy in a mouse model of glioma *in situ*. *Adv Funct Mater.* 2021; 31: 2100969.
235. Wu D, Li BL, Zhao Q, Liu Q, Wang D, He B, et al. Assembling defined DNA nanostructure with nitrogen-enriched carbon dots for theranostic cancer applications. *Small.* 2020; 16: 1906975.

Author biography



Cheng-Long Shen is an assistant research fellow at School of Physics and Microelectronics, Zhengzhou University. He received his B.S. degree (2015) and Ph.D. degree (2021) from Zhengzhou University. Since 2021, he entered into Zhengzhou University as a research fellow in the Diamond Optoelectronic Materials and Devices Group directed by Prof. Chong-Xin Shan. His present research interests are carbon-related materials and their applications.



Hang-Rui Liu obtained her M.M. degree in Oncology from Zhengzhou University in 2021. Currently, she is resident physician of the Second Affiliated Hospital of Zhengzhou University. Her research interests mainly focus on the diagnosis and treatment of breast cancer, lung cancer, esophageal cancer, gastric cancer, colorectal cancer, liver cancer, lymphoma, multiple myeloma, cervical cancer, ovarian cancer, and prostate cancer.



Qing Lou earned his B.S. degree from Chongqing University and Ph.D. degree from Changchun Institute of Optics, Fine Mechanics and Physics, Chinese Academy of Sciences. In 2015, he entered into Zhengzhou University as a lecturer in the Diamond Optoelectronic Materials and Devices Group directed by Prof. Chong-Xin Shan. His research is mainly focused on diamond and carbon nanodots and their optoelectronic devices.



Feng Wang is a professor in the Department of Oncology at the First Affiliated Hospital of Zhengzhou University. He earned his M.M. degree from Zhengzhou University in 2002 and his Ph.D. degree from Zhengzhou University in 2008. His current research interests are the diagnosis and treatment of breast cancer, lung cancer, esophageal cancer, gastric cancer, colorectal cancer, liver cancer, lymphoma, multiple myeloma, cervical cancer, ovarian cancer, prostate cancer.



Kai-Kai Liu received his B.S. degree in Applied Physics from Shandong University (2013) and Ph. D. degree in Condensed Matter Physics from Changchun Institute of Optics, Fine Mechanics and Physics, Chinese Academy of Sciences (2018). Since 2018, he worked at School of Physics and Microelectronics, Zhengzhou University. Currently, his research focuses on luminescent nanomaterials.



Lin Dong received his B.S. (1998) and M.S. degree (2001) in Chemistry from Jilin University, and the Ph.D. degree (2005) in Condensed Matter Physics from Changchun Institute of Optics, Fine Mechanics and Physics, CAS, and joined Zhengzhou University in 2005. He is currently a full professor in School of Physics & Microelectronics, Zhengzhou University. His research mainly focuses on luminescent performance and piezotronic/piezophototronic effects of nano-devices.



Chong-Xin Shan is a Professor of Zhengzhou University. He received his B.S. degree from Wuhan University in 1999, and Ph.D. degree from Changchun Institute of Optics, Fine Mechanics and Physics, Chinese Academy of Sciences in 2004. His current research focuses on carbon based semiconductor materials and devices.